

Loughborough University
Institutional Repository

*Evaluation of the wind
patterns over the Yucatán
Peninsula in México*

This item was submitted to Loughborough University's Institutional Repository by the/an author.

Additional Information:

- A Doctoral Thesis. Submitted in partial fulfillment of the requirements for the award of Doctor of Philosophy of Loughborough University.

Metadata Record: <https://dspace.lboro.ac.uk/2134/5988>

Publisher: © Rolando Soler-Bientz

Please cite the published version.

This item was submitted to Loughborough's Institutional Repository (<https://dspace.lboro.ac.uk/>) by the author and is made available under the following Creative Commons Licence conditions.



CC creative commons
COMMONS DEED

Attribution-NonCommercial-NoDerivs 2.5

You are free:

- to copy, distribute, display, and perform the work

Under the following conditions:

 **Attribution.** You must attribute the work in the manner specified by the author or licensor.

 **Noncommercial.** You may not use this work for commercial purposes.

 **No Derivative Works.** You may not alter, transform, or build upon this work.

- For any reuse or distribution, you must make clear to others the license terms of this work.
- Any of these conditions can be waived if you get permission from the copyright holder.

Your fair use and other rights are in no way affected by the above.

This is a human-readable summary of the [Legal Code \(the full license\)](#).

[Disclaimer](#) 

For the full text of this licence, please go to:
<http://creativecommons.org/licenses/by-nc-nd/2.5/>

Thesis Access Form

Copy No.....Location.....

Author... Rolando Soler-Bientz.

Title... Evaluation of the wind patterns over the Yucatán Peninsula in México.

Status of access **OPEN** / RESTRICTED / CONFIDENTIAL

Moratorium Period:.....years, ending...../.....200.....

Conditions of access approved by (CAPITALS):.....SIMON MARTIN.....

Supervisor (Signature)..........

Department of... Electronic and Electrical Engineering Department

Author's Declaration: *I agree the following conditions:*

Open access work shall be made available (in the University and externally) and reproduced as necessary at the discretion of the University Librarian or Head of Department. It may also be digitised by the British Library and made freely available on the Internet to registered users of the EThOS service subject to the EThOS supply agreements.

The statement itself shall apply to ALL copies including electronic copies:

This copy has been supplied on the understanding that it is copyright material and that no quotation from the thesis may be published without proper acknowledgement.

Restricted/confidential work: All access and any photocopying shall be strictly subject to written permission from the University Head of Department and any external sponsor, if any.

Author's signature..........Date.....

users declaration: for signature during any Moratorium period (Not Open work): <i>I undertake to uphold the above conditions:</i>			
Date	Name (CAPITALS)	Signature	Address

Loughborough University
Department of Electronic and Electrical Engineering
Centre for Renewable Energy Systems Technology

**Evaluation of the wind patterns
over the Yucatán Peninsula in México**

by

Rolando Soler-Bientz

A Doctoral Thesis

Submitted in partial fulfilment of the requirements

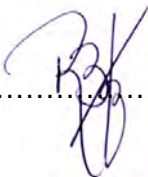
for the award of

Doctor of Philosophy of Loughborough University

2010

CERTIFICATE OF ORIGINALITY

This is to certify that I am responsible for the work submitted in this thesis, that the original work is my own except as specified in acknowledgments or in footnotes, and that neither the thesis nor the original work contained therein has been submitted to this or any other institution for a degree.

.....  (Signed)

Abstract of Thesis

Wind power is seen as one of the most effective means available to combat the twin crises of global climate change and energy security. The annual market growth has established wind power as the leading renewable energy technology. Due to the availability of sparsely populated and flat open terrain, the Yucatán Peninsula located in eastern México is a promising region from the perspective of wind energy development but no comprehensive assessment of wind resource has been previously published.

A basic requirement when developing wind power projects is to study the main characteristic parameters of wind in relation to its geographical and temporal distribution. The analysis of diurnal and seasonal wind patterns are an important stage in the move towards commercial exploitation of wind power. The research developed during the PhD has comprehensively assessed the wind behaviour over the Yucatán Peninsula region covering long term patterns at three sites, a spatial study using short term data for nine sites, a vertical profile study on one inland site and an offshore study made on a pier at 6.65km from the North shore.

Monthly trends, directional behaviours and frequency distributions were identified and discussed. The characteristics of the wind speed variation reflected their proximity to the coast and whether they were influenced by wind coming predominantly from over the land or predominantly from over the sea. The atmospheric stability over the eastern seas was also analysed to assess thermal effects for different wind directions. Diurnal wind speed variations are shown to be affected in particular by the differing wind conditions associated with fetches over two distinct offshore regions. Seasonal behaviour suggests some departure from the oscillations expected from temperature variation. The offshore wind is thermally driven suggesting largely unstable conditions and the potential development of a shallow Stable Internal Boundary Layer.

Keywords: Wind resource assessment, Seasonal wind patterns, Diurnal wind patterns, Wind frequency distribution, Atmospheric stability, Offshore winds, Vertical wind profile, Temperature patterns.

Acknowledgements

I would like to take this opportunity to thank to the support given to the research project by:

- The Yucatán Office of the “Servicio Meteorológico de la CNA”, facilitating the access to the data used in the chapters II and III .
- The administration of the API (Administración Portuaria Integral) at the Yucatán state, allowing access to the “Progreso Pier”.
- The regional office of a mobile communications company “TELCEL”, which allow installing measurement system on its communication towers.

I would also like to thank the members of the Energy laboratory of the Faculty of Engineering of the Autonomous University of Yucatán who were responsible for the installation and the operation of the measurements stations installed as part of the work done in the chapters IV and V .

Special thanks are also due to Prof. David Infield, who was my supervisor during the first stages of my PhD, because his initial support allowed the development of the research project and for his commitment to continue the supervision activities even when he was not based at Loughborough University.

I am also very grateful to my supervisor Dr. Simon Watson for his support, his guidance and for presenting increasing challenges that lead the research project to levels beyond the initial expectations.

Finally, but extremely relevant, I would like to thank my wife Tere, my daughter Karen , my son Alex and my entire family for being my inspiration and for their constant support and patience throughout my PhD studies.

Table of Contents

I	GENERAL INTRODUCTION	15
I.1	Research context.....	16
I.2	Literature review	18
I.3	Wind speed profiles	23
I.4	The Weibull probability Distribution	26
I.5	Satellite SST images.....	28
I.6	The Yucatán Peninsula and the Gulf of México	30
I.7	Thesis outline	32
II	LONG TERM TEMPORAL WIND PATTERNS.....	34
II.1	Introduction	35
II.2	The measurements at the observation sites.....	35
II.2.1	Measurement sites	35
II.2.2	Study period and data validation	37
II.3	Main environmental parameters	38
II.4	Wind behaviour	39
II.4.1	Wind speed patterns	40
II.4.2	Wind directional patterns	42
II.5	Wind frequency distribution and wind power density.....	43
II.6	Remarks.....	45
III	SPATIAL BEHAVIOUR OF THE WIND RESOURCE	47
III.1	Introduction	48
III.2	Measurement conditions.....	48
III.2.1	Study region	48
III.2.2	Measurement stations	50
III.3	Directional characteristics of the wind in the study region.....	52
III.4	Daily patterns	54
III.4.1	Environmental parameters	54
III.4.2	Wind behaviour	55
III.5	Seasonal variation	57
III.5.1	Environmental parameters	57
III.5.2	Wind behaviour	60
III.6	Atmospheric stability over the surrounding sea.....	60
III.7	Remarks.....	66
IV	INLAND VERTICAL WIND PROFILE.....	67
IV.1	Introduction	68
IV.2	Study site	68
IV.2.1	Geographical location.....	68
IV.2.2	Measurement sensors.....	69

IV.2.3	Main obstacles	70
IV.3	Directional behaviour	73
IV.4	Diurnal behaviour.....	76
IV.5	Seasonal behaviour	80
IV.6	Remarks.....	82
V	OFFSHORE WIND CHARACTERISTICS.....	84
V.1	Introduction	85
V.2	Site description	85
V.3	Onsite measurements.....	87
V.4	Effects of the solid mast on the measurements.....	88
V.5	Wind speed patterns	90
V.6	Temperature analysis	96
V.6.1	Satellite thermal images	96
V.6.2	Correlation between Satellite SST and underwater temperature measurements	98
V.6.3	Satellite SST data for the study period	100
V.6.4	Vertical temperature profile	102
V.7	Offshore wind speed ratio as function of stability	103
V.7.1	Stability measures derived from onsite measurements	104
V.7.2	Stability measures derived from Satellite SST measurements.....	106
V.8	Distribution of the atmospheric stability classes	107
V.9	The Stable Internal Boundary Layer	110
V.10	Remarks.....	111
VI	MAIN RESULTS, GENERAL CONCLUSIONS AND RECOMMENDATIONS.....	113
VII	REFERENCES	116
VIII	APPENDICES.....	122
VIII.1	Classified critical literature review.....	122
VIII.1.1	Temporal assessment	123
VIII.1.2	Spatial assessment	127
VIII.1.3	Inland vertical wind profile	132
VIII.2	Devices and sensors.....	138
VIII.3	Sea surface temperature maps from GEOS Satellite.....	141
VIII.4	Published results.....	144
VIII.4.1	Energy Conversion and Management Journal, 2009	145
VIII.4.2	Energy Conversion and Management Journal, 2010	146
VIII.4.3	Wind Engineering Journal, 2009	147
VIII.4.4	European Wind Energy Conference 2009	148
VIII.4.5	European Wind Energy Conference 2010.....	149

List of Figures

Figure I.1. Example of the original full thermal map produced hourly by the GEOS Satellite.....	29
Figure I.2. (a) Geographical location of the Yucatán Peninsula in relation to the North American subcontinent. (b) Yucatán Peninsula map representing the terrain heights by means of shadow zones.	30
Figure I.3. A 3D representation of the Gulf of México region.	31
Figure II.1. Map of the Yucatán Peninsula area representing the geographical position of the meteorological observatories: Campeche, Mérida and Chetumal.....	36
Figure II.2. Monthly (a) and yearly (b) averages of the ambient temperature for the three observatories for data measured between 1996 and 2005.	38
Figure II.3. Monthly (a) and yearly (b) averages of atmospheric pressure for the three observatories for data measured between 1996 and 2005.	39
Figure II.4. Monthly (a) and yearly (b) averages of the wind speed for the three observatories for data measured between 1996 and 2005.	40
Figure II.5. Wind speed averages for each direction using 16 directional sectors for the three observatories using all the data available at each site.	42
Figure II.6. Wind roses representing the full study period for the three observatories.	43
Figure II.7. Wind speed frequency distributions and Weibull PDFs using the wind data for the whole study period for the three observatories.	44
Figure III.1. Location of the study sites (see details in Table 1) on the Yucatán Peninsula. Terrain height represented by the shading is also shown.	49
Figure III.2. Satellite images of 500m radius centred on each automatic meteorological station.	50
Figure III.3. Photos showing the two types of meteorological measuring structures used at the study sites (Type A: Scaffolding and Type B: Tower), in these cases, the RIO and CAN stations.	51
Figure III.4. Wind roses for the nine study sites.	53
Figure III.5. Hourly averages of the main parameters for each study sites, grouped by sites with winds coming predominantly from the sea (column "A") and sites with winds coming predominantly from the land (column "B").	55
Figure III.6. Hourly averaged wind speeds for each study site, grouped by sites with winds coming predominantly from the sea (column "A") and sites with winds coming predominantly from the land (column "B").	57
Figure III.7. Monthly average of the main parameters for each study site, grouped by the sites with winds coming predominantly from over the sea (column "A") and sites with winds coming predominantly from over the land (column "B").	59
Figure III.8. Wind monthly averages for each study site, grouped by the sites with winds coming from sea (column "A") and sites with winds coming from land (column "B").	60

Figure III.9. Locations of the two selected NOAA marine stations (buoys) in the vicinity of the Yucatán Peninsula: "1. East Gulf" and "2. Yucatán Basin".	61
Figure III.10. Wind roses representing the directional distribution of wind for the data available from the EG and YB marine stations.	62
Figure III.11. Average hourly (a and b) and monthly (c and d) wind speed and wind direction for EG and YB marine buoys over the available data periods described in Table III.4.	63
Figure III.12. Daily (a and b) and yearly (c and d) sea surface and air temperatures for EG and YB marine stations averaged over the available data period described in Table III.4.	64
Figure III.13. Distribution of the stability classes from their values of the Obukhov length computed with equations I.3 and I.5 and classified using Table I.2 for EG and YB marine stations.	65
Figure IV.1. The geographical location of the measurement site is shown in the North of the Yucatán peninsula with a small star.	69
Figure IV.2. Images of the measurement tower: (a) overall view from the westerly direction, (b) view from the northerly direction showing the tower base, (c) close up view from the northerly direction showing the position of the installed sensors.	70
Figure IV.3. Satellite photos showing an aerial view of the measurement site. (a) A square area of 1600m x 1600m (b) a close up of the 400m x 400m area with the directional sectors around the measurement tower.	71
Figure IV.4. Panoramic views of the terrain surrounding the measurement tower grouped in four main directions.	72
Figure IV.5. (a) Wind frequency distribution for each directional sector over the whole study period and (b) the contribution to the whole wind distribution of the three main diurnal periods.	74
Figure IV.6. Wind speed averages over the whole study period for each direction sector.	74
Figure IV.7. Wind shear averages over the whole study period for each direction sector.	75
Figure IV.8. Frequency distribution of the wind shears over all directions.	76
Figure IV.9. (a) Hourly wind speed averages and (b) hourly wind direction averages, computed for the whole study period.	77
Figure IV.10. Distribution of the wind by directions, for the three main diurnal time periods. The shadowed region marks the directional sectors with less than 1.5% of wind over the whole study period, see distributions in Figure IV.5.	78
Figure IV.11. Diurnal pattern over the full study period for the averages of wind shear and ambient temperature.	78
Figure IV.12 Diurnal pattern for each season for the averages of ambient temperature (a) and wind shear (b).	79
Figure IV.13. Frequency distribution of the wind shear for the three main diurnal periods.	79
Figure IV.14. Wind shear as a function of rate of change of temperature.	80
Figure IV.15. (a) Monthly wind speed averages and (b) monthly wind direction averages computed for the whole study period.	81

Figure IV.16. Combined plot of the monthly averages for the wind shear (left axis) and the averages of the seasonal ambient temperature (right axis).....	81
Figure IV.17. Wind shear frequency distributions for the months January, March, July and August.....	82
Figure V.1. Data availability by month over the whole measurement period.....	88
Figure V.2. Correlation between the ten minute averages of wind speed at API and API2 for both measurement heights: (a) 10m and (b) 16.5m.....	89
Figure V.3. Correlation between the ten minute averages of air temperature at API and API2 for both measurement heights: (a) 10m and (b) 16.5m.....	90
Figure V.4. Frequency distribution by direction of the measurements over the whole study period: (a) at both measurement heights and (b) during every season for the "hi" height measurements.	91
Figure V.5 Directional frequency distributions for the data measured at 8 different hours over the whole study period: (a) from midnight up to before midday, (b) from midday up to before midnight.	91
Figure V.6 Diurnal frequency distributions for the main directional sectors over the whole study period: (a) for winds coming from the land, (b) for winds coming from the sea.	92
Figure V.7 Diagram for the directions of the dominant wind during the diurnal cycle.....	92
Figure V.8. Wind speed averages over the whole study period for each direction (a), diurnal cycle (b) and seasonal pattern (c).....	93
Figure V.9. Frequency distribution of the wind speeds over the whole study period at both measurement heights.	94
Figure V.10. Frequency distribution of wind speed over the whole study period at the "hi" height: (a) for four directional groups, (b) for three periods within the day and (c) during each season.....	95
Figure V.11. Average of ambient temperature at both measurement heights: (a) Diurnal pattern and (b) Seasonal pattern	96
Figure V.12. Available SST measurements during the correlation period for onsite (API), satellite (GEOS) and the synchronized data where values from both sources were available simultaneously.....	98
Figure V.13. Examples of hourly behaviour for: (a) and (c) underwater measurements of SST at API site; and (b) and (d) GEOS Satellite SST.....	99
Figure V.14. Correlation between the SST measured from GEOS Satellite and the underwater measurements at API site: Examples of hourly data for six days in the correlation period (a) and daily average for the whole correlation period (b).	99
Figure V.15. SST data available from GEOS Satellite during the day averaged over the entire study period between 25/07/2007 and 26/06/2009.	100
Figure V.16. Four examples of diurnal SST pattern from the GEOS Satellite.....	101
Figure V.17. Averages of SST from the GEOS Satellite over the whole study period: (a) daily and (b) hourly... ..	101
Figure V.18. Vertical temperature profile using the measurements from the GEOS Satellite for SST and from the API mast at "hi" and "lo" heights: (a) average and extreme values over the whole study period (b) hourly averages for selected times of the day.	102

Figure V.19. Ratio of wind speed at “lo” and “hi” heights versus the stability measure z/L calculated using the Gradient Richardson number (Ri) and Bulk Richardson number (Rb Thi-Tlo). (a) No filter applied, (b) Filter applied to the wind speed variations and (c) Filter applied to the wind speed standard deviation.	105
Figure V.20. Frequency distributions of the stability measure z/L calculated using Ri and “Rb Thi-Tlo”.	106
Figure V.21. Ratio of wind speeds at “lo” and “hi” height as function of the stability measure “ z/L ” using SST and air temperature at “lo” height (a) and “hi” height (b) to compute the Bulk Richardson number. The filter for mean wind speed variations was applied in both cases.	106
Figure V.22. Frequency distributions of the stability measure z/L computed from the SST and air temperature at “lo” and “hi” heights.....	107
Figure V.23. Distribution of stability classes during the whole measurement period using as stability measure: (a) “Rb Tlo-SST”, (b) “Rb Thi-SST”, (c) “Rb Thi-Tlo” and (d) “Ri”.....	107
Figure V.24. Stability classes for each directional sector using as stability measure: (a) “Rb Tlo-SST” and (b) “Rb Thi-SST”.	108
Figure V.25. Distribution of stability classes over the day using as stability measure: (a) “Rb Tlo-SST” and (b) “Rb Thi-SST”.	109
Figure V.26. Seasonal distribution of stability classes using as stability measure: (a) “Rb Tlo-SST” and (b) “Rb Thi-SST”.	109
Figure V.27. Schematic of the SIBL profile ($\delta_\theta(x)$) created when warm air is advected over colder sea ($\theta_s < \theta$).	110

List of Tables

Table I.1. Wind data sources that were available for this research	17
Table I.2. Stability classes in terms of the Obukhov length scale (L)	24
Table I.3. Values of roughness length for common landscape [70].....	25
Table I.4 Wind power classes definition as function of the wind speed and the Wind power density at 10m, 30m and 50m height.	27
Table II.1. Geographical coordinates of the meteorological observatories.....	36
Table II.2. Details of the meteorological parameters measured at each site.....	36
Table II.3. Available data for each measurement site where the darker shaded boxes represent the years with measured data.	37
Table II.4. Monthly averages of wind speed and wind direction measured at 10m a.g.l. during the study period for each site.	40
Table II.5. Percentage of wind between North (N) and South-East (SE) sectors for each site.	43
Table II.6. Shape (K) and scale (C) parameters for the fitted Weibull distributions and the estimated power densities at the three study sites.	45
Table III.1. Locations, elevations and WMO codes of the nine study sites N.B. GM=Gulf of México coast, CS=Caribbean Sea coast.	49
Table III.2. Main characteristics of the parameters recorded.	51
Table III.3. Data availability for all sites studied. The shaded boxes represents the periods with available data.....	52
Table III.4. Information concerning the NOAA marine stations used to evaluate the atmosphere stability [73].	62
Table IV.1. Parameters for the geographical location of the measurement tower.....	69
Table IV.2. Technical specifications of the sensors installed on the measurement tower.	70
Table V.1 (a) Location of the "Progreso" pier in relation to the Yucatán Peninsula, (b) location relative to the North shore, (c) One kilometre radius and (d) 250m radius around measurement tower.	85
Table V.2 Different terrestrial views of the measurement tower showing the location of the tower on the pier and the position of the sensors on the tower.	86
Table V.3 Panoramic views of surrounding areas taken at 25m height above the pier surface.	86
Table V.4. Measurement parameters.....	87
Table V.5. Summary of the main sensor characteristics.....	87
Table V.6 (a) Locations of API and API2 towers. (b) A view of API2 from API tower. Sensors position on API (c) and API2 (d) masts.....	88
Table V.7 Distance from the mast to the edge of the pier (fetch) at (a) API and at (b) API2 for each directional sector.....	89

Table V.8 (a) Gulf of México and (b) "Progreso" pier areas with an example of an SST temperature map for each region (c) and (d).	97
Table V.9. Percentages of remaining data after the filters were applied for each stability measure.	103
Table VIII.1. Temporal data researches.	123
Table VIII.2. Spatial data researches.	127
Table VIII.3. Vertical wind profile researches.	132
Table VIII.4. Example of hourly Satellite SST images of the Gulf of México region selected from four days with the higher amount of images available. The temperature-colour scale is the same introduced in Table V.8 (c) and (d). N/A stands for "Not Available" in the following tables.....	141
Table VIII.5. Continuation of Table VIII.4	142
Table VIII.6. Continuation of Table VIII.5	143

Glossary and Acronyms

Symbol Definition/Meaning

α	Wind shear exponent of the power law
a.g.l.	Above the ground level
a.m.s.l.	Above the mean sea level
ABL	Atmospheric Boundary Layer
AirT	Air Temperature
API	Administración Portuaria Integral
C	Scale parameter of the Weibull probability density function
CAM	Automatic meteorological station located at Campeche city
CAN	Automatic meteorological station located at Cancún city
CBL	Convective Boundary Layer
CEL	Automatic meteorological station located at Celestún town
CHE	Automatic meteorological station located at Chetumal city
CMN	Automatic meteorological station located at Ciudad del Carmen city
C_p	Specific heat of air at constant pressure
CS	Caribbean Sea coast
E	East
EG	Eastern of the Gulf of México
ENE	East-North-East
ESE	East-South-East
f(u)	Weibull probability density function
g	Gravity acceleration
γ	Empirical parameter in the stability function
GEOS	Geostationary Operational Environmental Satellites
GM	Gulf of México coast
GWEC	Global Wind Energy Council
hi	A sub-index indicating that a magnitude is referenced to the lower measurement height
IBL	Internal Boundary Layer
ITCZ	Intertropical Convergence Zone
k	von Karman constant
K	Shape parameter of the Weibull probability density function
L	Obukhov length
lo	A sub-index indicating that a magnitude is referenced to the higher measurement height
LoF	Level of Filter
MCP	Measure-Correlate-Predict
MDA	Automatic meteorological station located at Mérida city
N	North

NE	North-East
NNE	North-North-East
NNW	North-North-West
NOAA	National Oceanic and Atmospheric Administration
NW	North-West
PDF	Probability density function
PO.DAAC	Physical Oceanography. Distributed Active Archive Center
P_w	Wind power density
R	Richardson number
R_b	Bulk Richardson number
Rb Thi-SST	Bulk Richardson number computed with the temperature measured at “hi” height and SST
Rb Thi-Tlo	Bulk Richardson number computed with temperatures measured at “hi” and “lo” heights
Rb Tlo-SST	Bulk Richardson number computed with the temperature measured at “lo” height and SST
R_i	Gradient Richardson number
RIO	Automatic meteorological station located at Rio Lagartos town
S	South
SBL	Surface Boundary Layer
SD	Standard Deviation
SE	South-East
SIBL	Stable Internal Boundary Layer
SKN	Automatic meteorological station located at Sian Ka An town
SSE	South-South-East
SST	Sea Surface Temperature
SSW	South-South-West
SW	South-West
T	Temperature
TAN	Automatic meteorological station located at Tantakin town
T_v	Virtual temperatures
u	Wind speed
u*	Friction velocity
W	West
WaterT	Sea temperature
WCL	Wind Coming from over Land
WCS	Wind Coming from over Sea
WECS	Wind Energy Conversion System
WMO	World Meteorological Organization
WNW	West- North-West
WS	Wind speed
WSW	West- South-West
YB	Yucatán Basin
z, z_r, z'	Measurement height

- z_0 Roughness length
- θ Potential temperature
- ρ Air density
- Ψ_m Stability function
- Δm Increment of a generic magnitude "m"
- \bar{m} Average of a generic magnitude "m"
- Γ Incomplete Gamma function
- $\delta_\theta(\mathbf{x})$ Height of the SIBL at a fetch of x

I General Introduction

This chapter presents the foundation for the subjects studied during this PhD research project. The main sources of data are defined in order to evaluate the temporal, horizontal and vertical wind resource in the Yucatán Peninsula, México. A general literature review is introduced to present previous work published which relates to the research during this PhD. Then, the theoretical models that support the research are introduced as well as a general description of the Yucatán Peninsula and the Gulf of México. Finally an outline of the PhD thesis is presented.

I.1 Research context

Wind power is seen as one of the most effective means available to combat the twin crises of global climate change and energy security, providing a possible solution to the problems associated with volatility in the fossil fuel markets for coal, gas and oil. The “Global Wind Energy Council” (GWEC) in their report “Global Wind Report 2006” [1] presented the state of development in each geographical region for the period 2000 to 2006 for leading countries in wind energy. According to this report, the annual market for wind energy grew at a rate of 32% in 2006, with over 15GW of new capacity installed worldwide. The market continued to broaden with installations in over 70 countries, establishing wind power as the leading renewable energy technology. Globally, the value of new generating plant installed in 2006 reached US\$24 billion with Europe was the world leader, with 65% of the global market. Recently, the GWEC reported a global wind power industry of 120.8 GW at the end of 2008 [2], mainly driven by the growth in the USA up to 25.2GW and the Chinese market which doubled its installed capacity reaching 12.2GW.

The capacity installed in Latin America and the Caribbean during 2006 was 296MW, increasing the total installed capacity to 508MW. México is one of the most promising regions for wind energy development being in the list of countries that more than doubled its installed capacity to 87MW, mainly located in the Isthmus of Tehuantepec in the State of Oaxaca. Due to the availability of sparsely populated and flat open terrain, the Yucatán Peninsula located in eastern México is a promising region from the perspective of wind energy development but no comprehensive assessment of wind resource has been previously published.

A basic requirement when developing wind power projects is to study the main characteristic parameters of wind in relation to its geographical and temporal distribution. The predicted energy yield for a Wind Energy Conversion System (WECS) is highly dependent on the measurement precision of the wind speeds used to compute the wind energy potential. In order to assess the wind power potential for a wide area, it may not be feasible to install a large number of masts with measurements made at typical wind turbine hub heights (presently 80m - 120m). Therefore, wind speed data from existing meteorological stations are often used for this purpose with an additional test tower, measuring at several heights, which helps to compute the wind shear and estimate the wind speed at the turbine hub height.

The research during this PhD has been concerned with a comprehensive assessment of the wind behaviour over the Yucatán Peninsula region using long-term data measured from three sites, short-term data from nine sites, detailed vertical profile data from one inland site

and data from a tower installed on a pier in order to study offshore wind patterns. Table I.1 below shows the data available for each measurement period.

Table I.1. Wind data sources that were available for this research

Data sources		Available averages	Measurement period	Stations
Local Meteorological centres	Observatories	Daily	1986 - 2005	3
	Automatic Stations	10 minutes	2000 - 2007	9
Inland tower to study wind vertical profile		10 minutes	2003 - 2005	1
Offshore measurement tower		10 minutes	2007 - 2009	1

The data described in Table I.1 can be classified in three research dimensions to assess the temporal, horizontal and vertical wind resources in the Yucatán Peninsula on and offshore. More specific information about these data sources is given below:

- a) Local meteorological centres provide data from three observatories and nine automatic stations, installed around the Yucatán Peninsula:
 - a.1) Observatories monitor sensors every 15 minutes and have recorded daily averages since 1986, in the best-case, and since 1997, in the worst-case. Thus, the diurnal behaviour is not represented and just seasonal and yearly patterns could be studied using these data to describe the long-term temporal behaviour of the wind resources in the Yucatán Peninsula.
 - a.2) Automatic Stations distributed across the whole Yucatán Peninsula measure data every 2 seconds to record 10 minutes averages since 2000, in the best-case, and since 2004, in the worse-case. This geographically distributed short-term data is later used to describe the spatial behaviour of the wind resources over the most relevant areas of the Yucatán Peninsula with regard to wind power.
- b) An inland wind measurement tower, which was the first measurement system installed in Yucatán Peninsula to specifically study the wind resources, with two mechanical polar anemometers (installed at 10m and 30m above ground level (a.g.l.)), a temperature sensor and an atmospheric pressure sensor. The data measured on this tower were used to evaluate the behaviour of the vertical wind profile.
- c) An offshore measurement station installed on a pier 6.65km from the North shore of the Yucatán Peninsula. Two ultrasonic orthogonal anemometers and two temperature sensors were configured at two different heights to monitor offshore winds.

I.2 Literature review

An initial detailed review of the scientific literature was undertaken to identify the appropriate research direction for this PhD, and this has been included in Appendix VIII.1 .

In this section, the review is concerned with previous studies of measurement sites with similar characteristics to the Yucatán Peninsula, in particular, sites where the wind resource has not been extensively studied, but where raw data were collected at intervals between 10 minutes and a day. This included measurements on towers at more than one height, and regions close to coastal zones. The review was classified according to the three main research dimensions defined in the previous section:

Long term temporal research

A basic requirement when developing wind power projects is to study the geographical distribution of wind and its main characteristics. Herbert et al [3] presented in 2007 a general review of wind energy technologies briefly describing the main results published in the scientific literature, covering more than 20 research projects undertaken around the world. The review revealed the critical role of the wind resource assessment over the temporal and spatial scales in the determination of the wind energy potential. Average wind speed and temporal wind patterns have been identified using short-term measurements, such as in the study by Essa and Embaby [4] to describe the winds of a site close to the Egyptian Mediterranean coast over one year. Similarly, Li and Li [5] analyzed data over five years to determine the annual, seasonal and diurnal wind characteristics for the Waterloo region in Canada.

Long-term studies for periods of at least 10 years have been reported using wind data measured at meteorological stations on islands and in coastal areas. Farrugia and Scerri [6], collated wind data over 24 years at a height of 11m above the ground level (a.g.l.) from Luqa International Airport in the Maltese Archipelago to analyze wind parameters and to identify diurnal trends. Shata and Hanitsch, [7,8] presented two complementary studies, where the wind power potential of two different Egyptian coastal regions was analyzed in terms of their wind characteristics over 10 years at a height of 10m a.g.l. using monthly averaged measurements for a total of 17 coastal meteorological stations.

Another Mediterranean coastal study, in the eastern region of Turkey, was undertaken by Sahin et al [9] with the explicit purpose of “quantifying the wind energy potential of and identify locations with better wind resources”. Seven meteorological stations were chosen in this study at sites situated between 4m and 100m above mean sea level (a.m.s.l.) with hourly measurements over 10 years (1992-2001). The Weibull parameters were computed for all

sites using the last five years of the study period. A diurnal pattern was identified with the lowest wind speeds around 7:00 in the morning local time and the highest wind speeds during the afternoon. The monthly mean wind speeds showed a seasonal pattern with the highest wind speeds in July and August and the lowest in November and December, in almost all of the stations that were studied.

Long-term studies for peninsular regions have been also undertaken. For a site located on the west coast of Saudi Arabia, Rehman [10], studied the annual, seasonal and diurnal patterns of the wind speed over 14 years in order to make wind energy yield calculations using wind turbines of different capacities. Because of the relatively low wind speeds identified, the author found better capacity factors for smaller wind turbines. Later, Rehman and Ahmad [11], extended their study to five meteorological stations located at coastal sites around Saudi Arabia. In this study, long-term hourly mean wind speeds were estimated at three different heights by means of the power law and the authors presented the hourly mean wind speeds during an average day and the monthly mean wind speeds during an average year at four different heights for each site.

In tropical regions, Tchinda and Kaptoum [12] reported in 2003 a study of the wind energy distributions for two Cameroon provinces using ten years of meteorological data. The authors found that the annual mean wind speeds for the windiest site exceeded 2m/s for over 53% of the time and that the wind resource could be useful for applications such as small distributed water pumping systems. Further studies to reinforce the results presented were proposed.

Many of the studies mentioned above used a Weibull probability distribution function (PDF) to represent the statistical behaviour of the wind. Nevertheless, other distributions have been used for this purpose. Akpinar and Akpinar initially used the Weibull PDF to characterize the wind energy potential in Turkey [13] but later, in 2007, extended the study reporting better results using the Maximum Entropy Principle (MEP) when assessing the wind energy potential for the range of study sites [14]. More recently, in 2008, Vicente [15], published the results of a comprehensive study undertaken in the Canary Islands, which showed that the use of probability distribution functions more complex than the Weibull distribution to fit wind speed experimental data did not give a significant improvement in the prediction of annual mean energy yield, particularly in cases where the probability of null wind speed was close to zero. The results described in this subsection have shown that the study of long-term wind patterns over periods of time of 10 years or more can be undertaken using daily averages in environments similar to islands and peninsulas.

Spatial wind research

Wind energy potential for five coastal regions of the Kingdom of Saudi Arabia was evaluated by Rehman and Ahmad in 2004 covering a period between 1970 and 1983 [16] using hourly mean values of wind speed and wind direction, thus the turbulence intensity were not studied. The authors analysed seasonal and diurnal changes in wind speed values and identified Yanbo site as the best location for exploiting in terms of wind power. This site was later studied in detail by Rehman [17]. To the North-West of Saudi Arabia, in the State of Kuwait, Al-Nassar et al. in 2005 [18] presented a study with hourly averaged wind speeds from six meteorological stations made at 10m a.g.l. over a four year period (January 1998 - December 2002). Monthly averages for the wind power density at 10m a.g.l. and their extrapolation to 30m a.g.l. were tabulated for each study station by means of the power law. The authors highlighted that the summer season showed higher potential wind power coinciding with the period of highest electricity demand during the year.

An assessment of wind energy in Egypt was carried out by Essa and Mubarak in 2006 [19]. Data were collected from 18 meteorological stations around Egypt measuring at 10m a.g.l. and recording averages every 15 minutes over a five years period (April 2000 to December 2004). The hourly, daily, monthly and yearly behaviour of the wind speeds were computed. The authors concluded that the Red Sea, Mediterranean (El-Arish) and some inland zones (Aswan and Ismailia) would be favourable locations for wind energy applications and that the Red Sea winds were strongest in the summer while in the Mediterranean coastal zones, winds were strongest in winter and spring seasons.

The eastern Mediterranean region of Turkey was studied by Sahin et al. in 2005 [20] using hourly data from seven meteorological stations which were measured between 1992 and 2001. The authors computed the wind energy at 10m and 25m a.g.l. using a linear wind flow model (WAsP) developed by Troen et al. [21]. Three areas with wind energy potential up to $500\text{W}/\text{m}^2$ were identified. Also in Turkey, Akpınar et al. in 2005 [22] studied different regions using hourly averages of wind data between 1998 and 2003 reporting the seasonal patterns and the energy available in the wind. The same authors in 2009 [23] focused their research on the probability density distribution of wind for 4 weather stations over 8 years proposing a mixture of distributions to represent the wind patterns for the area studied.

For the Indian region of Karnataka, Ramachandra et al. in 2005 [24] studied the wind resource using a geographical information system. The authors studied the spatial and seasonal patterns reporting wind speed averages between 0.9m/s and 9.2m/s with the higher seasonal values registered between May and September.

In the case of México, Jaramillo et al [25] in 2004 undertook a study of the wind potential along the coast line of "Baja California Sur" in the North-West of México. Measurement masts at 15 sites were installed with instruments at 10m a.g.l. and a year of data was

collected (February 1997 to February 1998) by the Electrical Research Institute. After a preliminary evaluation of all 15 sites, the authors chose one site to study the monthly wind speed behaviour, calculating the wind rose and the frequency distribution. Also, Cancino-Solórzano and Xiberta-Bernat [26] in 2009, studied the diurnal and seasonal patterns of wind speed in the eastern Mexican state of Veracruz using 5 meteorological stations, during 2001 - 2006. The authors reported maximum seasonal wind in winter and minimum over the summer in the majority of the studied sites. A clear diurnal pattern was also reported conditioned by the geographical distribution of the studied sites along or close to the coastal regions.

Onshore and offshore vertical wind profile research

In the case of offshore conditions, Van Wijk et al. [27] obtained good estimates for the seasonal mean wind speed in the North Sea after applying a “diabatic” approach to calculate the wind speed profile as a function of height when wind speed, sea water temperature and air temperature are known and when neutral conditions are not dominant in the atmosphere. This diabatic method was also used by Coelingh et al. to study offshore [28] and onshore sites [29]. These two studies of the North Sea and its coastal areas concluded that diurnal variations are very similar in autumn and winter and that the thermal circulation leads to sea breezes with important effects up to 30km offshore for wind speeds lower than 7m/s.

For the marine environment of the Danish Baltic Sea, Lange et al. [30] studied the influence of thermal effects on wind speed profiles computing the Obukhov length using three different methods. Their results showed that the standard Monin-Obukhov theory predicted lower wind speed values than measured for stable and near-neutral conditions, especially at large distances from the shore.

Using wind speed and air temperature data measured from one onshore site and two offshore towers, Pryor and Barthelmie [31] applied parameterization methods to compute the Monin-Obukhov length in a study of wind speed, stability and surface roughness. They reported that wind speed distributions onshore and offshore were statistically different for heights less than 20m regardless of the atmosphere stability conditions, at distances less than 2km from the shore. In an extended study using data from the Danish monitoring network [32], the same authors concluded that sites located within 2km from the coastline could experience significant vertical shear and differing turbulence because the wind speeds close to the sea surface were frequently decoupled from the wind characteristics above 30m in height.

Lapworth [33] reported diurnal patterns with maximum winds overnight and minimum values occurring during the afternoon for the offshore surface winds around the English coast after applying numerical models for stable boundary layers to offshore measurements made in static vessels. On the other hand, Barthelmie et al. [34] studying the coastal meteorology of Denmark found that the offshore sites which receive winds from over the land showed a typical onshore pattern with lowest wind speeds overnight and highest wind speeds during the afternoon. The offshore wind speed generally presents the opposite pattern increasing overnight as a result of the lower roughness of the sea surface and the transition from stable conditions over land to less stable conditions over sea. While during the daylight time, the transition from unstable conditions over land to stable conditions offshore conditions that the surface layer becomes decoupled from higher wind speeds aloft and the wind speed close to the surface layer is lower, as was reported by Barthelmie et al. [35].

In cases where not enough data were available to apply the Monin-Obukhov similarity theory (this theory will be introduced in subsection 1.3 below), the use of the power law to compute the wind shear exponent has been used as an alternative to predict the vertical profile. Farrugia [36] studied the wind shear from measurements at two different heights on Malta's South West coast, in the central Mediterranean, reporting that the monthly values decrease in summer and increase in winter and that the daily pattern has a period of a minimum from 9:00 to 15:00 and a period of a maximum from 21:00 to 5:00. Similar diurnal patterns were found by Rehmana and Al-Abbadib over a period of 3 years [37] and 5 years [38] for a site in the coast of the Gulf region of Saudi Arabia. In this case, no regular seasonal trends were identified.

Kirchhoff and Kaminsky [39] remarked that basic errors could be introduced because of the random nature of the wind speed and the deterministic characteristic of the power law when computing the wind shear from measured wind speeds at two different heights. Kirchhoff and Kaminsky made 173 wind speed measurements to study the wind shear, in a statistically significant way. Their data analysis indicated a normal distribution for the wind shear in three of the synoptic weather categories: I (in a warm section), III (behind a cold front) and IV (under a continental polar or arctic high).

The review presented in this subsection has shown that there has been important research undertaken to study wind resource in regions with similar characteristics to the Yucatán Peninsula. Nevertheless, more research needs to be done and the following conclusions were identified:

- The three research dimensions (temporal, spatial and vertical) are relevant and timely.
- The wind data available for the Yucatán Peninsula, see Table I.1, are sufficient to undertake studies of the wind characteristics for each of the three research dimensions.
- The wind resource in the Yucatán Peninsula region has not been previously investigated.

I.3 Wind speed profiles

A widely accepted procedure to compute the theoretical wind speed profile is described by the Monin-Obukhov similarity theory, as can be seen below in equation (I.1):

$$u(z) = \frac{u_*}{k} \left[\ln \left(\frac{z}{z_0} \right) - \Psi_m \left(\frac{z}{L} \right) \right] \quad \text{I.1}$$

In the equation (I.1), k is the von Karman constant and the wind speed u at height z is represented as a function of the friction velocity u_* , roughness length z_0 and Obukhov length L . $\Psi_m(z/L)$ is the stability function which can be calculated with the equation (I.2), formulated by Businger [68]. In this equation the “ γ ” was evaluated by Högström [69] as 19.3.

$$\Psi_m = 2 \ln \left(\frac{1 + \Phi_m^2}{2} \right) - 2 \tan^{-1}(\Phi_m) + \frac{\pi}{2} \quad \text{where } \Phi_m = \left(1 - \gamma \frac{z}{L} \right)^{1/4} \quad \text{I.2}$$

An important magnitude to evaluate the behaviour of the wind is the stability conditions of the atmosphere. The atmosphere stability can be quantified by means of the Obukhov length L , Monin and Obukhov [76]. This parameter gives information about the relative magnitudes of vertical air movements produced by mechanically generated vertical turbulence as opposed to thermally generated vertical turbulence. Mechanically generated turbulence is the result of the surface roughness and thermally generated turbulence arises as a consequence of the air density gradients created when the temperature of the air and the sea surface are different. The atmospheric stability can be allocated to one of five stability classes [74], as given in Table I.2.

Table I.2. Stability classes in terms of the Obukhov length scale (L).

Stability class	Obukhov Length L [m]	z/L for 10m height
Very stable	$0 < L < 200$	$0.05 < z/L$
Stable	$200 < L < 1000$	$0.01 < z/L < 0.05$
Near-neutral	$ L > 1000$	$ z/L > 0,01$
Unstable	$-1000 < L < -200$	$-0.05 < z/L < -0.01$
Very unstable	$-200 < L < 0$	$z/L < -0.05$

A relation to compute the Obukhov length L was proposed by Businger [68] and Högström [69] in terms of the Richardson number R at z' height, see equation (I.3) below.

$$L = \begin{cases} \left(\frac{z'}{R}\right) & R < 0 \\ \frac{z'(1-5R)}{R} & 0 < R < 0.2 \end{cases} \quad \text{where } z' = \frac{z_{Lo} - z_{Hi}}{\ln\left(\frac{z_{Lo}}{z_{Hi}}\right)} \quad \text{I.3}$$

Equation (I.4) and (I.5) presents expressions to compute the Gradient and Bulk Richardson number respectively, from ambient temperatures and wind speeds measured at two different heights (z_{lo} and z_{hi}) [74, 75, 30]. These expressions are valid at the height z' defined in equation (I.3) which was proposed by Larsen [77]. Equation (I.4) is used when measurement of wind speed and temperature are available at both different heights. In this case, the differences in height, virtual temperature and wind speed are represented by Δz , ΔT_v and Δu while C_p and g are the specific heat of air at constant pressure and the gravity acceleration respectively.

$$R_i(z') = \frac{\frac{g}{T} \left(\frac{\Delta \bar{T}_v}{\Delta z} + \frac{g}{C_p} \right)}{\left(\frac{\Delta \bar{u}}{\Delta z} \right)^2} \quad \text{I.4}$$

$$R_b(z') = \frac{\frac{g}{T} \left(\frac{\Delta \theta}{\Delta z} \right) \bar{z}^2}{\bar{u}^2} \quad \text{I.5}$$

Equation (I.5) is used when just wind speed at high height is available. In this equation, $\Delta \theta_v$ is the difference between the virtual potential temperature at the two measurement heights.

Then, the theoretical wind speed ratio between high and low heights can be calculated by the relation shown below in the equation (I.6).

$$\frac{u(z_{hi})}{u(z_{lo})} = \frac{\ln\left(\frac{z_{hi}}{z_0}\right) - \Psi_m\left(\frac{z_{hi}}{L}\right)}{\ln\left(\frac{z_{lo}}{z_0}\right) - \Psi_m\left(\frac{z_{lo}}{L}\right)} \quad \text{I.6}$$

Table I.3 below presents the relation between roughness length and the terrain characteristics for common conditions used by Troen and Petersen for developing the European Wind Atlas [70].

Table I.3. Values of roughness length for common landscape [70].

Roughness Length [m]	Landscape Type
0.0002	Water surface.
0.0024	Completely open terrain with a smooth surface, e.g. concrete runways in airports, mowed grass, etc.
0.03	Open agricultural area without fences and hedgerows and very scattered buildings. Only softly rounded hills.
0.055	Agricultural land with some houses and 8m tall sheltering hedgerows with a distance of approx. 1250m
0.1	Agricultural land with some houses and 8m tall sheltering hedgerows with a distance of approximately 500m.
0.2	Agricultural land with many houses, shrubs and plants, or 8m tall sheltering hedgerows with a distance of approx. 250m.
0.4	Villages, small towns, agricultural land with many or tall sheltering hedgerows, forests and very rough and uneven terrain.
0.8	Larger cities with tall buildings.
1.6	Very large cities with tall buildings and skyscrapers.

In conditions close to neutral states of the atmosphere, the wind speed profile proposed by the Monin-Obukhov similarity theory, see equation (I.1), can be simplify to the Log law. Alternately to this adiabatic log law, the empirical power law, equation (I.7) below, simplify even more the estimation of the vertical wind profile.

$$u(z) = u(z_r) \left(\frac{z}{z_r} \right)^\alpha \quad \text{I.7}$$

where “ α ” represents the wind shear exponent which can be calculated, see equation (I.8), when the wind speed values at two different heights, $u(z)$ and $u(z_r)$, are available:

$$\alpha = \frac{\text{Log} \left(\frac{u(z)}{u(z_r)} \right)}{\text{Log} \left(\frac{z}{z_r} \right)} \quad \text{I.8}$$

I.4 The Weibull probability Distribution

An important statistical tool to estimate the frequency distribution of wind speed u is the Weibull function defined as a two parameter Probability Distribution Function (PDF) using the following equation (I.9) [51]:

$$f(u) = \left(\frac{K}{C}\right) \left(\frac{u}{C}\right)^{K-1} \exp\left[-\left(\frac{u}{C}\right)^K\right] \quad \text{I.9}$$

Equation (I.9) depends on the wind speed u and on two other parameters namely shape (K) and scale (C) which succinctly represent the characteristics of the wind speed distribution at a particular site. These two parameters can be found from a time series of wind speed using conventional graphical methods [52]. A better approach can be obtained using the Maximum Likelihood Estimator Method [53,54] by mean of equation (I.10) and equation (I.11):

$$K = \left(\frac{\sum_{i=1}^n u_i^K \ln(u_i)}{\sum_{i=1}^n u_i^K} - \frac{\sum_{i=1}^n \ln(u_i)}{n} \right)^{-1} \quad \text{I.10}$$

$$C = \left(\frac{\sum_{i=1}^n \ln(u_i^K)}{n} \right)^{\frac{1}{K}} \quad \text{I.11}$$

Where K is the dimensionless shape parameter and C is the scale parameter with dimensions of m/s^2 . The K parameter can be computed iteratively by means of numerical methods from a filtered dataset of n wind speed observations with u_i greater than zero. Then, C parameter can be directly evaluated from equation I.11.

The wind power density P_w can be estimated from the Weibull parameters using equation (I.12) [52]:

$$P_W = \frac{1}{2} \rho C^3 \Gamma(1 + 3/K) \quad \text{I.12}$$

Where " ρ " is the air density and " Γ " is the incomplete Gamma function defined by the equation (I.13) below, which can also be evaluated numerically.

$$\Gamma(1 + 3/K) = \int_0^{\infty} t^{3/K} e^{-t} dt \quad 1.13$$

The mean wind speed, its standard deviation and the most frequently wind speed value can also be expressed as function of the Weibull parameters [55,56] through equations (1.14), (1.15) and (1.16) respectively:

$$\bar{u}_m = C \Gamma\left(1 + \frac{1}{K}\right) \quad 1.14$$

$$\sigma = \sqrt{C^2 \Gamma\left(1 + \frac{2}{K}\right) - \Gamma^2\left(1 + \frac{1}{K}\right)} \quad 1.15$$

$$u_{\text{mod}} = C \left(1 - \frac{1}{K}\right)^{1/K} \quad 1.16$$

A widely used way to classify the wind power density is through the to use wind power classes. Table 1.4 below presents the wind power classes definition as function of the wind speed and the Wind power density [58]. In this classification, the equivalent mean wind power density was used with the Rayleigh Probability Distribution to compute the mean wind speeds. Wind speeds are considered at mean sea level conditions. Vertical extrapolation of wind speed to 30m and 50m height were calculated from the 1/7 power law. This is a general approximation to initially classify the type of wind available at a particular site.

Table 1.4 Wind power classes definition as function of the wind speed and the Wind power density at 10m, 30m and 50m height.

Height	10m		30m		50m	
	Wind power density [W/m ²]	Wind speed [m/s]	Wind power density [W/m ²]	Wind speed [m/s]	Wind power density [W/m ²]	Wind speed m/s
1	0 - 100	0 - 4.4	0 - 160	0 - 5.1	0 - 200	0 - 5.6
2	100 - 150	4.4 - 5.1	160 - 240	5.1 - 5.9	200 - 300	5.6 - 6.4
3	150 - 200	5.1 - 5.6	240 - 320	5.9 - 6.5	300 - 400	6.4 - 7.0
4	200 - 250	5.6 - 6.0	320 - 400	6.5 - 7.0	400 - 500	7.0 - 7.5
5	250 - 300	6.0 - 6.4	400 - 480	7.0 - 7.4	500 - 600	7.5 - 8.0
6	300 - 400	6.4 - 7.0	480 - 640	7.4 - 8.2	600 - 800	8.0 - 8.8
7	400 - 1000	7.0 - 9.4	640 - 1600	8.2 - 11.0	800 - 2000	8.8 - 11.9

I.5 Satellite SST images

The sea surface temperature (SST) is defined as the water temperature close to its surface. Significant differences can be found between measurements made at different depths, especially during the daytime when low wind speed and high sunshine conditions may lead to the formation of a warm layer at the ocean's surface and strong vertical temperature gradients (a diurnal thermocline). There are three layers to the ocean: the first is the surface layer; below this lie the already mentioned thermocline; and immediately below is the deep ocean which comprise the 75% of the ocean depth.

In practical terms, the exact meaning of the SST is conditioned by the method used to register the measurements:

- A satellite using an infrared radiometer: measures indirectly the temperature within a layer of approximately 10 μ m of depth of the sea (skin temperature) where the infrared radiation takes place [59, 60].
- A microwave sensor monitors the sub-skin temperature located around 1mm depth.
- An underwater thermometer installed below a marine buoy usually measures the temperature at 1m below the sea surface. This temperature is identified during the day with the temperature of the above mentioned warm layer.

Satellites have the advantage to monitor the spatial and temporal variation of the Sea Surface Temperature. Usually, the satellite monitor the radiation from the sea several wavelengths of the infrared spectrum which can then be empirically related to SST. These wavelengths are chosen because they are within the peak of the blackbody radiation expected from the earth, and able to transmit well through the atmosphere. However, there are several difficulties with satellite based absolute SST measurements [61, 62]:

- The infrared radiation monitored comes from the upper or "skin" layer of the sea (close to the top 0.01mm) which does not describe the bulk temperature of the upper meter of ocean due primarily to effects of solar surface heating in the daytime, reflected radiation, as well as sensible heat loss and surface evaporation.
- Satellites are unable to monitor through clouds, creating a "fair weather bias" in the long term trends of SST.

The NOAA's GOES (Geostationary Operational Environmental Satellites) are located in geostationary orbit above the Western Hemisphere. This characteristic enables hourly measurements.

GOES SST data are derived from imagers with five-band multispectral capability, 10 bit precision and high spatial resolution derived from GOES East and GOES West Satellites. This data is available in the form of one hour gridded sea surface temperatures with the following main characteristics:

- **Temporal resolution:** One hour, three hour, and 24 hour gridded sea surface temperatures.
- **Spatial resolution:** 6 km
- **Region grid:** Western Hemisphere bounded horizontally from 180°W to 30°W and vertically from 60°N to 45°S.

The GOES 6km hourly SST, generated by GOES 11-12, is available from the Physical Oceanography / Distributed Active Archive Centre (PO.DAAC) within a few hours of real time since May 2003 [63]. These data are in the form of flat binary files which include 2100 rows of 3000 unsigned one-byte binary integers that contain the SST values. This two dimensional matrix represents a rectangular grid of 3000 longitude coordinates by 2100 latitude coordinates aligned by longitudes from 179.975°W to 30.025°W and by latitudes from 59.975°N to 44.975°S with a spatial resolution of 0.05 degrees.

In this research, the Physical Oceanography/Distributed Active Archive Centre (PO.DAAC) software was used to decode the binary files and to generate temperature maps such as that shown in Figure I.1 below.

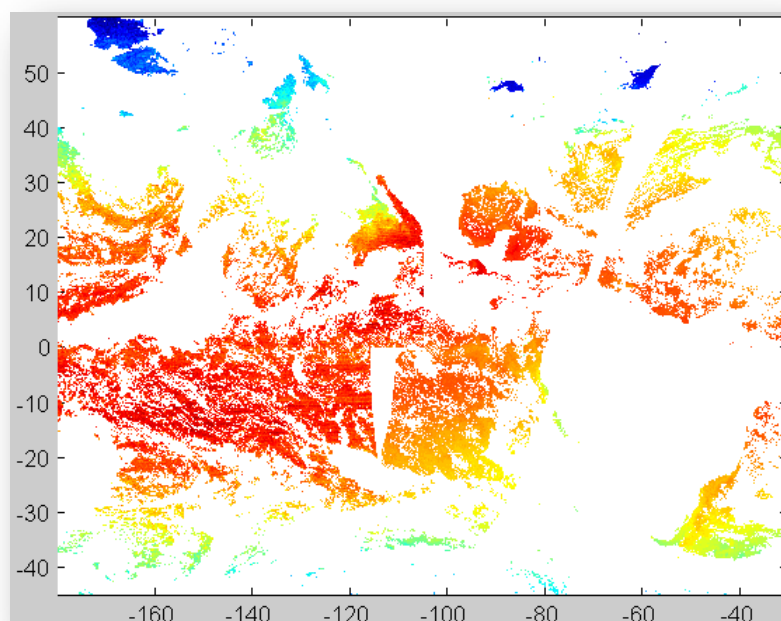


Figure I.1. Example of the original full thermal map produced hourly by the GEOS Satellite.

I.6 The Yucatán Peninsula and the Gulf of México

The geographical location of the Yucatán peninsula at the western of Mexico is show below in Figure I.2(a). It could be also appreciated from Figure I.2(b) that the topography of this region is mainly flat particularly in sites close to coastal zones.

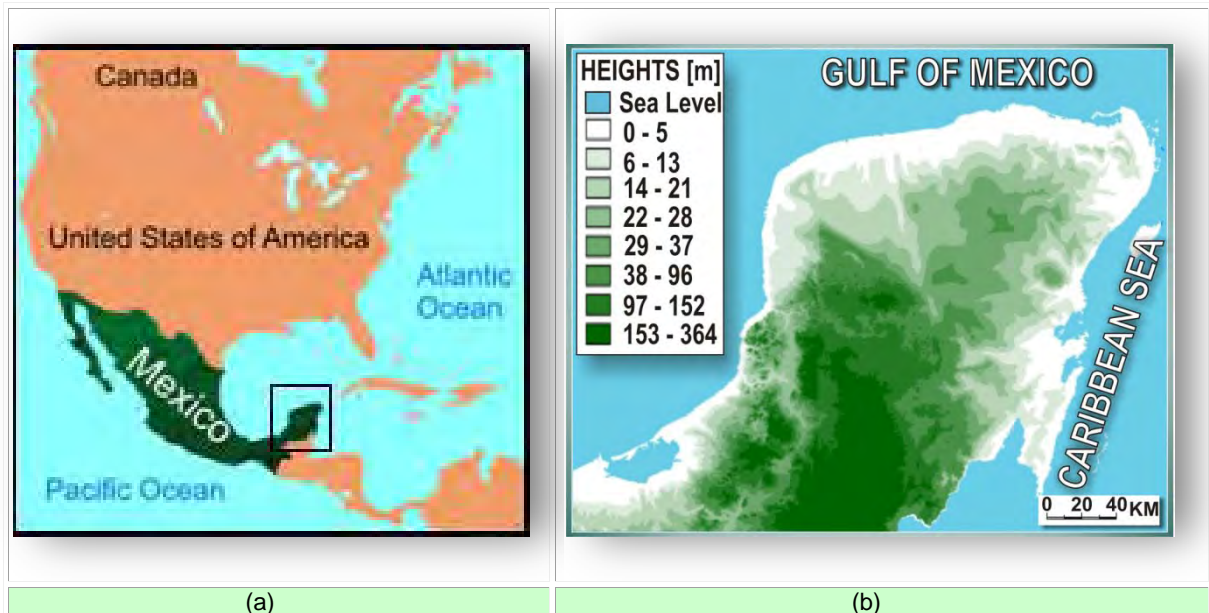


Figure I.2. (a) Geographical location of the Yucatán Peninsula in relation to the North American subcontinent. (b) Yucatán Peninsula map representing the terrain heights by means of shadow zones.

The North coast of the Yucatán Peninsula is located at the South-East of the Gulf of México close to the tropic of Cancer covering almost 400km of coast approximately parallel to the tropic line. Its sea depth is very shallow increasing around 1m every 1km in the majority of the regions while the onshore terrain is almost flat reaching just 7m above the sea mean level at 30km inland. The vegetation grows up to an average of 3m height. These particular characteristics make the North of the Yucatán Peninsula a strategic natural laboratory to study the ABL at coastal regions. Field measurements under these naturally controlled conditions can potentially simplify the validation of numerical models.

On the other hand, the Gulf of México covers a surface area of approximately 1.5 million km² [57]: ~1600km from East to West and ~900km from North to South. The average depth is ~1.61km and approximately [64]:

- 38% of shallow and intertidal areas (less than 20m deep).
- 22% of continental shelf (less than 180m)
- 20% of continental slope (between 180m and 3km)
- 20% of abyssal areas (deeper than 3km).



Figure I.3. A 3D representation of the Gulf of México region.

The Gulf of México is the 9th biggest body of water in the world. Often identified as part of the Atlantic Ocean, it is an ocean basin surrounded by the South Coast of the United States, the East Coast of Mexico and the North West of the island of Cuba, see Figure I.3. The reduced area of contact with the Atlantic produces small tidal regimes (shallow intertidal waters cover roughly half of the basin). The Gulf of México could be created ~300 million years ago driven by sinking processes developed in its seafloor [65].

Seven main regions area usually classified within the Gulf of México [66]:

- Gulf of México Basin: including the Sigsbee Deep and the Mississippi Cone.
- Northeast Gulf of México: from the East of the Mississippi Delta to the Eastern of Appalachian Bay.
- South Florida Continental Shelf and Slope: Along the coast, from Appalachian Bay to the Straits of Florida.
- Campeche Bank: from the Yucatán Straits in the East to the “Tabasco/Campeche Basin” in the west, covering all the North and West coast of the Yucatan Peninsula.
- Bay of Campeche (isthmian embayment): from the Western edge of Campeche Bank to the East of Veracruz’s Port.
- Western Gulf of México: from Veracruz to the “Rio Grande”.
- Northwest Gulf of México: from Alabama to the USA/México border.

The Gulf Stream is a strong warm ocean current originating in the Gulf of México as a result of the extension of the current system created from the “Caribbean Current” / “Yucatán Current” Loop. The warm temperature of the water in the Gulf of Mexico usually create conditions for the formation of highly intense Atlantic hurricanes [67].

I.7 Thesis outline

This thesis presents the results of the research organised into eight chapters. A general introduction section is presented to describe the foundation for this research as well as a general literature review covering the main findings published in the scientific literature which relate to this PhD, the theoretical foundations that support the research in this PhD thesis to evaluate the wind resource in the Yucatán Peninsula and a general description of the Yucatán Peninsula and the Gulf of Mexico considering the characteristics relevant for wind resource assessment.

Chapter II studies the wind patterns and their long-term behaviour by means of data measured at three meteorological stations for a period between 10 and 20 years. Monthly trends of ambient temperature, atmospheric pressure and wind speed data were identified and are discussed. The directional behaviour of the winds, their frequency distributions and the related Weibull parameters are presented.

Chapter III analyzes the spatial distribution of winds around the Yucatán Peninsula based on ten-minute averaged wind speed data from nine meteorological stations. Hourly and monthly patterns of the main environmental parameters are examined. The characteristics of the wind speed variation observed at the studied sites reflected their proximity to the coast and whether they were influenced by wind coming predominantly from over the land or predominantly from over the sea. The atmospheric stability over the eastern seas of the Yucatán Peninsula was also analysed to assess thermal effects for different wind directions.

Chapter IV studies the vertical wind profile for a site at the Autonomous University of Yucatán which experiences the tropical conditions of the Yucatán Peninsula in México. The wind shear is analyzed in terms of the directional, diurnal and seasonal patterns. A detailed look at frequency distributions has been undertaken to facilitate a comprehensive understanding of the local climatic conditions. Diurnal wind speed variations are shown to be affected in particular by the differing wind conditions associated with fetches over two distinct offshore regions. Seasonal behaviour suggests some departure from the oscillations expected from temperature variation.

Chapter V analyzes the properties of the offshore wind close to the North coast of the Yucatán Peninsula using a communication tower installed on a pier 6.65km from the coast. The results show that the offshore is wind thermally driven and sea breezes which veer to blow parallel to the coast in the late afternoon under the action of the Coriolis force. Mast measurements suggested largely unstable conditions, yet the observed shear was greater than that predicted using standard Monin-Obukhov theory. A dataset of sea surface

temperatures was also used to study stability and the results potentially suggested the development of a shallow Stable Internal Boundary Layer.

Finally, the main results and general conclusions from the research undertaken as well as the recommendations for further research are presented. The thesis concludes with a reference section listing the literature reviewed and an appendices section which presents additional information related with the work undertaken in relevant stages of the research.

II Long term temporal wind patterns

This chapter presents an analysis of the meteorological parameters relevant to an evaluation of the wind resource in order to identify patterns in their long-term behaviour and to establish a foundation for subsequent research into the wind power potential of the Yucatán Peninsula. Three meteorological stations with data measured for a period between 10 and 20 years were used in this study. The monthly trends of ambient temperature, atmospheric pressure and wind speed have been identified and their main features have discussed. The directional behaviour of the winds, their frequency distributions and the related Weibull parameters are presented. Wind power densities have been also estimated for the study sites showing a relatively low wind potential (Wind Power Class 1).

II.1 Introduction

The studies described in the reference review, section I.2 , have been undertaken mainly in the last ten years in different regions around the world close to coastal sites. The majority of these studies used wind data measured at meteorological stations at 10m a.g.l. over long-term periods to compute wind averages, identify trends over different time scales and to analyze the wind energy potential at the study sites. At the beginning of this research, no proper assessment of the wind resource in the Yucatán Peninsula of México had been published.

The first step in this work was to select three coastal sites following a survey conducted to locate available data recorded by the Observatories of the “Servicio Meteorológico Nacional de la Comisión Nacional del Agua” (National Meteorological Service). Secondly, a conventional procedure to validate the data measured over a period of between 10 and 20 years was applied for each study site. Then, the monthly and yearly behaviour of the main environmental parameters were studied. Finally, wind speed data were analysed to assess temporal patterns as well as the wind direction statistics, wind frequency distributions and estimated power densities.

The main purpose of this chapter is to present, for the first time, a preliminary analysis of the long-term behaviour of meteorological parameters relevant to the wind resource in the Yucatán Peninsula.

II.2 The measurements at the observation sites

II.2.1 Measurement sites

A detailed study was undertaken to select suitable meteorological measurement sites within the Yucatán Peninsula. Ideally, more than 30 years of data contribute to describe properly the variability of the long-term patterns. Nevertheless, following quality checks for completeness and reliability of the available meteorological data, three strategic locations around the Yucatán Peninsula were chosen where meteorological data had been collected over a period of between 10 and 20 years. As can be seen from Figure II.1, these sites, also known as observatories, are distributed around the Yucatán Peninsula close to the coast line that surrounds the West, North and East of the Peninsula. Each site was identified by the name of the city where it is located, namely: “Campeche”, “Mérida” and “Chetumal”.

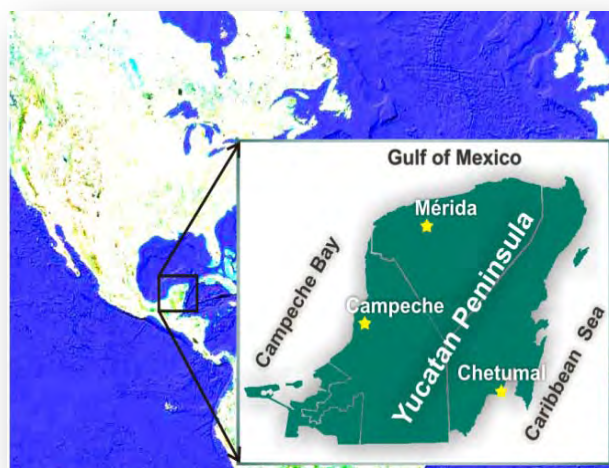


Figure II.1. Map of the Yucatán Peninsula area representing the geographical position of the meteorological observatories: Campeche, Mérida and Chetumal.

The geographical coordinates of the measurement sites and their heights a.m.s.l. are presented in Table II.1. This table also shows the distance between each observatory and its closest coast line. As shown in Figure II.1, these coasts are the Bay of Campeche, the Gulf of México and the Caribbean Sea for Campeche, Mérida and Chetumal, respectively.

Table II.1. Geographical coordinates of the meteorological observatories.

Station	Latitude	Longitude	Height a.m.s.l. [m]	Distance from the closest coast
Campeche	19° 50'N	90° 30'E	5	4.3km in West direction to Bay of Campeche
Mérida	20° 57'N	89° 39'E	11	38.4km in North direction to Gulf of México
Chetumal	18° 30'N	88° 19'E	9	2.1km in East direction to Caribbean Sea

The main meteorological parameters recorded for each observatory are listed in Table II.2. As can be seen from the Table II.2, the daily averages for wind data were computed from 96 values measured each 15 minutes. The other parameters were measured every hour and thus their daily averages were produced using 24 measured values.

Table II.2. Details of the meteorological parameters measured at each site.

Parameters	Height a.g.l. [m]	Units	Measurement's Frequency	Stored average data
Wind speed	10	m/s	15 minutes	Daily average, maximum and minimum.
Wind direction	10	Degrees	15 minutes	Daily preferential direction
Ambient temperature	1.5	°C	Hour	Daily average, maximum and minimum.
Atmospheric pressure	1.5	hPa	Hour	Daily average, maximum and minimum.

II.2.2 Study period and data validation

Ambient temperature, atmospheric pressure, wind speed and wind direction data were processed for the observatories described above. These long-term data consist of daily averages that cover 20 complete years for the Mérida observatory, 16 complete years for the Campeche observatory and 10 complete years for the Chetumal observatory within a period between 1986 and 2005, as shown Table II.3.

Table II.3. Available data for each measurement site where the darker shaded boxes represent the years with measured data.

Mexican state	Observatory	1986	1987	1988	1989	1990	1991	1992	1993	1994	1995	1996	1997	1998	1999	2000	2001	2002	2003	2004	2005
Yucatán	Mérida	■	■	■	■	■	■	■	■	■	■	■	■	■	■	■	■	■	■	■	■
Campeche	Campeche	■	■	■	■	■	■	■	■	■	■	■	■	■	■	■	■	■	■	■	■
Quintana Roo	Chetumal	■	■	■	■	■	■	■	■	■	■	■	■	■	■	■	■	■	■	■	■

Each of the meteorological observatories in the Yucatán Peninsula was scrutinised for their suitability in this study. This was done to discard the data that could be misleading due to local obstacles or poor instrumentation. Accordingly, the following data quality control measures were undertaken:

- All measured parameters with values outside the operational limits of their corresponding measurement sensors were excluded. Parameters with values below the sensor threshold were also eliminated and data values were rounded to the resolution appropriate to the sensor used.
- As the raw data represent daily averages from sites located in a tropical region, ambient temperatures below 0°C were discarded. Atmospheric pressure values were also screened for unrealistically high and low values.
- The directional values for each of the sites were homogenized as some sites reported direction in degrees and some using symbols representing compass points, e.g. N, NNE, NE, ENE, E, etc.
- A graphical browser tool was used to visually review the data and identify and filter out any remaining abnormal data points. In this case, just the data clearly outside of the physical range of each parameter was filtered in order to avoid to skew the data.

After applying this quality control stage, the percentage of remaining data compared with the full possible data in the measuring period shown in Table II.3 was 97.12% for Campeche, 96.84% for Mérida and 98.67% for Chetumal. Thus, each measurement site fulfilled the requirement of having at least 90% of the data available during the measurement period for subsequent analysis [42].

The daily average data recorded at each measurement site were used to compute the monthly and yearly averages for each of the measured parameters. In order to compare the measurements from the three study sites under the same conditions, only the common ten years between 1996 and 2005 were considered unless otherwise stated.

II.3 Main environmental parameters

Ambient temperature

Figure II.2 shows the ambient temperature (a) averaged monthly throughout the year and (b) averaged annually for the three study sites in the period 1996 to 2005. Figure II.2(a) seems to show two different temperature trends: one for Chetumal and the other for Mérida and Campeche. This difference is discussed below in relation to the directional characteristics of the winds. The three temperature patterns cover a range of 6°C from 23.5°C to 29.5°C with minimum values between December and January. The maximum temperature at Chetumal was reached between July and September while for Mérida and Campeche, the hottest month was May. Mérida had the lowest average temperatures among the study sites.

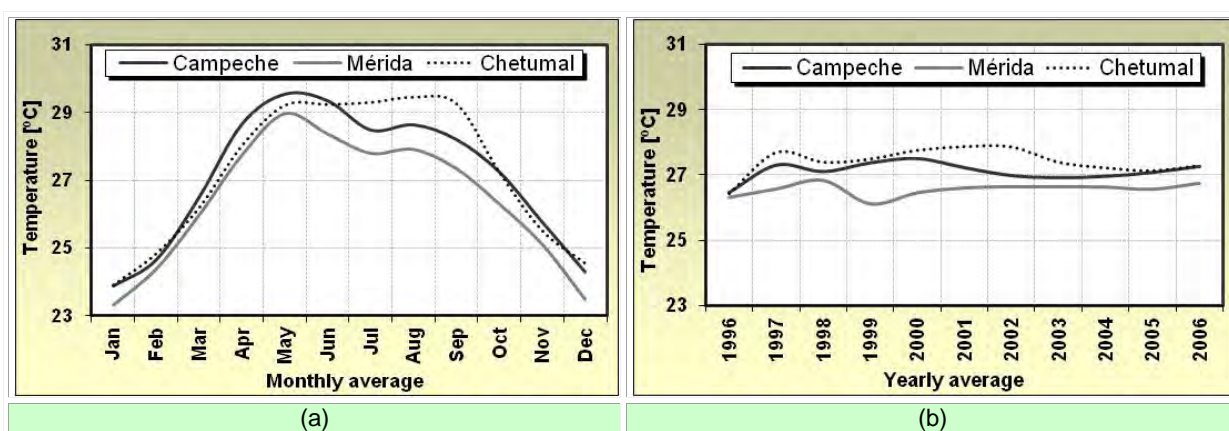


Figure II.2. Monthly (a) and yearly (b) averages of the ambient temperature for the three observatories for data measured between 1996 and 2005.

The yearly behaviour of temperature did not show any particular pattern for the study sites during the ten years included in the plots showed in Figure II.2(b). Yearly temperature for all sites was within a band of around 1°C.

Atmospheric pressure

The monthly average atmospheric pressure shows a semi-annual cycle as shown in Figure II.3(a) with a large maximum during January, a smaller maximum in July/August and minima during May/June and September/October. This semi-annual cyclic behaviour is also

confirmed by Amador et al [43] and is particularly associated with the annual movement of the Intertropical Convergence Zone (ITCZ) which perturbs the pressure gradients within this region. The range of the seasonal pressure differences is 7hPa.

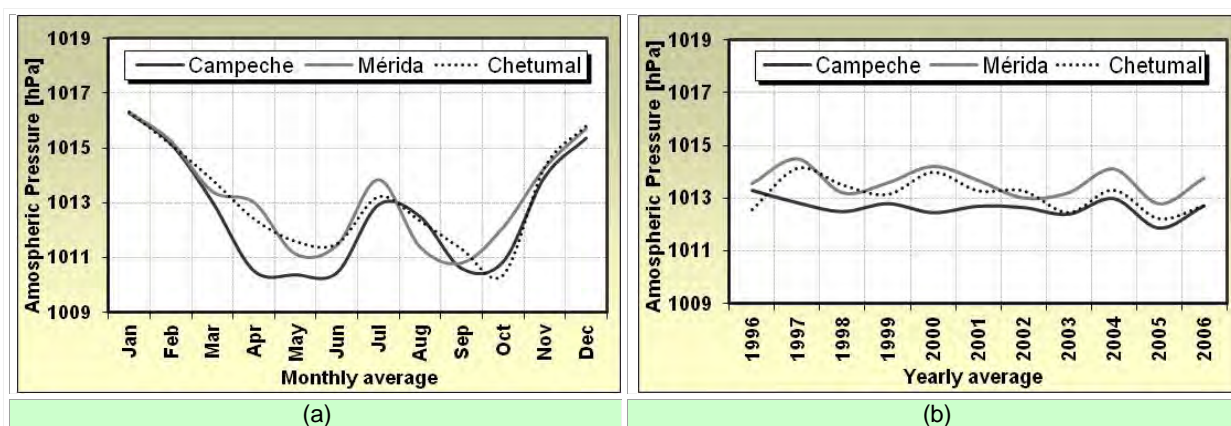


Figure II.3. Monthly (a) and yearly (b) averages of atmospheric pressure for the three observatories for data measured between 1996 and 2005.

There was little variation in annual average pressure values for the ten year study period (see Figure II.3(b)), with a range of annual values of less than 2hPa.

II.4 Wind behaviour

The monthly averages between 1996 and 2005 for each observatory are listed in Table II.4 for wind speed and wind direction, considering that the wind directions are measured from the North in clockwise direction. Of the three sites, Campeche showed the highest individual monthly average wind speed in April of 3.76m/s and the highest annual average wind speed of 2.93m/s at 10m a.g.l. Mérida registered an annual average wind speed 0.16m/s less than Campeche, and Chetumal had the lowest average annual wind speed of 2.24m/s. The majority of the monthly wind direction averages were concentrated within a range of 45 degrees to 96 degrees and the winds at all three sites were noted to be very directional as described below.

Table II.4. Monthly averages of wind speed and wind direction measured at 10m a.g.l. during the study period for each site.

		Wind speed averages [m/s]			Wind direction averages [degrees]		
		Campeche	Mérida	Chetumal	Campeche	Mérida	Chetumal
Months	January	2.94	2.74	2.20	47	64	54
	February	3.25	2.94	2.35	66	75	72
	March	3.61	3.43	2.81	85	88	89
	April	3.76	3.47	2.62	90	93	88
	May	3.40	3.41	2.34	94	95	89
	June	3.16	2.88	2.57	95	96	85
	July	2.68	2.50	1.96	92	91	85
	August	2.32	2.28	2.34	88	85	83
	September	2.39	2.12	1.87	70	80	80
	October	2.60	2.31	2.06	68	58	24
	November	2.53	2.54	1.86	56	55	45
	December	2.51	2.38	1.74	61	57	51
Yearly Mean		2.93	2.76	2.24	79	81	76

II.4.1 Wind speed patterns

In order to clearly visualize wind speed trends, Figure II.4 shows the monthly and yearly averages of the wind speed during the study period. In the case of the monthly averages, Figure II.4(a) shows that during the first 8 months of the year, between January and August, all the sites showed similar patterns with a maximum between March and April. It should be noted that the peak for Chetumal over this period is somewhat less pronounced. During the last four months of the year, there was not such a defined pattern and the variations in wind speed averages were below 0.42m/s for each site in this period. Over the year, Chetumal shows significantly less variation in wind speed than both Mérida and Campeche.

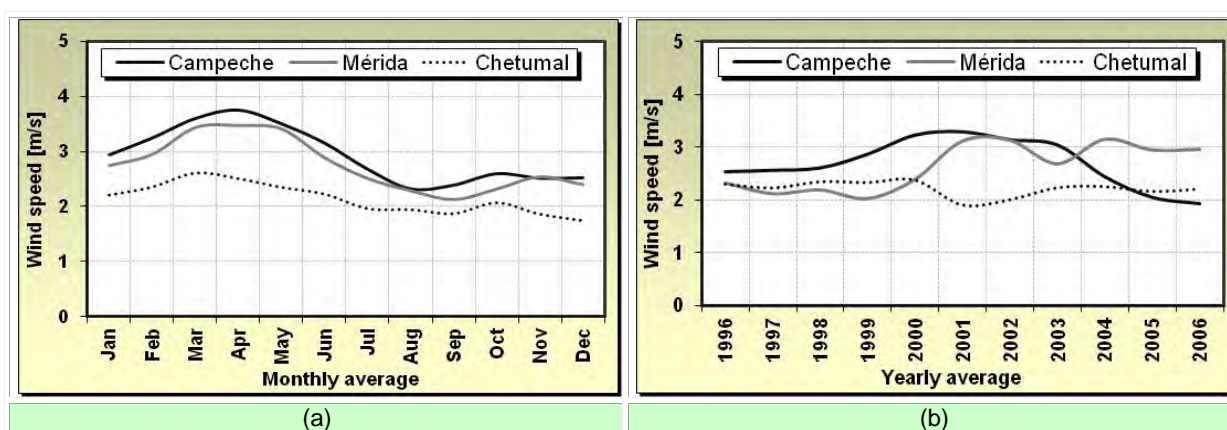


Figure II.4. Monthly (a) and yearly (b) averages of the wind speed for the three observatories for data measured between 1996 and 2005.

Figure II.4(b) shows the annual wind speed variation for three sites during the study period. It can be seen that both Mérida and Campeche show increases in wind speed from around

2000 and a reduction in wind speed around 2003/2004. This variation is not seen at Chetumal, where, once again, little variation in wind speed is seen over the study period.

In order to understand the results presented in Figure II.4(a) and Figure II.4(b), it should be remembered that the Atmospheric Boundary Layer (ABL) is essentially controlled by atmospheric motions governed by spatial variations of air pressure and temperature. The variations with height of horizontal pressure gradients or geostrophic winds occur in response to local temperature gradients created by surface topographical features. Because of the diurnal variations of solar energy at the surface, there are large diurnal variations in air temperature in the ABL over land surfaces, but in contrast, these are much smaller over the sea. Consequently, the ABL depth over the sea varies relatively slowly in space and time [44].

This difference in behaviour of the heating and cooling processes of the sea and land is produced by differences in the absorbed, transported and re-radiated energy. The opacity of the land concentrates the absorption in a very thin layer, producing rapid and intense heating, while the solar irradiation penetrates deeper in the water distributing the available energy in a wider zone because the fluid characteristics of water facilitate vertical and horizontal mixing. Thus, while land experiences significant temperature variations on a daily, inter-annual and intra-annual basis, sea water cools down and heats up far more slowly [45]. This in turn means larger changes in vertical temperature gradients over the land compared with the sea. Because these temperature gradients are responsible for the transfer of momentum from upper levels, then it can be seen why greater temporal changes in wind speed are seen for winds coming off the land than for those coming off the sea.

As can be seen in Figure II.6, the prevailing wind comes from an easterly direction over the Caribbean shore of the Yucatán Peninsula. Thus, Chetumal, which is situated just 2km from the shore, is influenced primarily by wind coming off the sea. This is not the case for Mérida and Campeche which are located more than 250km from the Caribbean shore. It can also be seen that the monthly temperatures at Mérida and Campeche seen in Figure II.2(a) peak earlier in the year (May/June) compared to Chetumal (August/September). This is consistent with air which is heated by the land as opposed to that by the sea. The far greater thermal mass of the sea means that there is a greater lag between temperature and absorbed solar irradiation for the sea, i.e. maximum annual sea temperature is reached several months later than maximum annual land temperature. In summary, different vertical temperature gradient and wind behaviour is observed in the case of Mérida and Campeche compared with Chetumal. The changes in wind speed during the year and over the study period driven by heating and cooling cycles over the land at Mérida and Campeche are thus far more pronounced than for the marine winds observed at Chetumal.

II.4.2 Wind directional patterns

In this section, wind direction statistics for the three sites are presented individually and so the whole period for which data were measured are used in each case, namely: 20 years for Mérida, 16 years for Campeche and 10 years for Chetumal. Figure II.5 shows the wind speed averages classified for each direction using 16 direction sectors.

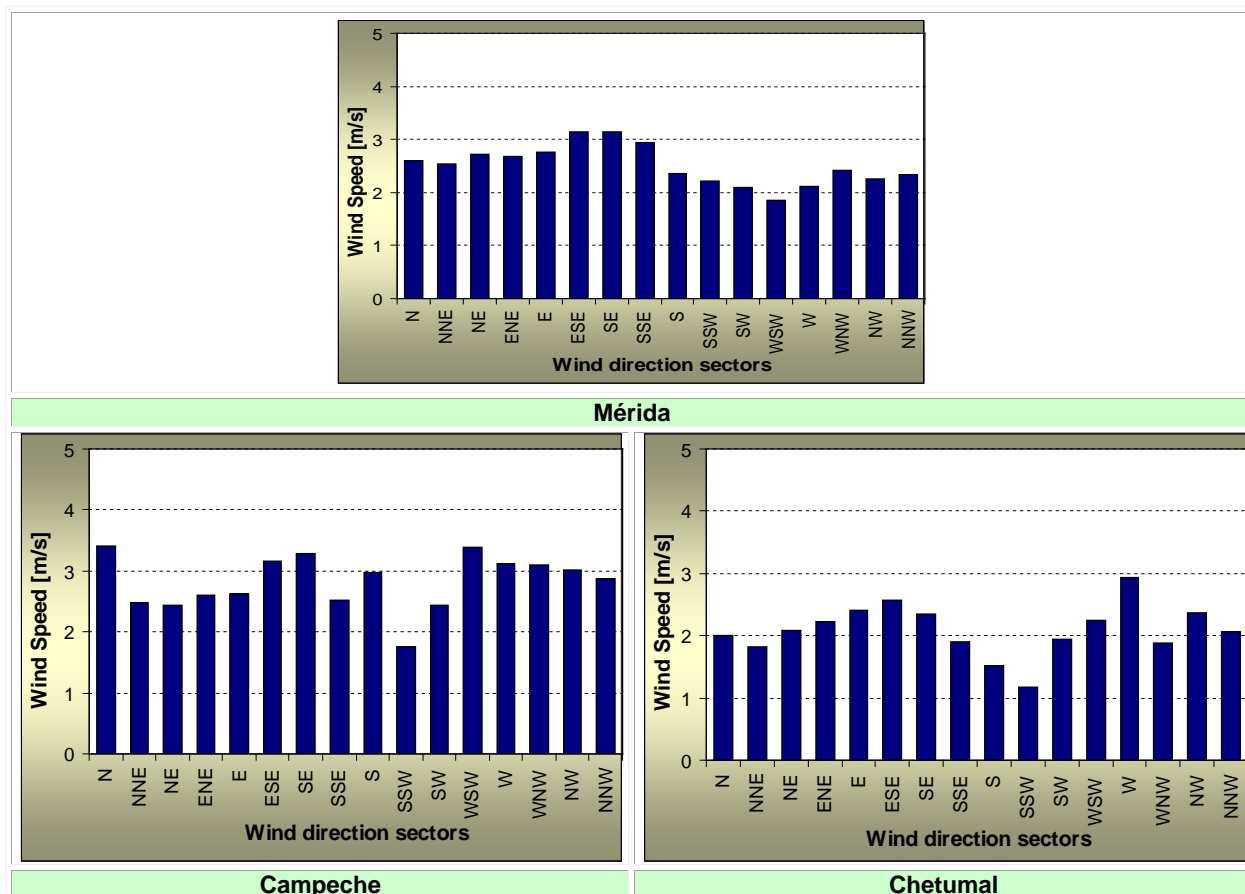


Figure II.5. Wind speed averages for each direction using 16 directional sectors for the three observatories using all the data available at each site.

Figure II.6 shows the wind roses for the three study sites. In this figure, the percentage of the time the wind blows from a given sector as well as the fraction of this time the wind speed is within a given range are both shown, represented by the length of each segment. It can be seen that the majority of the winds come from the East or East-South-East. In the case of Campeche and Mérida, there is also a smaller contribution from the North while northerly winds at Chetumal are negligible.

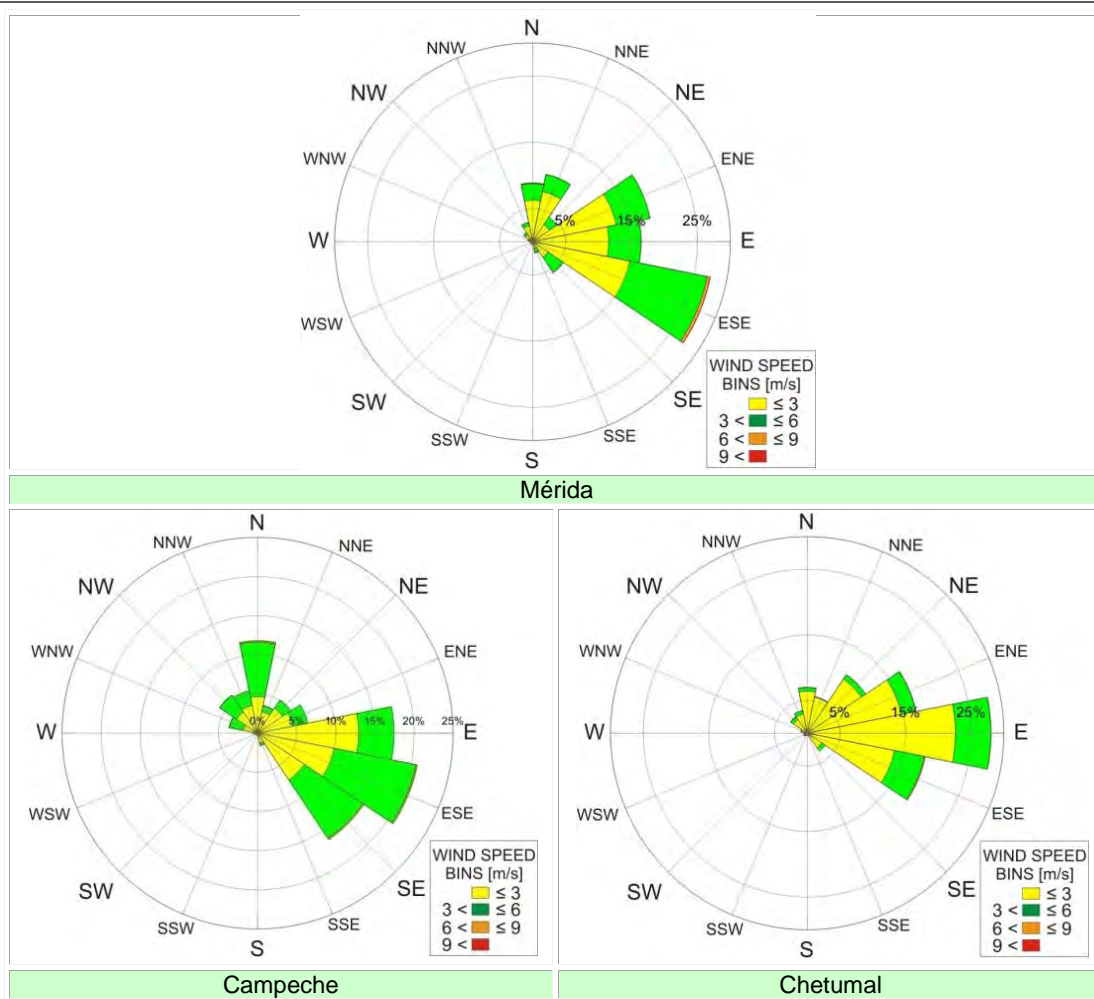


Figure II.6. Wind roses representing the full study period for the three observatories.

The results presented in Figure II.6 show that winds at the three study sites are highly directional. The results in Table II.5 confirm this. At least 89% of the winds between 1996 and 2005 in the Yucatán Peninsula came from directions between North and South-East. The proportion of the wind speed for each site at 10m a.g.l. is also tabulated when the wind speeds are higher than 3m/s.

Table II.5. Percentage of wind between North (N) and South-East (SE) sectors for each site.

	Campeche	Mérida	Chetumal
Percentage of all wind speed data	89%	93%	93%
Percentage where wind speed >3 m/s	61%	60%	38%

II.5 Wind frequency distribution and wind power density

As was already mentioned in the introduction, several studies have shown that the Weibull distribution function is suitable for representing wind speed frequency distributions, in particular for peninsulas [46] and islands [47]. More recently, other distributions have been

applied particularly in circumstances where the proportion of low winds is larger than predicted by a Weibull or where the observed distribution shows a variety of shapes which cannot be fitted by a Weibull distribution [48,49,50]. But as will be shown in Figure II.7, these characteristics are not present in the data of any of the three sites included in this study. Thus for ease of fitting, the Weibull distribution, see equation I.9, has been chosen to parameterize the frequency distribution of the measured wind speed data.

An iterative computer algorithm was implemented to calculate the K Weibull shape parameter using the Maximum Likelihood Estimator Method, see equation I.10. Then, the C Weibull scale parameter was evaluated with the equation I.11. In this case, the whole available data for each study site was used to compute the Weibull parameters. Figure II.7 shows the frequency distribution of the wind speed and the computed Weibull probability density function (PDF). It can be seen from these fits that the Weibull curve provides a relatively good fit to the data. There is no evidence of a high proportion of low wind speed values or unusual structure in the observed distributions that would merit more complicated distributions which are more difficult to fit. In addition, the Weibull distribution provides a simple way to calculate the wind power density.

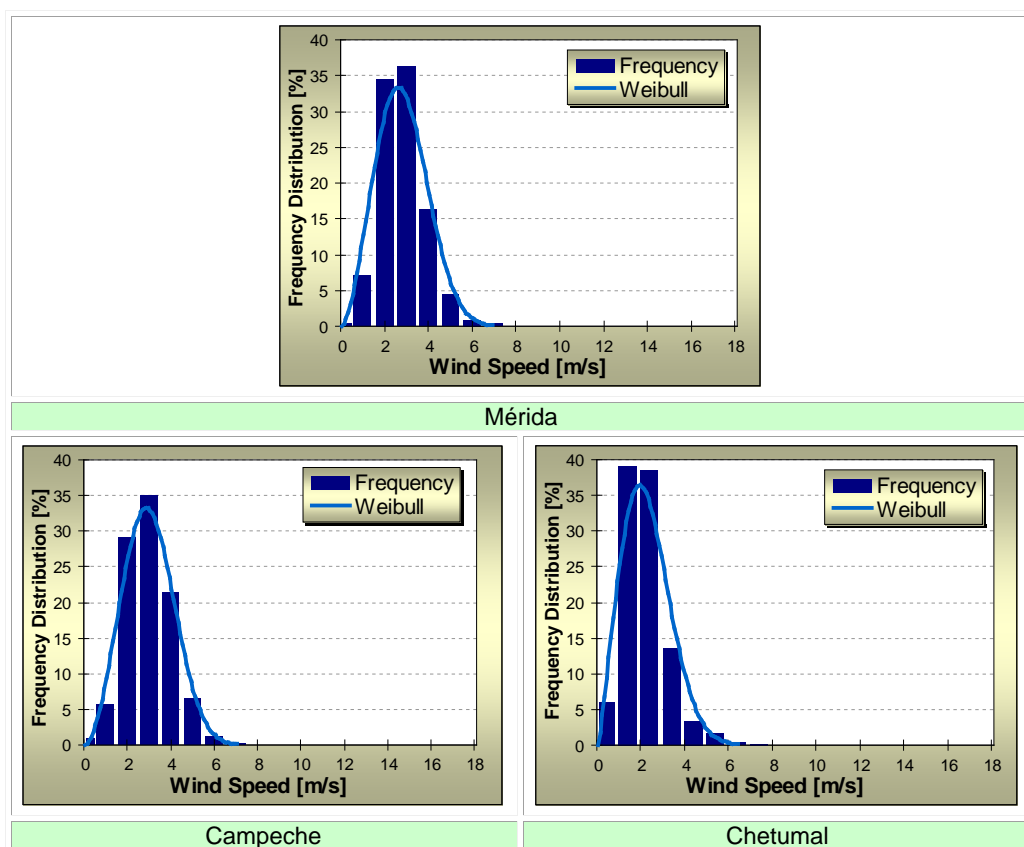


Figure II.7. Wind speed frequency distributions and Weibull PDFs using the wind data for the whole study period for the three observatories.

Table II.6 lists the associated K and C parameters of the Weibull PDF computed for each site.

Table II.6. Shape (K) and scale (C) parameters for the fitted Weibull distributions and the estimated power densities at the three study sites.

Station	Weibull parameters		Power density [W/m ²]
	K	C	
Campeche	2.79	3.33	23.3
Mérida	2.60	3.12	19.9
Chetumal	2.15	2.53	12.2

The wind power density calculated for the three sites using equation I.12 is shown in the final column in Table II.6. It can be seen that all three sites would be Wind Power Class 1 (<100W/m² at 10m a.g.l.), see Table I.4, which would not normally be economically viable for wind farm development. It should be noted, however, that the Weibull parameters here are based on daily averaged values of wind speed. This will give less wind speed variability than hourly averages and thus larger values of K than for hourly values. If hourly values were available and gave Weibull PDFs with K close to 2 (Rayleigh distributions), there would be a significant increase in power density, e.g. the power density at Campeche would increase from 23.3W/m² to 30W/m², close to 30%. Nonetheless, this increase does not represent a high power density compared with other sites usually reported with significant wind potential.

II.6 Remarks

This chapter has presented long-term wind statistics for three measurement sites spread around the Yucatán Peninsula in México. Trends in the long-term behaviour of pressure, temperature, wind speed and wind direction have been identified. The first important conclusion is that the winds are highly directional with the majority of wind coming from the East and East-South-East sectors.

It has been seen that the two sites which experience predominantly land-based winds, Mérida and Campeche, show the larger degree of temporal variation in wind speed on intra-annual and inter-annual timescales compared with the site at Chetumal where the winds are predominantly marine in origin. This is due to the different thermal properties of land and sea giving rise to different degrees of vertical temperature variation and hence different degrees of vertical mixing.

Weibull PDFs have been fitted to the wind speed distributions at the three sites and appear to give relatively good representations of the wind speed variations at the three sites. The Weibull scale and shape parameters have been used to compute the estimated wind power densities at the three sites which all fall within Wind Power Class 1.

The results presented in this chapter have stated an important reference milestone producing the first dataset of long-term data for wind power applications from the most reliable data available in the meteorological observatories of the Yucatán Peninsula. Therefore, this dataset can be used through Measure-Correlate-Predict (MCP) to estimate the seasonal patterns of wind energy available in other regions of the Yucatán Peninsula.

The diurnal distributions of wind characteristics were not identified in this chapter because the dataset were based on daily averages. Another useful result that cannot be properly derived from the results at this stage is the vertical wind profile which allows the estimation of the wind potential at the usual height of the wind power generators. The identification of both characteristics will be addressed in the next chapters of this PhD thesis.

III Spatial behaviour of the wind resource

An analysis of the characteristics of the wind resource of the Yucatán Peninsula is presented in this chapter, based on ten-minute averaged wind speed data from nine meteorological stations, between 2000 and 2007. Hourly and monthly patterns of the main environmental parameters have been examined. Highly directional behaviour was identified that reflects the influence of winds coming from the Caribbean Sea and the Gulf of México. The characteristics of the wind speed variation observed at the studied sites reflected their proximity to the coast and whether they were influenced by wind coming predominantly from over the land or predominantly from over the sea. The atmospheric stability over the eastern seas of the Yucatán Peninsula was also analysed to assess thermal effects for different wind directions. The findings were consistent with the variation in average wind speeds observed at the coastal sites where winds came predominantly from over the sea.

III.1 Introduction

The reference review presented in section I.2 revealed that a study of the seasonal variation of the wind resource is an important stage in assessing the reliability of the energy produced by wind turbines. In addition, wind data collected from automatic meteorological stations, measured every two seconds and with averages recorded every ten minutes, give useful information for studying local wind patterns. Considering these facts and the lack of any detailed analysis of the short-term variability of wind speeds in the Yucatán Peninsula (Eastern México), this chapter describes the second stage in this PhD research project to characterize the wind resource in the Yucatán Peninsula. This stage complements the previous analysis by: covering a wider geographical region in the Yucatán Peninsula; increasing the number of meteorological stations; using data from offshore marine buoys; and increasing the resolution of the source data from 1 day to 10 minutes.

More specifically, the data analysed in this chapter consists of ten-minute averaged values recorded at nine onshore and inland meteorological stations between 2000 and 2007. Hourly and monthly patterns of the main meteorological parameters were studied to infer the temporal and spatial wind patterns. Finally, atmospheric stability, over the adjoining sea areas was computed using data from marine buoys of the National Oceanic and Atmospheric Administration (NOAA-USA) to identify thermal effects on the wind patterns observed at the nine meteorological sites, particularly those close to the coast.

III.2 Measurement conditions

III.2.1 Study region

Figure III.1 shows the locations of the measurement sites used in this more detailed study of the short-term variability in wind speed over the Yucatán Peninsula. The sites are denoted by their three ID letters, described in Table III.1. The terrain height represented by levels of shading over the map shows that, except for a small region in the South, the majority of the Yucatán Peninsula lies below a height of 50m a.m.s.l.

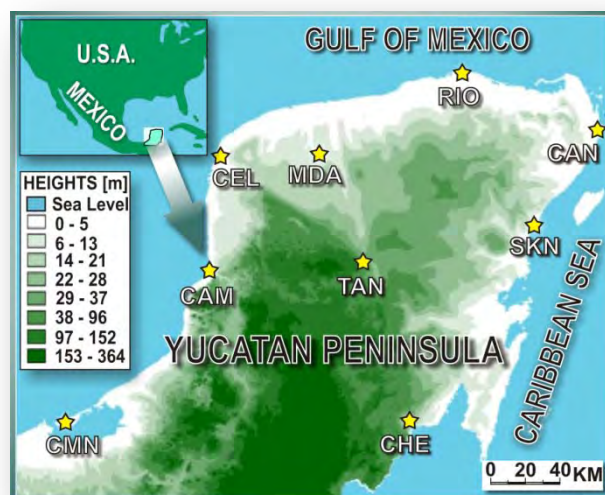


Figure III.1. Location of the study sites (sea details in Table 1) on the Yucatán Peninsula. Terrain height represented by the shading is also shown.

Nine automatic meteorological stations of the “Servicio Meteorológico de la CNA” (the National Meteorological Service) were selected to be analysed. Locations, elevations and the World Meteorological Organization (WMO) code of the nine stations are given in Table III.1. As will be shown in the next section, the main winds in the study region come mainly from sectors around the Easterly direction. Thus, two columns have been included in Table III.1 with the distances to the coast in the Easterly direction and additional observations of relevance to the wind characteristics.

Table III.1. Locations, elevations and WMO codes of the nine study sites N.B. GM=Gulf of México coast, CS=Caribbean Sea coast.

Meteorological station	ID	Station WMO code	Geographical coordinates	Station height a.m.s.l.	Distance to shore in east direction	Observations
Chetumal	CHE	MXCNA-QR02	18°30'02"N 88°19'40"W	14m	5km to CS	
Sian Ka An	SKN	MXCNA-QR03	20°07'40"N 87°27'56"W	8m	0.12km to CS	
Cancún	CAN	MXCNA-QR01	21°01'30"N 86°51'33"W	5m	4.7km to CS	7.5km to GM in North direction
Rio Lagartos	RIO	MXCNA-YC03	21°34'16"N 88°09'37"W	5m	120km to CS	10km to GM in East-North-East direction
Ciudad del Carmen	CMN	MXCNA-CM01	18°38'53"N 91°49'21"W	8m	430km to CS	Approx. 51km of harbour in East direction
Campeche	CAM	MXCNA-CM02	19°50'10"N 90°30'26"W	11m	304km to CS	
Celestún	CEL	MXCNA-YC02	20°51'29"N 90°22'59"W	10m	363km to CS	13km to GM in North direction
Mérida	MDA	MXCNA-YC01	20°56'47"N 89°39'06"W	8m	292km to CS	40km to GM in North direction
Tantakin	TAN	MXCNA-YC04	20°01'49"N 89°02'50"W	30m	164km to CS	

To complete the description of each measurement site, Figure III.2 shows a satellite image with a 500m radius around each measurement location. The ID codes used for each site image in Figure III.2 are described in Table III.1 and will be used during the rest of the thesis to denote each measurement station. As can be seen from Figure III.2, three of the nine measurement stations (CMN, CAM and MDA) have several buildings in their immediate vicinity.

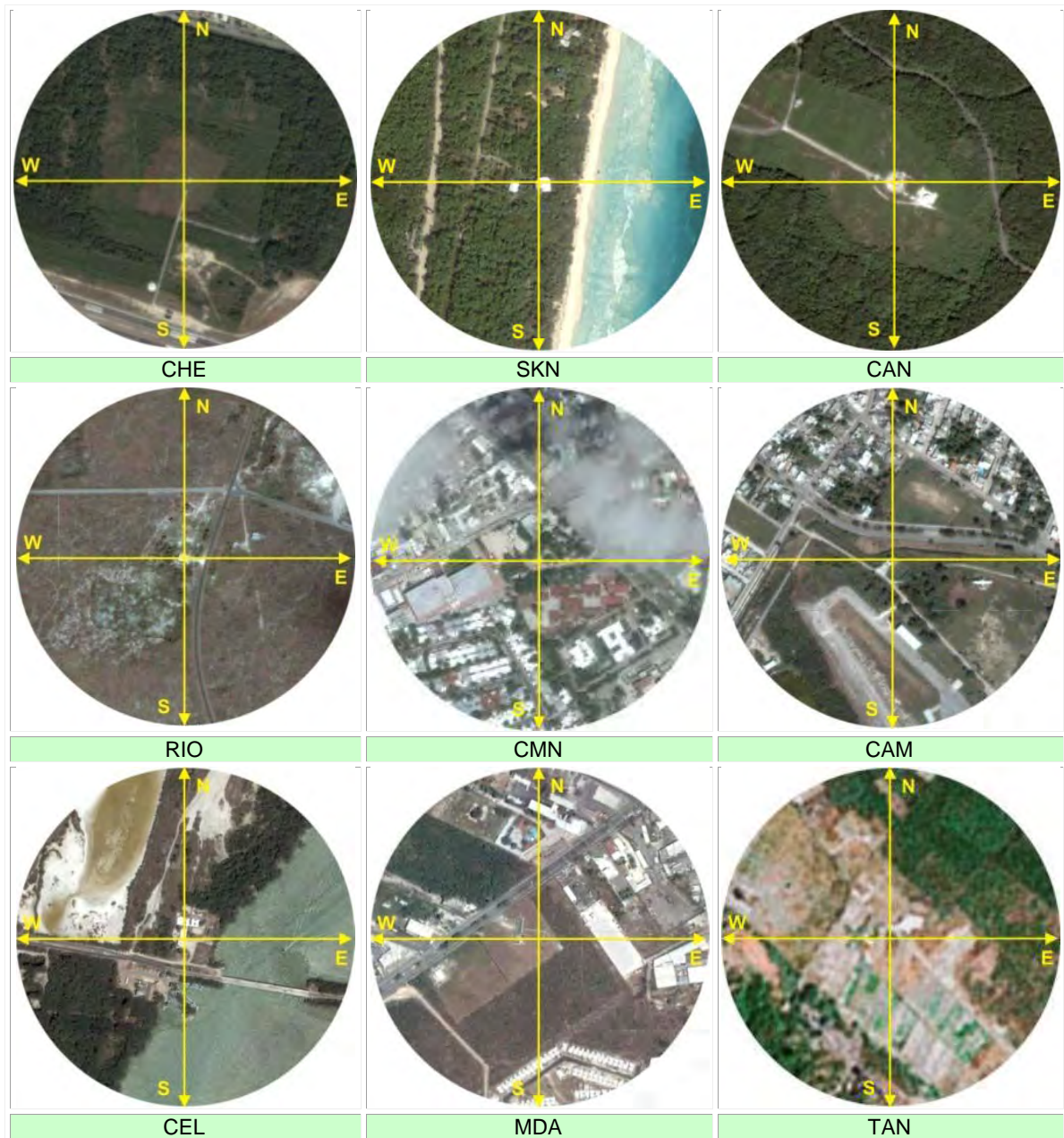


Figure III.2. Satellite images of 500m radius centred on each automatic meteorological station.

III.2.2 Measurement stations

The measurement stations selected for this research use two types of structures to support the sensors at 10m height, see Figure III.3. Type **A** stations support the sensors on a scaffolding structure and Type **B** stations locate the sensors on a tower. Figure III.3 shows

photographic examples of both types of structure; in these cases, RIO and CAN automatic measurement stations.



Figure III.3. Photos showing the two types of meteorological measuring structures used at the study sites (Type A: Scaffolding and Type B: Tower), in these cases, the RIO and CAN stations.

The main parameters measured by the automatic meteorological stations are described in Table III.2. These parameters were measured every two seconds to store averages every ten minutes by means of dedicated dataloggers.

Table III.2. Main characteristics of the parameters recorded.

Parameter	Unit	Range	Accuracy	Threshold	Resolution	Sensor height a.g.l. [m]	
						Type A station	Type B station
Wind speed	km/h	2.4 / 160	$\pm 2 \%$	2.4 km/h	0.1 km/h	10	10
Wind direction	Degrees	0 / 360	$\pm 5^\circ$	2.4 km/h	1°	10	10
Temperature	$^\circ\text{C}$	-51 / +60	0.2 $^\circ\text{C}$	-	0.1 $^\circ\text{C}$	10	10
Relative humidity	%	0 / 100	$\pm 2 \%$	-	0.10 %	10	10
Atmospheric pressure	hPa	600 / 1060	± 0.5 hPa	-	0.01 hPa	1.5	10
Solar radiation	W/m^2	305 / 2800 nm	-	-	-	5	10

Taking into account the range, accuracy, threshold and resolution of each sensor, the collected data were subject to quality checking, selection and some filtering to remove erroneous data points which were outside of the ranges specified in Table III.2. As mentioned above, the recorded data covered the period between 2000 and 2007. However, not all stations were fully commissioned by 2000 and several interruptions to data collection occurred, mainly as a result of hurricanes passing over the Yucatán Peninsula during the period of interest. Table III.3 shows the recording periods for each station from April 2000 to May 2007. Each rectangle represents a measurement month numbered from 1 for January to 12 for December.

Table III.3. Data availability for all sites studied. The shaded boxes represents the periods with available data.

Year	2000					2001					2002					2003					2004					2005					2006					2007								
Month	4	5	6	7	8	9	1	1	1	1	1	1	2	3	4	5	6	7	8	9	1	1	1	1	1	1	2	3	4	5	6	7	8	9	1	1	1	1	1	1	2	3	4	5
CMN																																												
CAM																																												
CEL																																												
MDA																																												
TAN																																												
CAN																																												
CHE																																												
SKN																																												
RIO																																												

III.3 Directional characteristics of the wind in the study region

The information recorded about the wind direction for each study site was classified into 16 directional sectors and four wind speed bins $\leq 3\text{m/s}$; $>3\text{m/s}$ and $\leq 6\text{m/s}$; $>6\text{m/s}$ and $\leq 9\text{m/s}$; and $>9\text{m/s}$. These results are represented in the form of wind roses in Figure III.4. It can be seen that for all of the study sites, the prevailing winds come from directional sectors between North-North-East (NNE) and East-South-East (ESE).

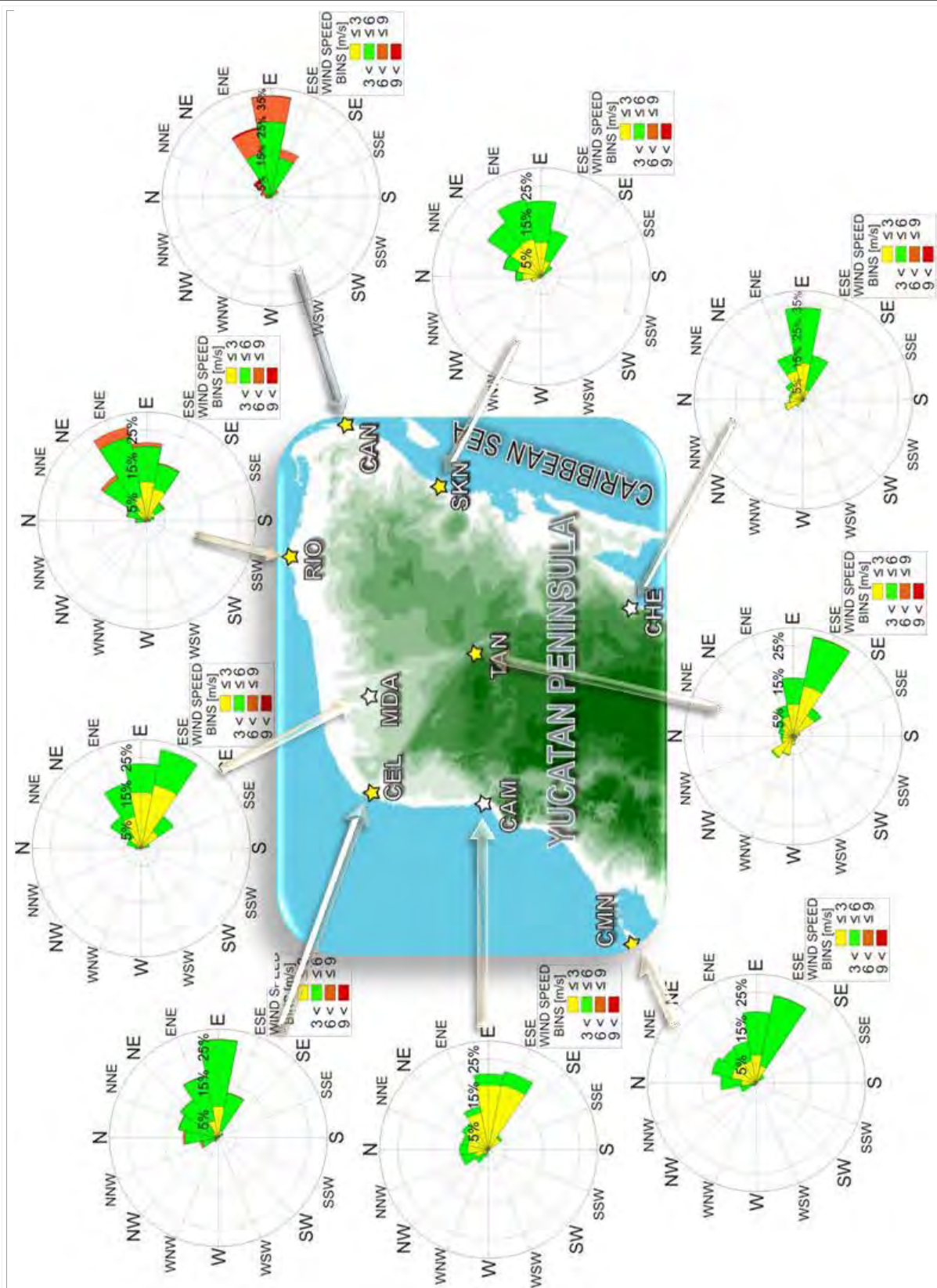


Figure III.4. Wind roses for the nine study sites.

Following the results presented in Figure III.4 and the geographical locations of the study sites (Figure III.1), the sites have been grouped according to whether the prevailing Winds Come from over the Sea (WCS) or Winds Come from over Land (WCL). The results presented in the next two sections, Figure III.5 to Figure III.8, are organized in two columns:

the first column (A) to showing four WCS sites (CHE, SKN, CAN and RIO) and the second column (B) showing the remaining five WCL sites (CMN, CAM, CEL, MDA and TAN). This classification takes into account that each group of sites should have different wind characteristics reflecting the different heating and cooling patterns of the sea and the land around them and their impact on the atmospheric boundary layer [71].

III.4 Daily patterns

III.4.1 Environmental parameters

Figure III.5 shows the daily patterns of ambient temperature, atmosphere pressure and relative humidity based on hourly averages throughout the study period given in Table III.3.

The ambient temperatures for the WCS sites show the least variation between the daily minimum and maximum temperatures ranging from 2°C for CAN to 7°C for RIO. In the case of the WCL sites, TAN (located in the middle of the Peninsula) shows the largest temperature range of 12°C whereas CMN, with a range of around 5°C, exhibits the least variation. Globally, the maximum daily temperature for the sites with WCS is on average 3°C lower than the sites with WCL. As was expected, the WCL sites registered less thermal influence from the air which has been heated over the sea. This sea-heated air will see a much lower range of temperature variation due to the large thermal capacity of the sea compared to the air which has been heated over the land.

The shape of the relative humidity patterns follows in general, as expected, an inverse relationship with the temperature pattern. The atmospheric pressure for all study sites shows a double peaked variation within the day. The first peak is located between the 08:00 and 10:00 and the second one between 20:00 and 00:00. This diurnal and semi-diurnal behaviour of atmospheric pressure, particularly pronounced near the equator is well known and is due to solar radiation causing eddy convection and the generation of gravity waves propagating throughout the atmosphere at integral values of the length of the day [72]. The semi-diurnal (S_2) component of pressure variation is larger than the diurnal (S_1) for the WCS sites and the amplitude of the S_1 component is larger for the WCL sites which would appear to be consistent with Dai and Wang [72], who reported a similar behaviour in similar geographical conditions.

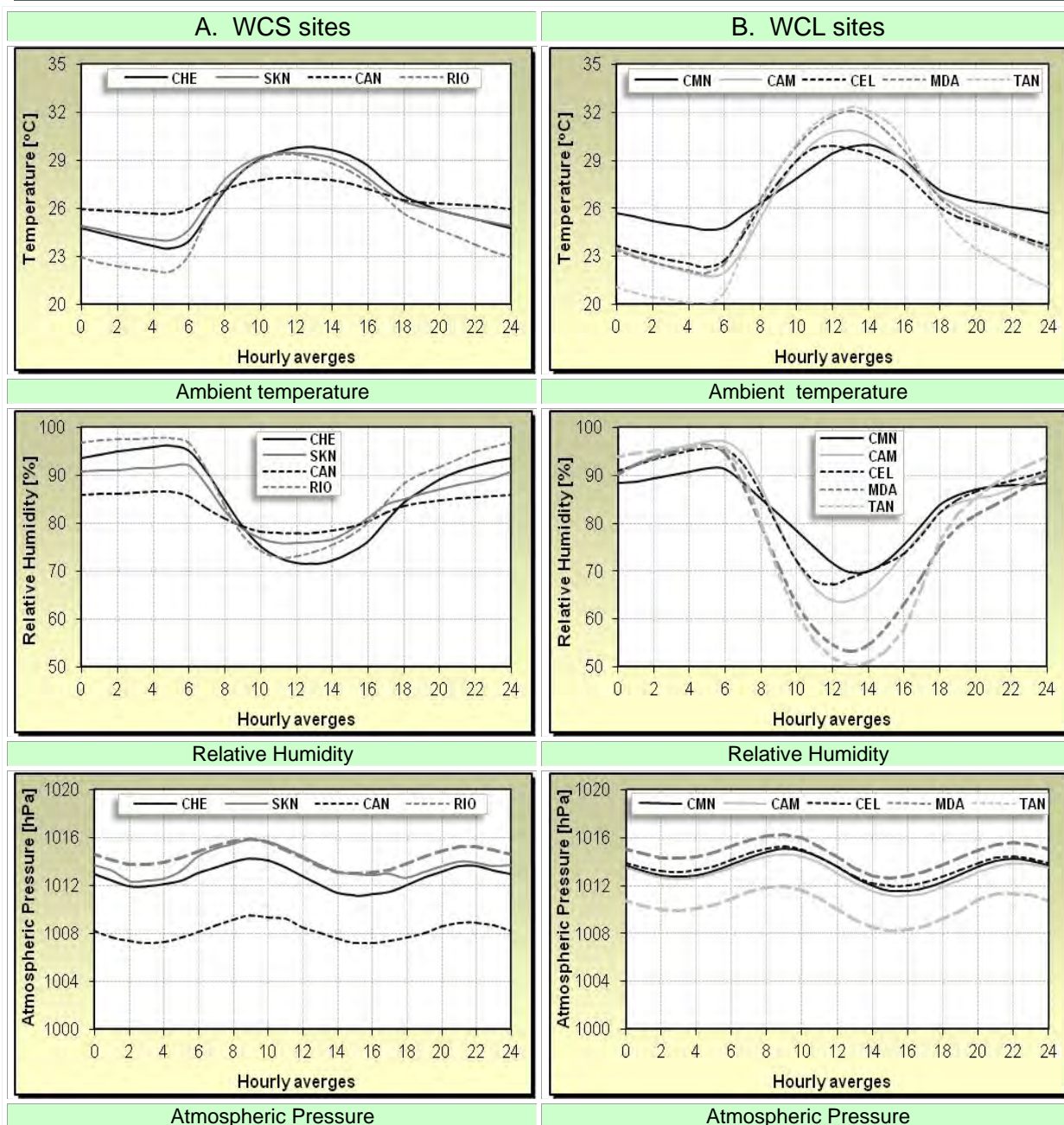


Figure III.5. Hourly averages of the main parameters for each study sites, grouped by sites with winds coming predominantly from the sea (column “A”) and sites with winds coming predominantly from the land (column “B”).

III.4.2 Wind behaviour

In the case of the WCS sites shown in column A of Figure III.6, the diurnal wind variation reduces due to convective mixing transferring momentum from higher in the atmospheric boundary layer to the surface. The overall magnitude of the wind speed increases moving from CHE in the South-East, through to SKN in the East, to CAN in the North-East of the Yucatán Peninsula, see map in Figure III.1. These effects result from the contribution of the winds coming from ENE which are more influenced by the Northern part of the East coast and the thermal influence of the Gulf of México discussed later at the end of Section IV.3.

Due to its position on the North-East coast, the winds at RIO show more diurnal variation than the other WCS sites. The wind patterns at RIO reflect the contribution of wind coming not just from the Gulf of México in the ENE direction but also from the land in the E and ESE directions (see the Figure III.1 and the wind rose in Figure III.4). Therefore, RIO shows characteristics of being both a WCS and WCL type site.

In the case of the WCL sites, column B of Figure III.6, there is a pattern of higher wind speed during daylight hours but with a peak in the morning and another generally higher peak in mid afternoon. The reason for this double-peaked behaviour becomes apparent by observing the diurnal variation in wind direction in Figure III.6. There is little variation for the WCS sites, but the WCL sites see a significant backing from E to N at around 10:00 and then a gradual veer back to E after around 16:00. This would be consistent with a sea breeze developing in the early afternoon causing the wind to change to an onshore breeze which later changes to an along shore easterly breeze as the Coriolis force takes effect. In the case of the WCS sites, the effect is less apparent as the wind is already coming predominantly from over the sea. For the WCL sites, this effect results in a change in wind coming over the land to wind which comes from over the sea with an attendant increase in wind speed giving rise to the larger peak in the afternoon. This characteristic is less marked in the case of CMN than in the remaining four WCL sites and is due to the influence of a natural harbour situated within 51km and aligned with the prevailing winds (see Figure III.1 and details in Table III.1). Finally, CEL located on the North-West coast experiences higher winds than the other WCL sites because of the combined effect of the prevailing winds coming from the land and from the Gulf of México (see the wind rose for CEL in Figure III.4).

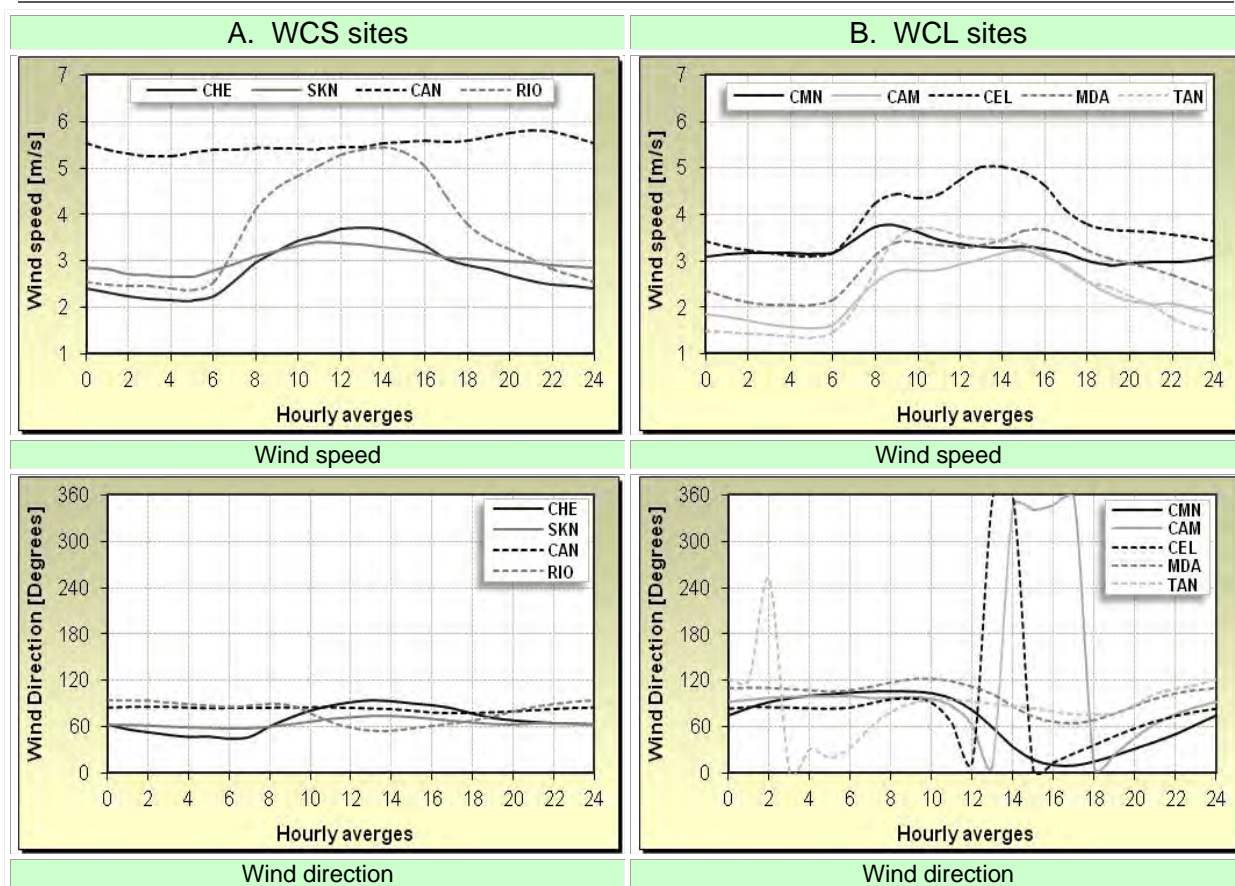


Figure III.6. Hourly averaged wind speeds for each study site, grouped by sites with winds coming predominantly from the sea (column “A”) and sites with winds coming predominantly from the land (column “B”).

III.5 Seasonal variation

III.5.1 Environmental parameters

This section examines the pattern of seasonal variation using monthly averages determined from the whole study period. Ambient temperature variation for WCS sites, column A in Figure III.7, indicates a maximum at around July-August while WCL sites show a double peak curve: with a global maximum reached in May and a less defined secondary peak located in the middle of September prior to a fall to a December-January annual minimum. This double peak in the temperature of the WCL sites can be explained by considering that the heat source (solar radiation) peaks in April-May and then again in July-August. This is due to the rainy season around June-July resulting in more cloud cover and the resulting reduced solar radiation. The temperature for sites where the winds are coming from over the land tends to reflect the changes in the solar radiation. On the other hand, the WCS sites receive winds from over the sea therefore the temperature shows a weaker correlation to the local solar radiation flux [71].

The relative humidity in the case of the WCL sites, column B of Figure III.7, has a well defined pattern for all sites: with a marked minimum in April and a less well defined maximum around September-October. From November to July, MDA and TAN (which is the site located deeper inland) show a less clear pattern for relative humidity than the rest of the WCL sites.

Generally, the atmospheric pressure shows an annual maximum at around January and a secondary peak in July. WCS sites have minimum values around September, in the middle of the Hurricane season.

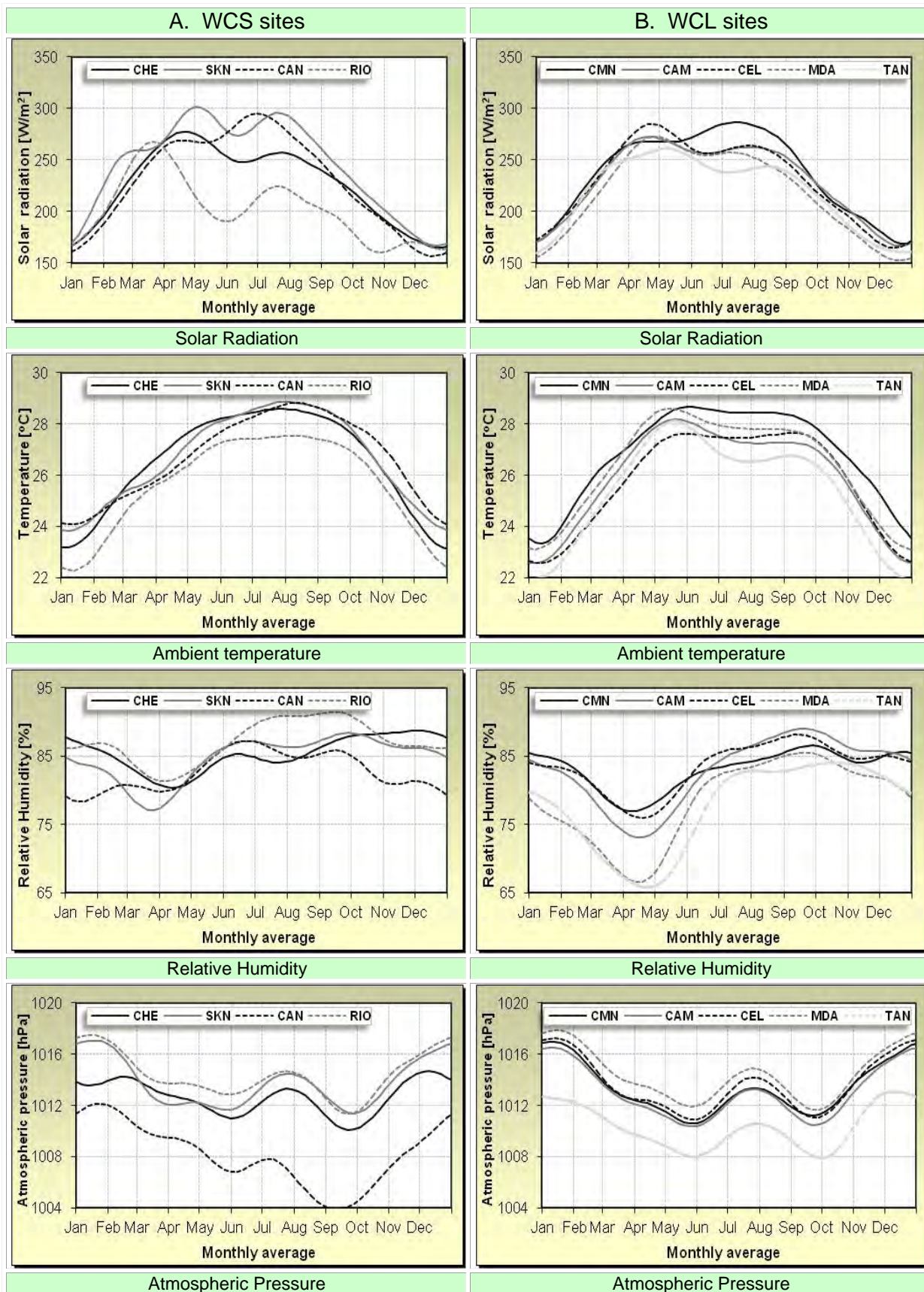


Figure III.7. Monthly average of the main parameters for each study site, grouped by the sites with winds coming predominantly from over the sea (column “A”) and sites with winds coming predominantly from over the land (column “B”).

III.5.2 Wind behaviour

Monthly behaviour of the wind is shown in Figure III.8. More significant variations in the wind speed are seen for the CAN and RIO sites on the most exposed part of the Yucatán Peninsula. These two WCS sites have similar trends between May and November but outside of this period, CAN shows a significant peak of monthly wind speed in December while RIO shows just a slight increase. The rest of the measurement sites show less variation in wind speed with generally higher wind speeds in the months between April and May and lowest wind speeds in the months between September and October. The average monthly wind directions for both classes of sites show just a few significant variations.

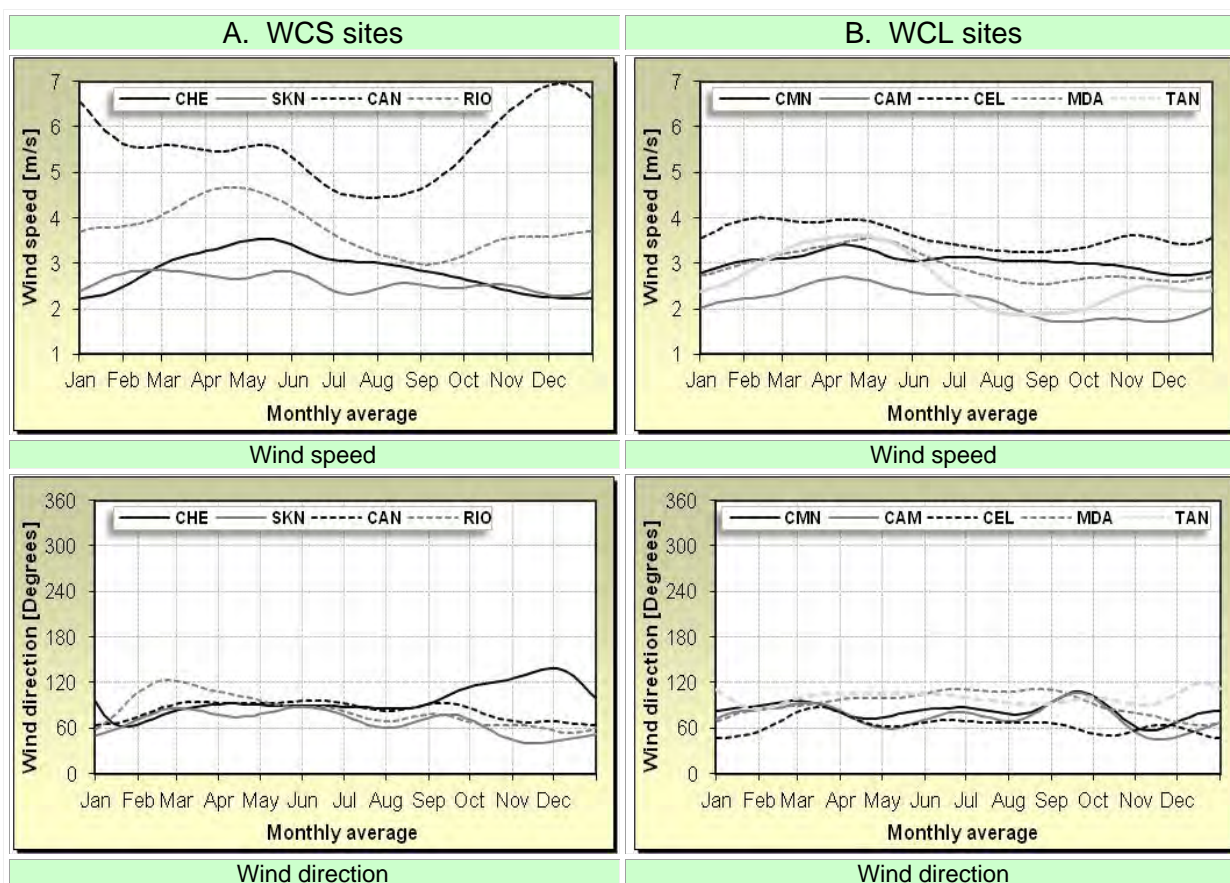


Figure III.8. Wind monthly averages for each study site, grouped by the sites with winds coming from sea (column “A”) and sites with winds coming from land (column “B”).

III.6 Atmospheric stability over the surrounding sea

As described above, the winds that arrive at the Yucatán Peninsula come mainly from NNE to ESE where the Easterly part of the Gulf of México and the Westerly part of the Caribbean Sea are located, as can be seen in Figure III.1. The stability of the atmosphere over these seas influences the winds that arrive on the Yucatán Peninsula. Thus to study this in more

detail, the wind speeds, air and sea temperatures available from marine buoys of the NOAA [73] have been used to evaluate the atmospheric stability.

Marine buoys

Two of the NOAA marine buoys were selected due to their geographical position and availability of data during the study period. They are located as shown in Figure III.9, where buoy “1” lies in the Eastern Gulf of México (EG), and buoy “2” in the West of the Caribbean Sea (YB, “Yucatán Basin”).

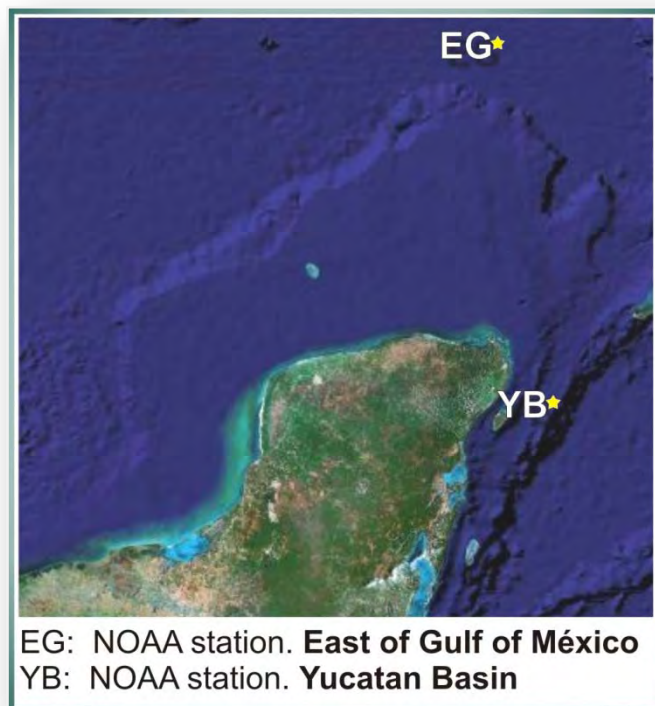




Figure III.9. Locations of the two selected NOAA marine stations (buoys) in the vicinity of the Yucatán Peninsula: “1. East Gulf” and “2. Yucatán Basin”.

The EG buoy is located in water which is approximately 1.2km shallower than that of the YB buoy. In addition, the YB buoy is inside the tropical region, whilst the EG buoy is located around 4 degrees North of the Tropic of Cancer as confirmed by data shown in Table III.4.

Table III.4. Information concerning the NOAA marine stations used to evaluate the atmosphere stability [73].

	East Gulf (EG)	Yucatán Basin (YB)
Marine buoy image		
Buoy diameter	10m	12m
Coordinates	25.74 N, 85.73 W	19.87 N, 85.06 W
Site elevation	sea level	sea level
Air temperature height	10m above site elevation	10m above site elevation
Sea temperature depth	1m below site elevation	1m below site elevation
Anemometer height	10m above site elevation	10m above site elevation
Barometer elevation	sea level	sea level
Water depth	3233m	4446m
Averaging period	Hourly	Hourly
Available measurement months	Jan. 2005, Aug. 2005 – Dec. 2006	May 2005 – Jan. 2006, Apr. 2006 – Dec. 2006

The EG buoy is located in water which is approximately 1.2km shallower than that of the YB buoy. In addition, the YB buoy is inside the tropical region, whilst the EG buoy is located around 4 degrees North of the Tropic of Cancer as confirmed by data given in Table III.4. Figure III.10 below shows that the wind roses in both cases follow the same pattern described for the WCS sites.

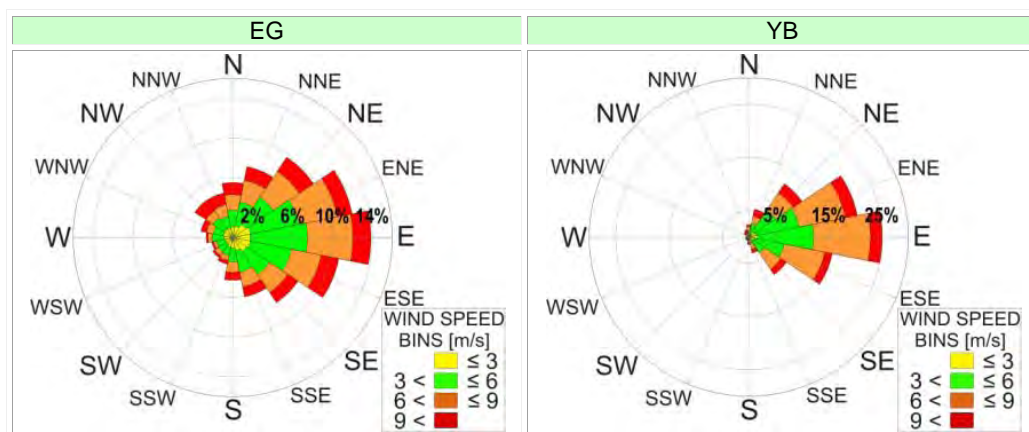


Figure III.10. Wind roses representing the directional distribution of wind for the data available from the EG and YB marine stations.

An analysis of the hourly averages during the day, shown in Figure III.11(a) and Figure III.11(b), shows that the winds at YB are up to 1m/s higher than for EG while the average

hourly wind direction for both sites remains almost constant at around 90 degrees (E). An analysis of monthly averages during the year, shown in Figure III.11(c) and Figure III.11(d), indicates lower wind speeds in September and the maximum towards the end of the year. A change in the direction of the winds from E to S, during August and September, can be seen (Figure III.11(c)) for EG buoy around the same period that the lower wind speeds are evident. The limited data available for the YB buoy, see Figure III.11(d), does not allow an analysis of wind speed and direction trends for the first three months of the year. Both offshore wind speed profiles show an important wind potential; this result suggests the relevance of studying offshore sites closer to the coastline.

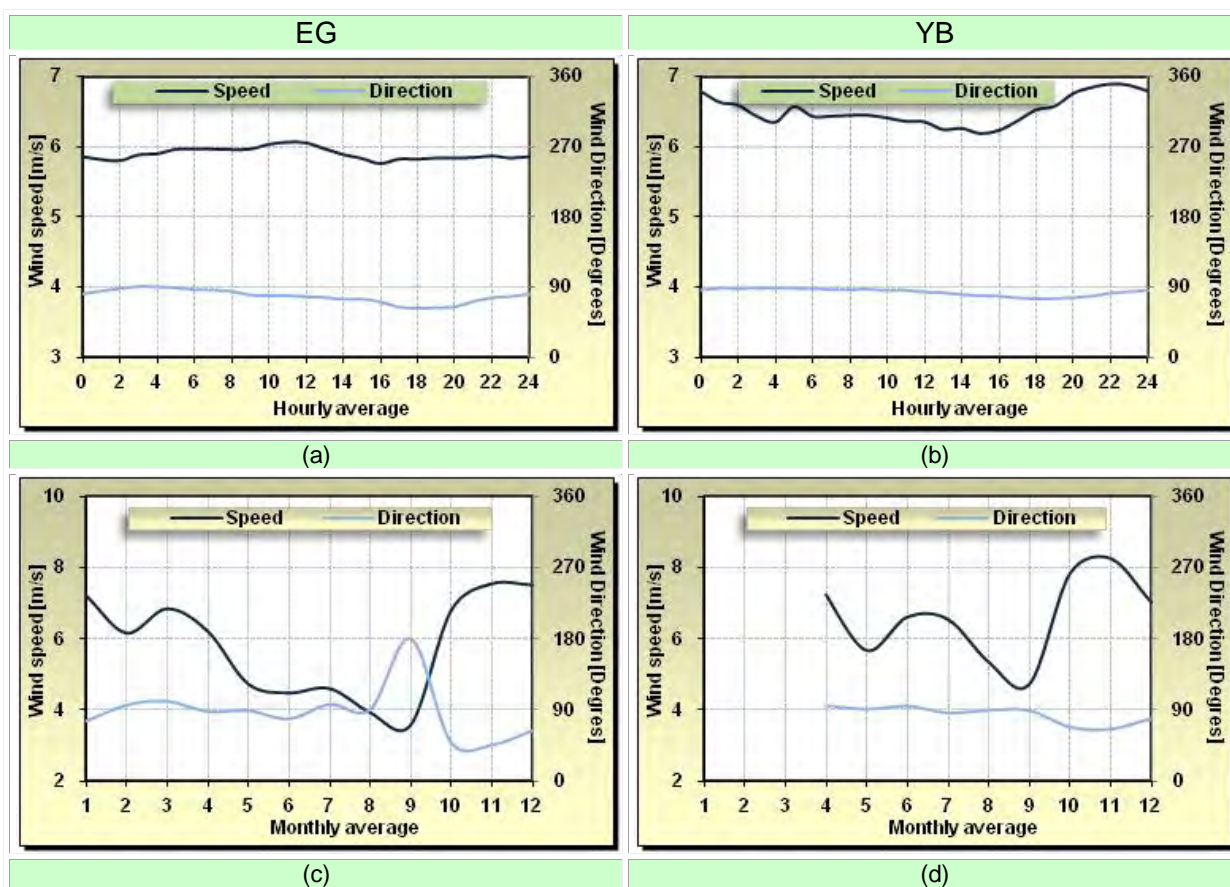


Figure III.11. Average hourly (a and b) and monthly (c and d) wind speed and wind direction for EG and YB marine buoys over the available data periods described in Table III.4.

Temperature patterns

Temperature data for the sea surface (WaterT) and the air (AirT) are required in order to evaluate the atmosphere stability at the two buoys. Figure III.12(a) and Figure III.12(b) show the hourly variation through the day where a significant difference between sea surface and air temperatures is revealed. This difference is approximately twice as large for EG than for YB. The YB air temperature is around 3°C higher than the EG air temperature while the sea surface temperature is around 1.5°C higher at YB than at EG over the entire day. Little

diurnal fluctuation in either air or sea surface temperature is seen at both sites as would expected due to the high thermal mass of the water.

Monthly averages for the temperature variation throughout the year are presented in Figure III.12(c) and Figure III.12(d). These show that the maximum annual air and sea surface temperatures occurred in August having approximately the same magnitude at both buoys. EG air temperature in December was around 4°C colder than YB air temperature and the sea surface temperature was 2°C colder at EG than at YB. With the limited data available at YB, it would seem that there was less annual variation in air and sea surface temperature in the Yucatán basin (YB) compared with the Eastern Gulf (EG); which cannot be explained with the results obtained so far although it should be related with stability of the atmosphere as will be analyzed in the next subsection.

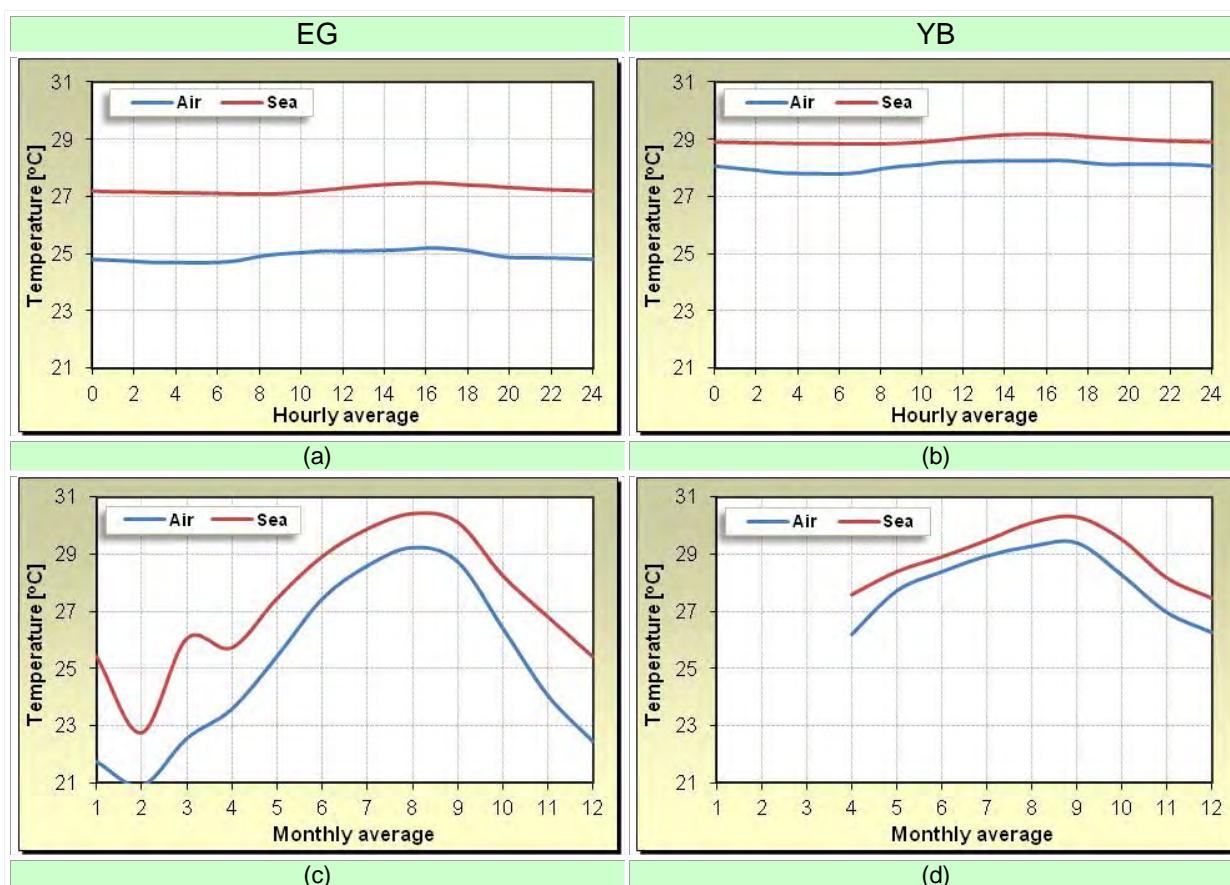


Figure III.12. Daily (a and b) and yearly (c and d) sea surface and air temperatures for EG and YB marine stations averaged over the available data period described in Table III.4.

Stability classes

The atmosphere stability, which can be estimated by the Obukhov length L through the equation 1.3, was computed using the Bulk Richardson number parameterization, see equation (1.5), where z' is 10m height, u is the wind speed measured at 10m height, \bar{T} is the average of the air and sea surface temperatures and $\Delta\theta_v$ is the difference between the virtual

potential temperature at 10m height and sea surface temperature. Then, the values of L were grouped according to the stability classes defined in Table I.2 and the frequency distribution of these classes shown in Figure III.13.

Considering that the sign of the Bulk Richardson number is negative for both sites, because the temperature gradient is negative as was shown by Figure III.12 above, it should be expected that the atmosphere present very low stable states in both sites. It can be seen that the atmosphere at EG is unstable or very unstable approximately 70% of the time and near-neutral for 30% of the time. On the other hand, the atmosphere at YB is near-neutral for approximately 65% of the time and the rest of the time is unstable or very unstable.

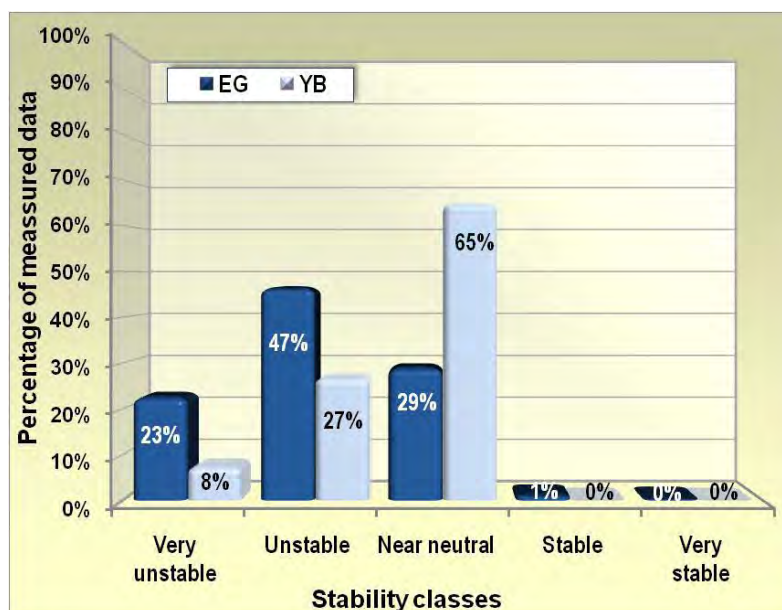


Figure III.13. Distribution of the stability classes from their values of the Obukhov length computed with equations I.3 and I.5 and classified using Table I.2 for EG and YB marine stations.

In a neutral atmosphere, mechanically generated turbulence is dominant and the wind speed at a specific height depends solely on the roughness of the sea surface and the geostrophic wind speed. Thus, the winds coming from the Caribbean Sea will tend to be influenced mainly due the surface properties following the predominance of near-neutral conditions observed at YB.

In an unstable atmosphere, the air virtual potential temperature is lower than the sea surface virtual potential temperature. Under these conditions, thermally generated turbulence dominates causing enhanced vertical mixing allowing greater transfer of wind momentum downwards and increased wind speed at lower heights compared with near-neutral conditions. Therefore, the sites with wind coming from over the Eastern Gulf of México should see higher wind speeds which is consistent with the results shown for CAN and RIO as seen in column A and for CEL and CMN (despite the proximity of buildings) as seen in column B of Figure III.6.

III.7 Remarks

The results obtained confirm that the winds on the Yucatán Peninsula are highly directional in nature which is not surprising given its location in the tropics and its proximity to the sea. Due to its geographical position, the mainly unstable atmosphere of the Eastern Gulf of México plays a key role in determining the higher wind speeds seen on the North and North East coasts of the Yucatán Peninsula, despite the slightly higher winds observed at the buoy in the West Caribbean Sea. It was seen that the atmosphere over the Eastern Gulf was near neutral for less than the 30% of the time studied, whilst the atmosphere over the Western Caribbean was predominantly near neutral.

In the main, the wind climatology seen at each study site reflects the geographical position in relation to the coast. Just two sites, Celestún (CEL) and Rio Lagartos (RIO), exhibited mixed behaviour with characteristics of both land and sea wind sites.

The sites with higher wind were Cancún (CAN), Rio Lagartos (RIO) and Celestún (CEL), all located in the Northern part of the Yucatán Peninsula with winds coming predominantly from over the Eastern Gulf. These more exposed sites have the best wind potential though, in absolute terms, the wind speeds at these sites, with the possible exception of Cancún (CAN), are modest in terms of wind energy potential.

It can also be noticed that another important reference for wind energy applications has been created through a geographically distributed dataset from the most reliable data available in the automatic meteorological stations of the Yucatán Peninsula. In this case, this dataset can be used through Measure-Correlate-Predict (MCP) to estimate the diurnal and seasonal patterns of wind energy in other regions of the Yucatán Peninsula.

The results presented in this stage of the PhD research have improve the level of description of the wind characteristic in the Yucatán Peninsula revealing the diurnal patterns, the conditions of the atmosphere in the surroundings seas and confirming the behaviour of the seasonal patterns identified in the long-term study undertook in the previous chapter. They have also stated the relevance of the surface roughness and the stable nature of the winds coming from eastern directions especially for the sites locates inland in the Yucatan Peninsula. In the next chapter, an inland site will be study to identify the vertical profile of the wind and the corresponding wind shear behaviour.

IV Inland vertical wind profile

This chapter presents an analysis of wind speed and wind shear in terms of the directional, diurnal and seasonal patterns for a site at the Autonomous University of Yucatán which experiences the tropical conditions of the Yucatán Peninsula in México. This analysis takes a detailed look at frequency distributions to facilitate a comprehensive understanding of the local climatic conditions. Diurnal wind speed variations are shown to be affected in particular by the differing wind conditions associated with fetches over two distinct offshore regions. Seasonal behaviour suggests some departure from the oscillations expected from temperature variation. In addition, the use of rate of change of temperature at one height is proposed as an alternative to vertical temperature gradient inferred from two heights as an approximate indicator of atmospheric stability which will affect the wind shear.

IV.1 Introduction

Many research results have been published addressing the subject of the vertical wind profile in the surface boundary layers and have considered, among other factors, the amount and kind of meteorological data available, the geographical location (inland, onshore or offshore), the topography and the distribution of buildings around the study site (mainly for urban cases). When the atmospheric stability is neutral and the terrain is reasonably flat and homogeneous, the adiabatic log law is reasonably effective in predicting the wind profile, but for other stability conditions additional information is required to accurately estimate the wind shear according to Monin-Obukhov similarity theory [76,78].

The simplicity of the power law has made it perhaps the most widely applied model of wind shear. Nevertheless, atmospheric conditions and geographical characteristics of a particular region can create important variations in the wind shear patterns. This chapter presents a comprehensive analysis of the wind speed and wind shear at a specific site in the Yucatán Peninsula in terms of the directional, diurnal and seasonal patterns. In particular the frequency distribution of the key parameters is examined to account for the diverse wind shear characteristics identified. This research is focused on a region where the vertical behaviour of the wind has not been studied previously.

IV.2 Study site

IV.2.1 Geographical location

The measurement site is located in eastern México in the State of Yucatán close to the north coast of the Yucatán peninsula. This is therefore a tropical climate which should be strongly influenced by the proximity of the Caribbean Sea to the East and the Gulf of México to the North and West. The measurement tower is installed at the Science and Engineering Campus of the Autonomous University of Yucatán which is shown in Figure IV.1 with a small star.



Figure IV.1. The geographical location of the measurement site is shown in the North of the Yucatán peninsula with a small star.

The topography of the North of the Yucatán Peninsula is mainly flat. Particularly, the measurement site which is located at around 25km from the North shore is just about 7m a.m.s.l. Table IV.1 lists the main geographical parameters for the measurement site.

Table IV.1. Parameters for the geographical location of the measurement tower.

Site parameters	Values	
Geographical coordinates	GPS GEO	21°02'55.69" N, 89°38'36.68" W
	UTM WGS84-16	225262 E, 2329831 N
Site height a.m.s.l.	6.9m	
Distance from the near coast	25.3km (Northerly direction)	
Measurement heights a.g.l.	10m and 30m	

IV.2.2 Measurement sensors

Figure IV.2(a) shows an overall view of the measurement tower which was designed, installed and operated as part of the works undertaken in this research project. The nearest obstacle is located to the west of the tower at a distance of 5m with a height of 7m; see Figure IV.2(b). In the right hand side image, Figure IV.2(c), a close up of the measurement tower is presented to identify the relative positions of the wind sensors at 10m and 30m a.g.l. and at a distance of 1.5m from the measurement tower. The wind sensors were installed facing the ENE direction as preliminary measurements showed that the westerly direction contributes less than 10% of the total winds at the site.



Figure IV.2. Images of the measurement tower: (a) overall view from the westerly direction, (b) view from the northerly direction showing the tower base, (c) close up view from the northerly direction showing the position of the installed sensors.

As well as two cup anemometers at 10m and 30m a.g.l. and a wind vane installed at 10m a.g.l., a temperature sensor was also installed at 10m a.g.l. The wind sensors were fully calibrated by the manufacturer and at the end of the study period this calibration was verified using a new ultrasonic wind sensor. The basic operational characteristics of the sensors are shown in Table IV.2.

Table IV.2. Technical specifications of the sensors installed on the measurement tower.

Parameters	Sensors		
	Anemometer	Wind Vane	Temperature
	RM Young 3101	RM Young 3101	Vaisala CS500
Measurement range	0 to 50 m/s	0° to 360°	- 40 °C to 60 °C
Resolution	0.01 m/s	0.1°	0.01 °C
uncertainty	1 %	± 5°	± 0.5 °C
Starting threshold	0.5 m/s	0.8 m/s	N/A

The data used in this work comprise 64,451 records which were computed over 18 months of measurements since April 2003. These records contain the average every 10 minutes of the measurements sampled every 2 seconds from the installed sensors. The directional, diurnal and seasonal patterns were computed applying conventional averaging statistical methods from the 10 minute records. Frequency distribution patterns of wind speed and wind shear were also obtained classifying and processing the 10 minute records.

IV.2.3 Main obstacles

The behaviour of the wind speeds, especially at low heights, is affected by the surface characteristics. Thus, the immediate surroundings, as with all meteorological sites, are of

importance because of their influence on the wind speeds and the wind shear in particular. Figure IV.3(a) shows a satellite photo of approximately 1.6km around the measurement tower. The closest region to the measurement point is marked with a square in the centre of Figure IV.3(a) and it has been magnified in Figure IV.3(b). This magnified area of approximately 400m x 400m shows the closer obstacles that could influence the wind patterns across the site.

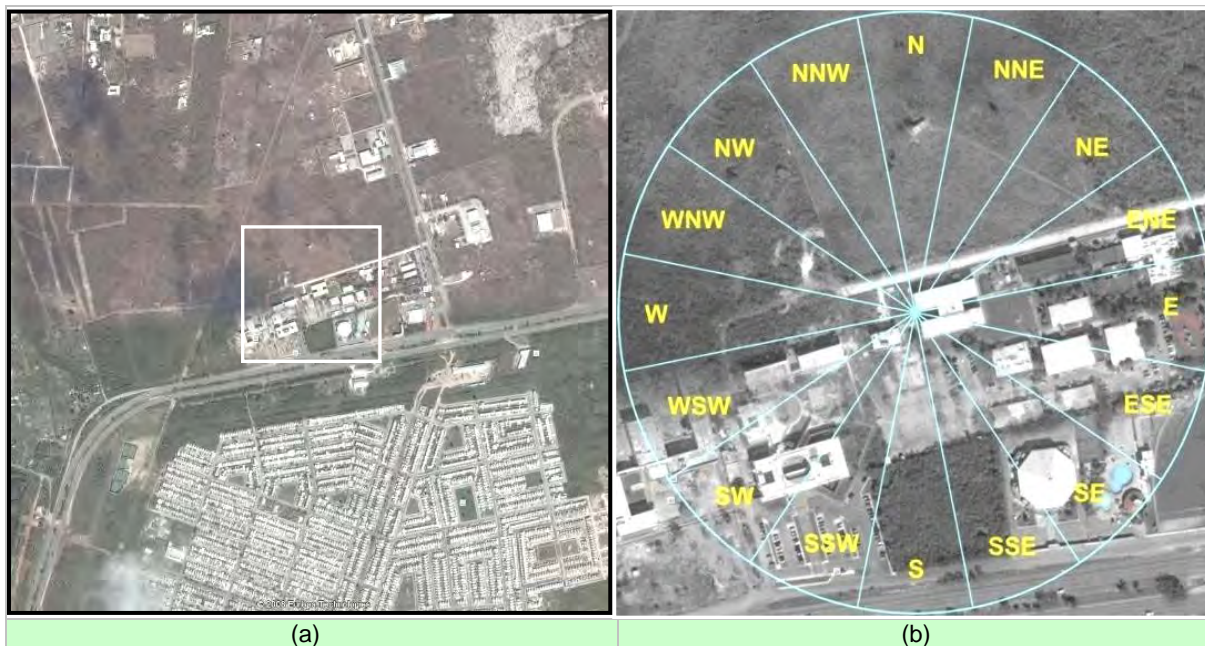


Figure IV.3. Satellite photos showing an aerial view of the measurement site. (a) A square area of 1600m x 1600m (b) a close up of the 400m x 400m area with the directional sectors around the measurement tower.

Sixteen directional sectors have been drawn in Figure IV.3(b) to identify the angular position of the main obstacles relative to the measurement tower. Figure IV.4 shows panoramic views of the four main regions that surround the measurement tower. These regions were defined considering the position of the main group of obstacles and the results presented in the following sections. The photos show a view as seen from the sensors installed at 10m a.g.l. on the measurement tower.



Figure IV.4. Panoramic views of the terrain surrounding the measurement tower grouped in four main directions.

Due to the number of obstacles close to the tower, the analysis is concentrated on the relative wind shear observed rather than absolute wind speed values. It is assumed that for the purposes of assessing wind energy potential at wind turbine hub height that, as mentioned in the theoretical background, the wind profile in the atmospheric surface layer is commonly described by the Monin-Obukhov similarity theory [76], which predicts an extended log-linear form shown in equation I.1. It describes the wind speed u at a particular height z as function of the friction velocity u_* , the roughness length z_0 and the Obukhov length L . Different models have been proposed to compute the parameters in the equation I.1 which usually involve the measurement of the ambient temperature at two different heights.

In this case, temperature measurements were only available at one height. In addition equation I.1 requires estimates of the surface roughness which are quite complex to infer with buildings in the immediate vicinity of the mast. The main item of concern here is the wind shear observed at the mast from the wind speeds measured at two heights and thus the empirical power law is used as given in equation I.8 to calculate the wind shear exponent (α).

In the case presented in this chapter $z=30\text{m}$ and $z_r=10\text{m}$, thus equation 1.8 can be expressed as:

$$\alpha = 2.0959 \cdot \text{Log} \left(\frac{u(30)}{u(10)} \right) \quad \text{IV.1}$$

IV.3 Directional behaviour

The distribution of the wind over 16 direction sectors is presented in Figure IV.5(a) for all of the data available in the study period. The majority of the winds comes from the sectors clustered around the South and less than 8% of the wind comes from the West to the North-East, which have been shaded in Figure IV.4(a). Therefore in the rest of this chapter, the directions from West to North-East will not be considered.

In order to study the diurnal directionality of the wind at the site, the wind distribution for each hour was grouped in three time periods according the daytime/night-time and rate of change of temperature: 1) from 21:00 to 8:00 for predominantly night-time/negative rate of change of temperature, 2) from 9:00 to 14:00 for predominantly daytime/positive rate of change of temperature and 3) from 15:00 to 20:00 for predominantly daytime/negative rate of change of temperature. The resulting wind distributions for the three time periods have been plotted in Figure IV.5(b) along with the wind distribution for the whole day (denoted 00:00 to 23:00). It can be seen that during the night, the wind comes over the land from around the South, and during the morning, the contribution to the wind is greater from the South to the South-West while in the afternoon the contribution from the East to the South-East are greatest. This behaviour is fairly typical of a coastal site where the winds are thermally driven and a land-sea breeze develops during the day.

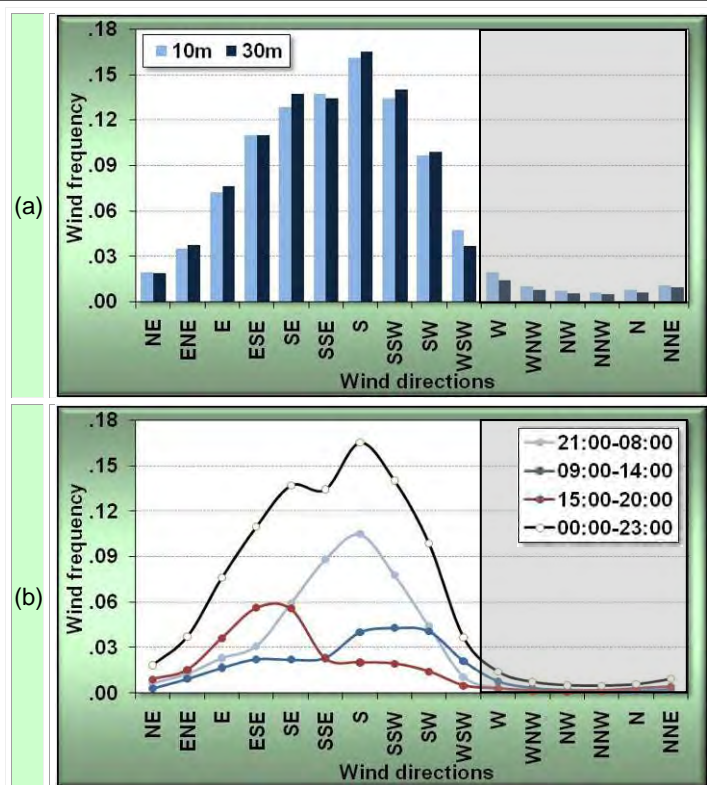


Figure IV.5. (a) Wind frequency distribution for each directional sector over the whole study period and (b) the contribution to the whole wind distribution of the three main diurnal periods.

The wind speed average for each direction, see Figure IV.6, shows that the highest wind speeds are located between the East and South-West direction sectors. As might be expected, the largest differences in wind speed measured at 30m and 10m a.g.l. were also located in the directions with the highest wind speeds reflecting the effect of the buildings which tend to reduce the wind speed at 10m a.g.l. but give some degree of acceleration at 30m a.g.l. (see the location of the obstacles in Figure IV.3(b) and Figure IV.4(a)). This result makes evidence the role of wind shear as a measure of the percentage of increase of the wind with the height, as will be study in the following sections.

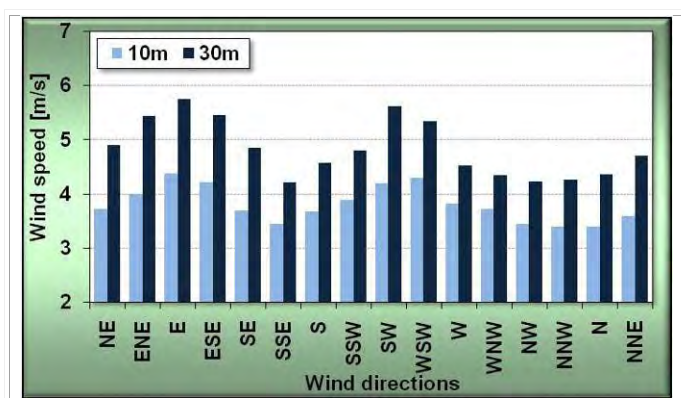


Figure IV.6. Wind speed averages over the whole study period for each direction sector.

Generally, the wind shear over a relatively flat surface with short vegetation can be computed by the one-seventh power law, i.e. $\alpha=0.14$ in equation I.7. For the study site, as was

expected because of the surroundings, the wind shear average computed, using equation IV.1, over the whole study period was 0.21 varying between 0.17 and 0.26 over the different direction sectors as shown in Figure IV.7. Notably, the largest and closest region of buildings located from the NE to the SE (NE-SE) gives rise to wind shear averages above 0.22 while the region with fewer and further obstacles from the SSW to the WSW (SSW-WSW) gives rise to wind shear averages above 0.19. There is a small region, from the SSE to the S (SSE-S), and a larger region, from the WSW to the NNE, giving wind shear averages under 0.19 corresponding with regions where there are no obstacles close enough to the measurement tower to have an appreciable effect, as can be in Figure IV.3(b) and Figure IV.4. The wind shear averages in Figure IV.7 are not significantly influenced by the obstacles with average heights under 10m located further than 300m away (ten times the height of the measurement tower), namely: the large region of buildings to the South and another group of buildings located to the North, see Figure IV.3(a) and Figure IV.4. The main influence on the wind shear comes from the closer obstacles.

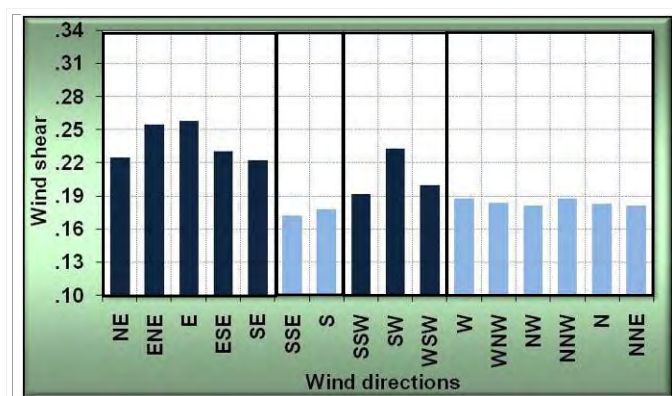


Figure IV.7. Wind shear averages over the whole study period for each direction sector.

Frequently in the literature [34,35,36,37] an average based analysis is used to evaluate the wind shear patterns but, as was reported by Kirchhoff and Kaminsky [39], basic errors could be obtained as result of the deterministic property of the wind shear computed from the power law. On the other hand, different stability conditions could be present in the atmosphere over the study period introducing unexpected values of wind shear. Thus, as the stability of the atmosphere cannot be derived from the data available in this research, the frequency distribution of the wind shear was computed to shed further light on the range of wind shear values.

The wind shear computed from the 10-minutes data was grouped by bins of size 0.05 before to be normalized to obtain the frequency distribution of the wind shear over all the directional sectors, see Figure IV.8. As can be seen the wind shear values are distributed between -0.2 and 0.6 with a peak at 0.2 which is consistent with the average value of 0.21 previously computed. However, it is noticeable that there is a significant range of wind shear values

observed which cannot be explained by differing roughness conditions by direction. Clearly, the effect of atmospheric stability is significant conditioning different rate of turbulence.

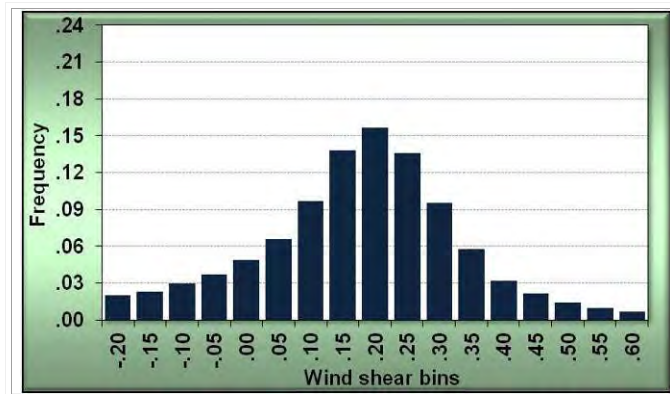


Figure IV.8. Frequency distribution of the wind shears over all directions.

IV.4 Diurnal behaviour

The diurnal wind speed behaviour is shown in Figure IV.9(a). Three particular features are notable: a period of reduced wind speed at night, an abrupt increase in the wind speed early in the morning followed by fairly constant wind speeds during the early afternoon and finally a peak in the wind speed during the late afternoon/early evening. In general terms, this diurnal pattern is consistent with results for other coastal regions, e.g. by Barthelmie et al. [34] in the marine environment of Denmark, by Farrugia [36] for Malta and by Rehmana and Al-Abbadib [37,38] in the Gulf region of Saudi Arabia.

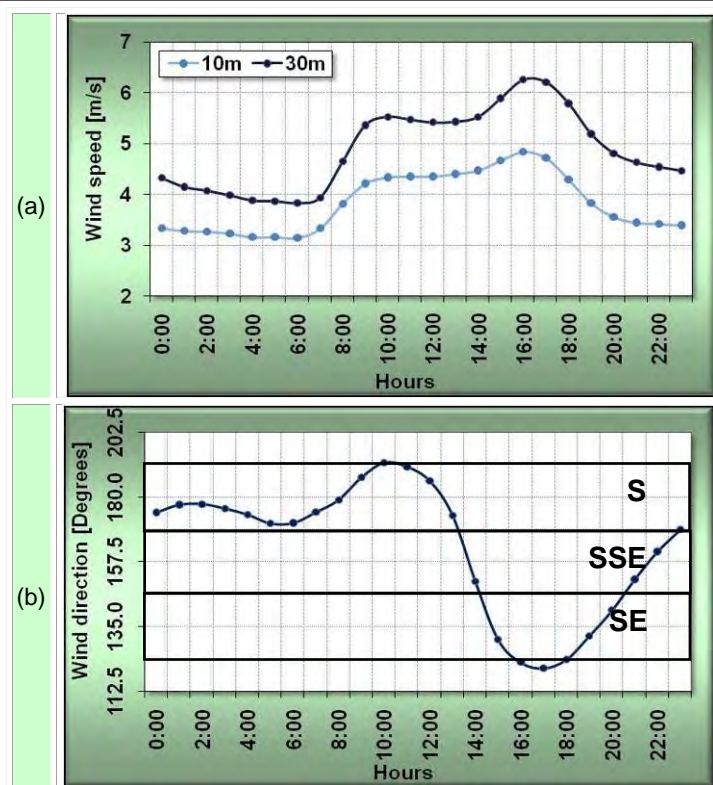


Figure IV.9. (a) Hourly wind speed averages and (b) hourly wind direction averages, computed for the whole study period.

In addition, the hourly average wind direction, shown above in Figure IV.9(b), was divided into two periods: from 23:00 to 13:00 with averages in the S sector and from 14:00-22:00 with average directions in the SE and SSE sectors. For both of these periods the wind is blowing from the landward direction; see Figure IV.1(b), which is not enough to explain the daily pattern shown by the wind speeds in Figure IV.9(a). To give more information, the distribution of the wind in each direction for the diurnal periods was computed, see Figure IV.10 below. The higher concentration of winds during the time period (21:00-8:00) came from the SE to the SW sectors, which is from the land area of the Yucatán Peninsula. Then, during the time period (9:00-14:00) the sun was rising and a larger fraction of the winds was coming from the SSW to the NNW sectors, which is from the West of the Gulf of México. Finally, during the time period (15:00-20:00) when the sun is setting, the winds were clearly concentrated in the NNW to the SE sectors from the North-East of the Gulf of México and the East of the Caribbean Sea, see maps in Figure IV.1.

In summary, the wind speed patterns in Figure IV.9(a) show wind mainly coming from the sea during the daytime and from the land during the night time. This is the standard pattern observed for sites close to the coast where the climate is determined not only by vertical thermal convection [79] but also by the horizontal movement produced by thermal circulation of the sea breeze [29,80]. However, in this case, a particular characteristic is seen for the daytime which shows two different sea regions driving the winds in different daylight periods and with different wind speed magnitudes.

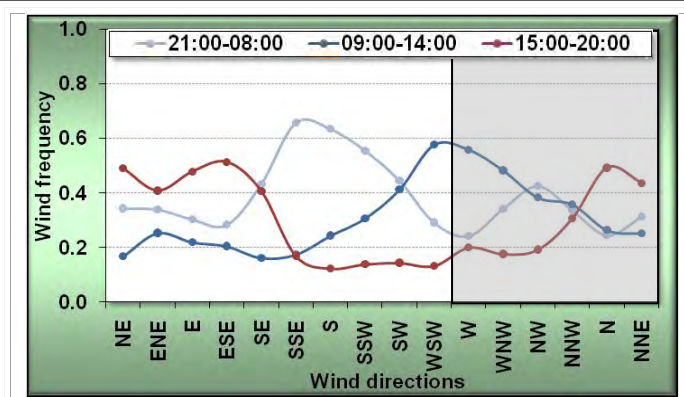


Figure IV.10. Distribution of the wind by directions, for the three main diurnal time periods. The shadowed region marks the directional sectors with less than 1.5% of wind over the whole study period, see distributions in Figure IV.5.

The diurnal pattern of the wind shear along with the ambient temperature averages are shown in Figure IV.11. The resulting pattern can be explained by means of the wind shear averages for each direction presented in Figure IV.7 and the distribution of winds for the three main diurnal time periods from Figure IV.10, excluding the low frequency region (W-NNE). During the night time (21:00-8:00) the wind comes mainly from the SSE-S with lower wind shear averages, whereas during the morning (9:00-14:00) the main wind from the SSW-WSW gives rise to an increase in the wind shear averages and finally during the afternoon (15:00-20:00) the wind from the NE-SE dominates with the highest wind shear averages. The wind shear observed in these cases results from the combined effect of the location of the main obstacles; see Figure IV.3(b), and from the thermal effects over the land and the sea around the measurement site.

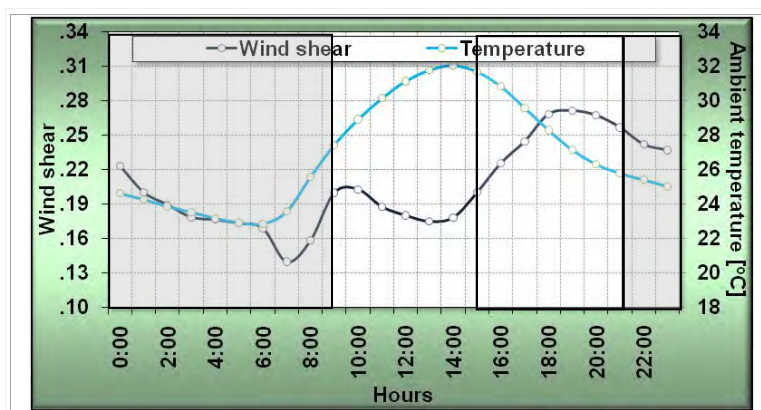


Figure IV.11. Diurnal pattern over the full study period for the averages of wind shear and ambient temperature.

Figure IV.12 below show the diurnal pattern for each season of the averages for the ambient temperature and the wind shear. It can be seen that with some degree of dispersion, the spring, summer and autumn patterns describe the same pattern presented above in Figure IV.11. In the case of the winter season, the distribution of lower temperatures create more

stable conditions in the atmosphere which condition a wind shear pattern dominated by diurnal cycles with higher values over the night than over the daylight times.

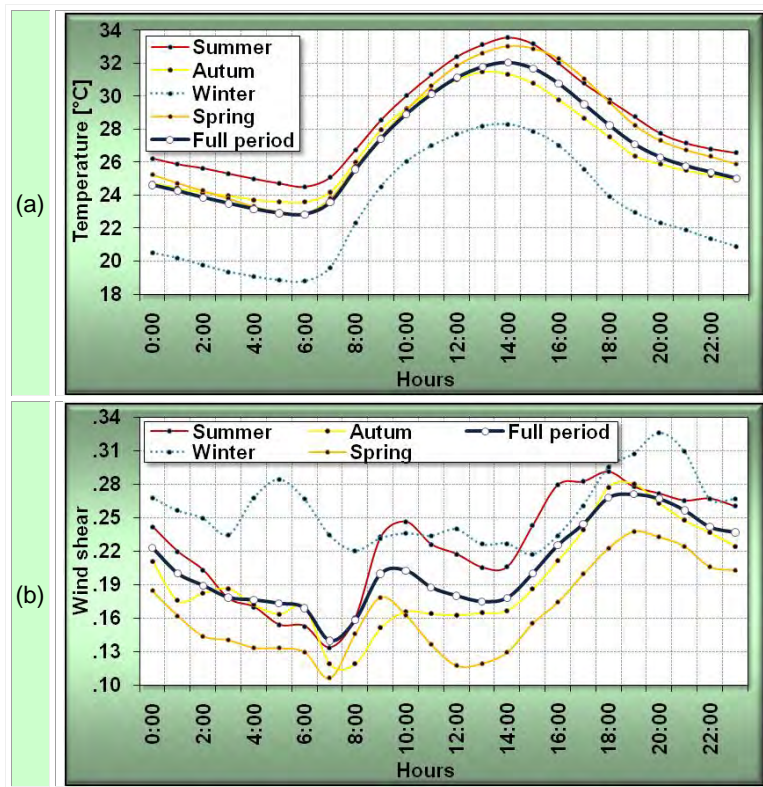


Figure IV.12 Diurnal pattern for each season for the averages of ambient temperature (a) and wind shear (b).

Figure IV.13 below shows the frequency distribution of the wind shear over the whole study period classified by the three main diurnal time periods. It can be seen that the night time (21:00-8:00) period gives the greatest spread of values indicating a larger range of stability conditions. In contrast, during the daytime (9:00-14:00 and 15:00-20:00) the distribution is more centred around 0.20 which could indicate stability values closer to neutral.

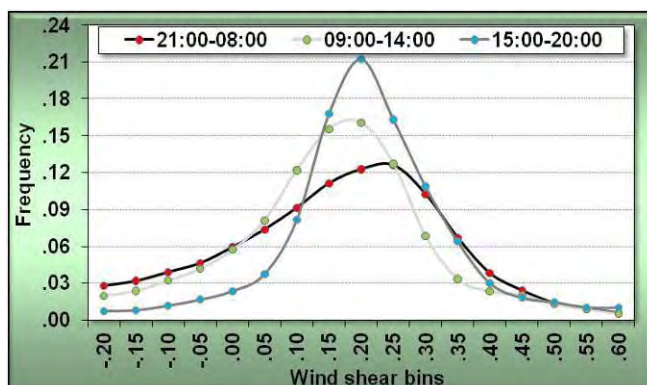


Figure IV.13. Frequency distribution of the wind shear for the three main diurnal periods.

Thermal effects

At this site, temperature measurements were only available at one height so it was not possible to calculate the Obukhov length L in equation I.1 to determine whether the change in the observed wind shear was consistent with that seen from the wind speed measurements. As an alternative, the rate of change of temperature at one height was used as a proxy for the stability. The data from Figure IV.8 was used to plot the wind shear as a function of rate of change of temperature $\Delta T/\Delta t$. Where ΔT is the temperature difference between the two consecutive instance represented by Δt . These results are shown in Figure IV.14.

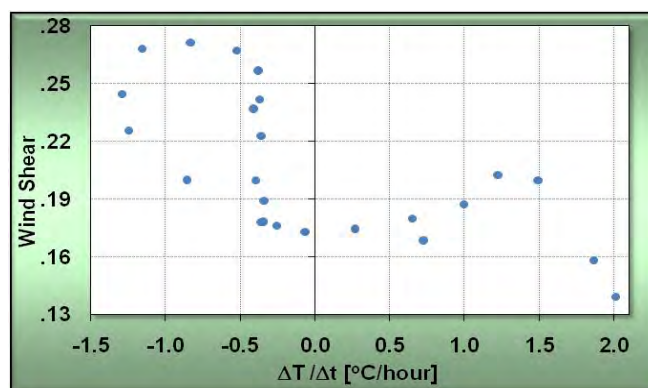


Figure IV.14. Wind shear as a function of rate of change of temperature.

It can be seen from Figure IV.14 that there is a clear trend whereby the wind shear decreases as the rate of change of temperature increases, though clearly there is some degree of scatter in the data. Negative values represent cooling which lead to stable conditions. This inhibits vertical mixing and leads to an increase in wind shear as expected. Positive values relate to heating and convection from the ground leading to unstable conditions. This increases mixing and reduces wind shear which is again what would be expected. In addition, the sensitivity of the wind shear to stable conditions is greater than that for unstable conditions. This is consistent with the Businger-Dyer relations [81,82] which, when integrated, give the diabatic term \square_n in equation I.1. Though further investigation is required and the lasso in Figure IV.14 reveals some influence of the surroundings, it is proposed that for a climate where strong diurnal heating and cooling is observed, the rate of change of temperature may be used as a proxy for vertical temperature gradient to infer atmospheric stability.

IV.5 Seasonal behaviour

The seasonal pattern of the wind speed can be seen in Figure IV.15(a) showing that the wind reaches its maximum in March and its minimum in September. Figure IV.15(b) shows that the monthly wind direction averages are close to the SSE for much of the year except for

May and June when the wind comes more from the South and during December when the wind comes more from the SE.

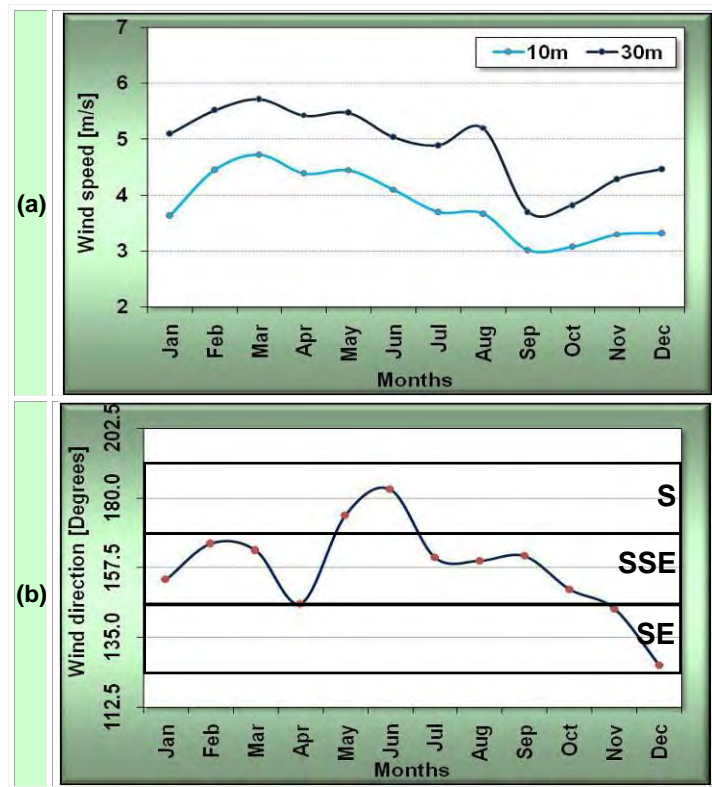


Figure IV.15. (a) Monthly wind speed averages and (b) monthly wind direction averages computed for the whole study period.

Figure IV.16 below shows the annual temperature pattern which has a double peak produced by a decrease in the ambient temperature during the rainy season in June, July and August. The wind shear shows an increase in the winter months which is consistent with cooler stable conditions and is lower in the summer when warmer convective conditions dominate. The exception to this is during the rainy season, particularly during July and August.

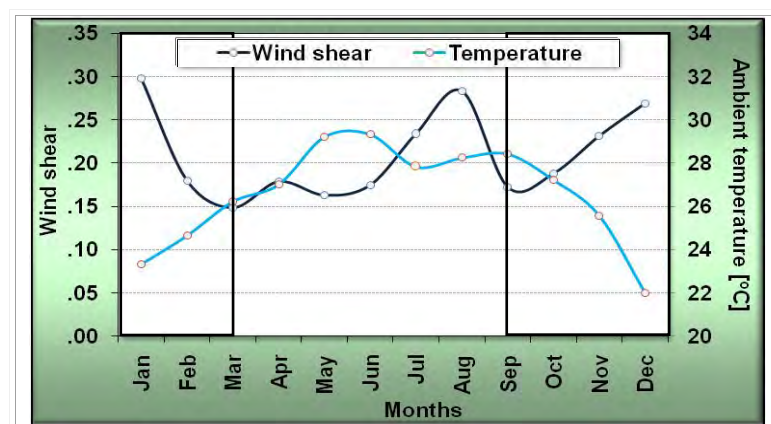


Figure IV.16. Combined plot of the monthly averages for the wind shear (left axis) and the averages of the seasonal ambient temperature (right axis).

During this period, an abrupt increase in the wind shear is seen. To shed further light on this, the frequency distribution of the wind shear for these two months and for the months where the minimum (March) and maximum (January) wind shear value are observed, is shown in Figure IV.17. The January and March distributions are fairly peaked while the distributions for July and August are more widely spread. It is clear that during the rainy season, a wider range of climatic conditions is observed and it is likely that the cloudier conditions are inhibiting ground heating and convection thus increasing the observed wind shear.

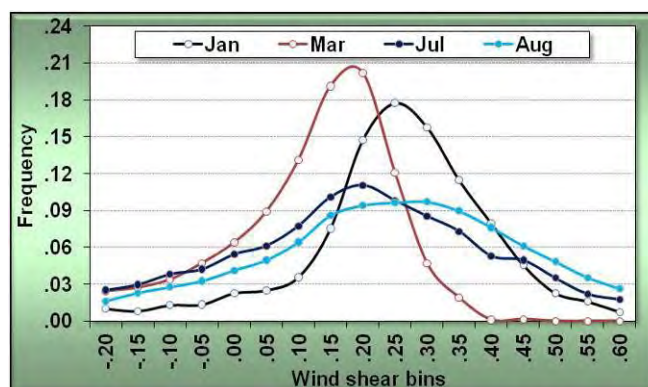


Figure IV.17. Wind shear frequency distributions for the months January, March, July and August.

IV.6 Remarks

Wind speed and wind shear patterns have been studied for a site at the Autonomous University of Yucatán which experiences the tropical conditions of the north Yucatán Peninsula of western México. Simple averaged values were found to be inadequate in describing the wind shear characteristics at the site in question. An analysis based on direction and frequency distribution proved to be more effective in describing the vertical wind profile.

Night time diurnal wind speed variations were identified with characteristics as expected for near coastal sites with lowest wind speeds blowing from land to sea. In contrast, during daytime, the higher winds coming from over the sea exhibit particular characteristics that reflect the two rather distinct fetches of offshore sea. At sunrise the wind tends to come from the west part of the Gulf of México while towards sunset, the highest wind speeds come from the north-east of the Gulf of México and the east of the Caribbean Sea where sea temperatures are rather different.

An analysis of the rate of change of temperature showed a correlation between wind speed and rate of change of temperature reflecting stable conditions during periods of cooling and unstable conditions during periods of heating. Though more data would be required to investigate this further, it is proposed that rate of change of temperature may be used as a proxy for vertical temperature gradient to infer atmospheric stability when temperature

measurements are only available at one height, particularly where winds are dominated by thermal conditions.

The seasonal characteristics of the wind shear appear to be mainly driven by the temperature changes with some anomalous values during the rainy season which reflect cooler conditions and lower levels of convection.

In summary, the study illustrates that a complex coastal environment, as provided by the proximity of both the Gulf of México and Caribbean Sea with their different sea conditions, can result in unusual wind characteristics, and in particular, non-standard diurnal wind variations and shear profiles.

At this stage, three different dimensions of the wind characteristics in the Yucatán Peninsula have been addressed: Temporal (long-term), spatial (short term, horizontal) and vertical wind profile (inland). Considering, the results presented in chapter III for the buoys in the surroundings seas, which reveals high wind patterns, and the current importance of the offshore wind power for the future use in the Yucatan Peninsula; the next chapter will present a comprehensive study of the wind characteristics in a site located offshore of the North coast of Yucatán Peninsula.

V Offshore wind characteristics

In order to complete the analysis of the wind characteristics for the Yucatán Peninsula, this chapter presents a study of the properties of the offshore wind close to the North coast of the Yucatán Peninsula. Around two years of measurements were recorded using a communication tower installed on a pier which extends 6.65km from the coast. The results show that the offshore wind is thermally driven by differential heating of land and sea producing sea breezes which veer to blow parallel to the coast in the late afternoon under the action of the Coriolis force. Most measurements of wind speed and temperature suggested largely unstable conditions, yet the observed shear was greater than that predicted using standard Monin-Obukhov theory. To investigate further, a dataset of sea surface temperatures derived from satellite thermal maps was combined with the onsite measured data to study stability measures at different measurement heights. The results potentially suggested the development during the day of a shallow Stable Internal Boundary Layer which occurs when warm air from the land advects over the cold sea.

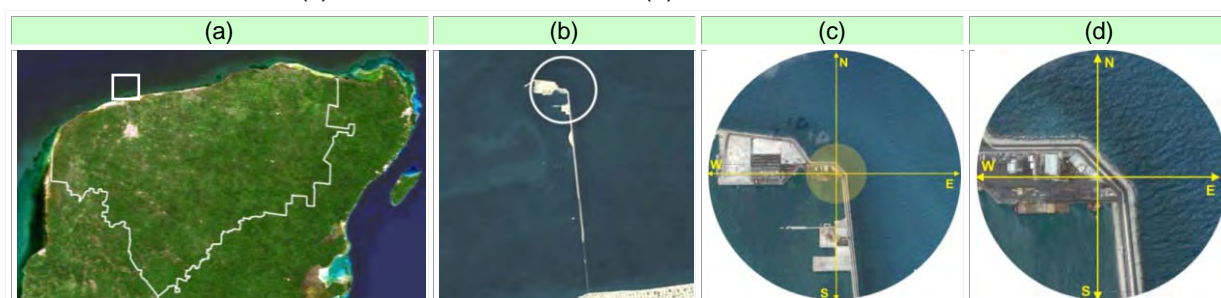
V.1 Introduction

In the previous chapters the temporal, spatial and vertical wind characteristics were studied for sites located inland and onshore of the Yucatán Peninsula. Also, a preliminary analysis of the winds for the Caribbean Sea and the Gulf of México was presented in chapter III section III.6 to support the analysis of these wind patterns. In order to complete the evaluation of the wind characteristics, this chapter presents a study of data recorded over a period of around two years 6.65km offshore of the North coast of the Yucatán Peninsula. The data were recorded using a 25m height communication tower installed at the end of a long pier that runs almost perpendicular to the shoreline. These data were analysed in order to study the characteristics of the wind speed and direction as well as the wind shear at the site and how it varied as a function of atmospheric stability.

V.2 Site description

The site that was available for the offshore study in this research project is located at the end of the “Progreso” pier. This pier extends 6.65km into the Gulf of México from the North shore of the Yucatán Peninsula with geographical coordinates: 21°20'45.18”N, 89°40'17.32”W. The mast erected on this pier that was available to this study will be referred to as the API tower. Table V.1 below shows satellite images of the pier and the location of the measurement tower close to the end of the pier on its east side.

Table V.1 (a) Location of the “Progreso” pier in relation to the Yucatán Peninsula, (b) location relative to the North shore, (c) One kilometre radius and (d) 250m radius around measurement tower.



The terrestrial view of the API tower in Table V.2 shows a solid cylinder, located above the pier surface, of 1m diameter at the tower base and 70cm at the top of the tower. An autonomous monitor system including sensors, a data-logger and a remote communication device was configured, installed and operated as part of the PhD research project. The relative position of the sensors, wind and air temperature, as well as the surroundings is also shown in Table V.2.

Table V.2 Different terrestrial views of the measurement tower showing the location of the tower on the pier and the position of the sensors on the tower.



Surrounding panoramic views are presented in Table V.3 below around the North, South, East and West directions. These images were taken from the top of the tower at 25m height and reveal an almost clear fetch for the wind coming from the East and North directions. A long road (around 6.65km) is located in the South direction and an area of approximately 1km long by 500m wide covered by isolated buildings of up to 4m height is located to the West.

Table V.3 Panoramic views of surrounding areas taken at 25m height above the pier surface.

	Upper view	Side view around the tower from 25m height
North		
East		
South		
West		

V.3 Onsite measurements

The parameters measured by the sensors installed on the API tower are listed in Table V.4 below. The sensor heights are given relative to the base of the API tower mounted on the pier surface. These sensors were installed on a boom at a distance of at least 1.5m from the side of the tower.

Table V.4. Measurement parameters.

	Parameter	Unit	Sensors height a.g.l. [m]
Orthogonal Ultrasonic anemometer Gill WindSonic 2-D	Wind Speed	m/s	10 and 25
	Wind Direction	Degrees	10 and 25
Vaisala CS500	Temperature	°C	10 and 25

Table V.5 shows the main operational characteristics of the installed sensors. The orthogonal wind sensor is a digital one which measured variations in the speed of two perpendicular ultrasonic beams to infer the wind speed and wind direction on the sensor plane. More details of all the sensors and devices installed as well as a scheme of the whole measurement system can be seen in Appendix VIII.2 .

Table V.5. Summary of the main sensor characteristics

Characteristics	Sensors		
	Wind Speed	Wind Direction	Air Temperature
Measurement Range	0 – 60m/s	0 – 360°	- 5°C to 95°C
Operation Temperature	-35°C to 70°C	-35°C to 70°C	- 5°C to 95°C
Uncertainty	±2%	±3°	±0.2°C
Resolution	0.01m/s	1°	0.1°C

The measurements were taken during 23 months starting in August 2007. A total of 87470 10-minute averaged values were available after filtering for measurement errors. Figure V.1 show the data available for each month over the whole measurement period. As can be seen, less than the 50% of the data were available during May and July due to maintenance problems at the end of the first year of measurement.



Figure V.1. Data availability by month over the whole measurement period.

V.4 Effects of the solid mast on the measurements

In order to evaluate the effect of the solid cylindrical tower on the measurements made at API mast, a second lattice tower (API2) located approximately 50m from the API tower was configured with two sets of wind and air temperature sensors, see Table V.6 (a) and (b) below. One set of sensors was installed at 10m height and the other one at 16.5m height which was the highest available position on the API2 tower, see Table V.6 (d). For this reason, an additional set of wind and air temperature sensors was also temporarily installed at 16.5m height on the original API tower, see Table V.6 (c). The sensors installed had the same operational characteristics as those installed on the API tower, see Table V.5.

Table V.6 (a) Locations of API and API2 towers. (b) A view of API2 from API tower. Sensors position on API (c) and API2 (d) masts.

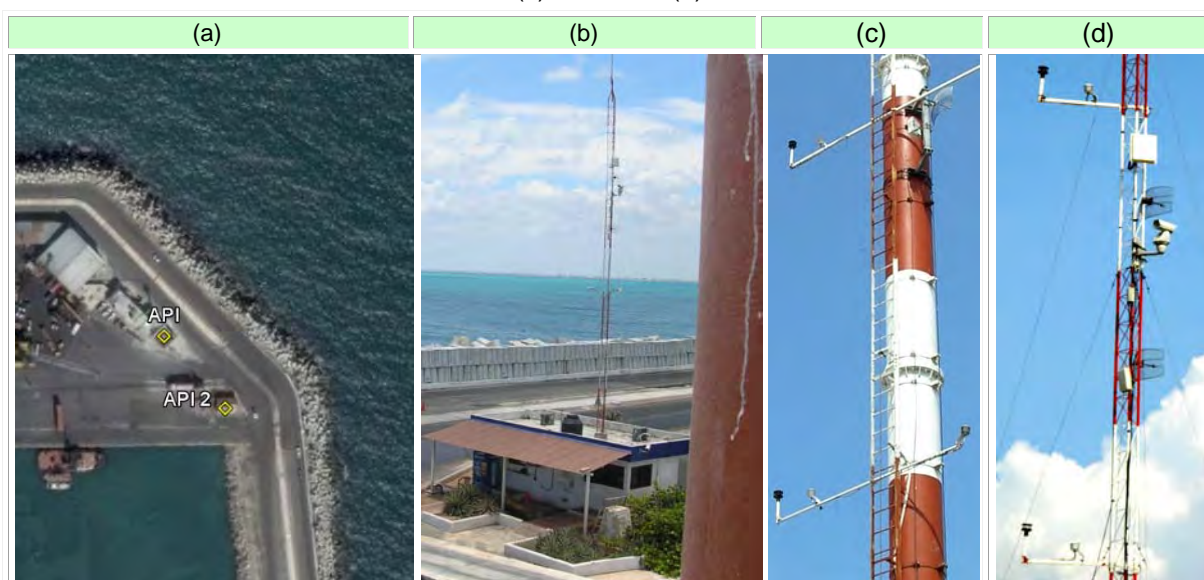
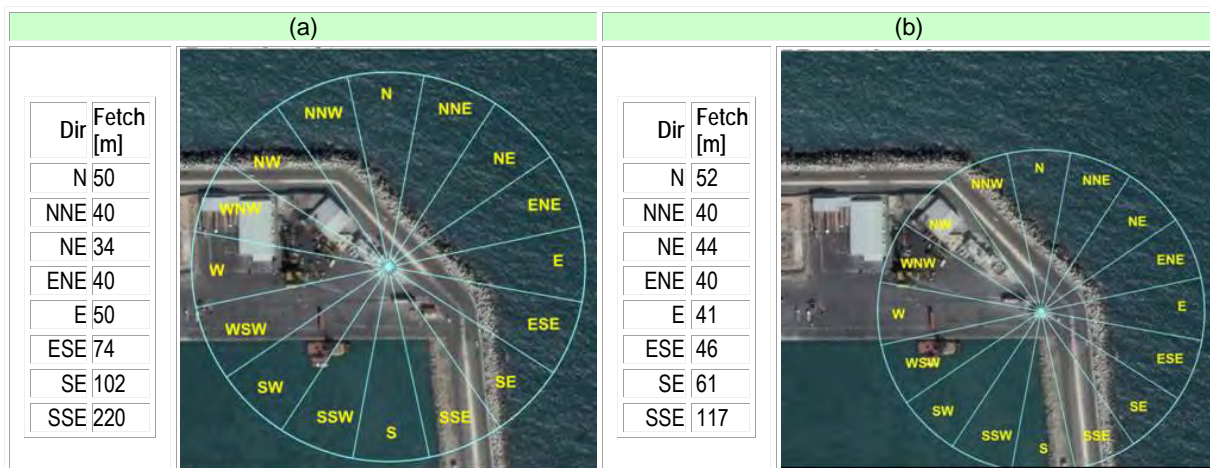


Table V.7 below shows the fetches (distances from mast to pier edge) for the main directional sectors for both measurement towers. These directional sectors, as can be seen in section V.5 , contained the majority of the winds observed during the study period.

Table V.7 Distance from the mast to the edge of the pier (fetch) at (a) API and at (b) API2 for each directional sector.



During 20 days, between 27/05/2009 and 15/06/2009, 2465 measurements of 10 minute averages of wind speed and air temperature were simultaneously measured at 10m and 16.5m heights on both towers API and API2. Figure V.2 and Figure V.3 show scatter plots of the data measured simultaneously on the two towers with a line of best fit shown in each case.

Figure V.2 shows that there was a relatively poor correlation between the wind speeds measured at 10m height but that the correlation coefficient increased significantly at 16.5m height. As the characteristics of both towers are the same at both measurement heights, the low correlation at the 10m height is not produced by the structure of the towers but by the surrounding conditions, see Table V.2 and Table V.6, or by different atmospheric conditions at the two measurement heights.

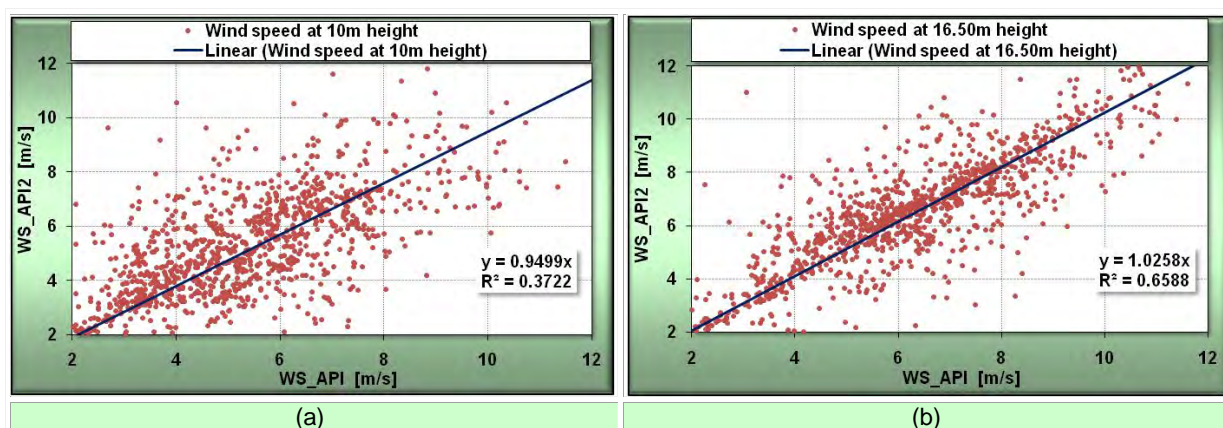


Figure V.2. Correlation between the ten minute averages of wind speed at API and API2 for both measurement heights: (a) 10m and (b) 16.5m.

Figure V.3 shows the air temperature correlation. It can be seen that there is no significant difference between the slope and the correlation coefficient at both heights. This would indicate the temperature measurements at the two masts were consistent.

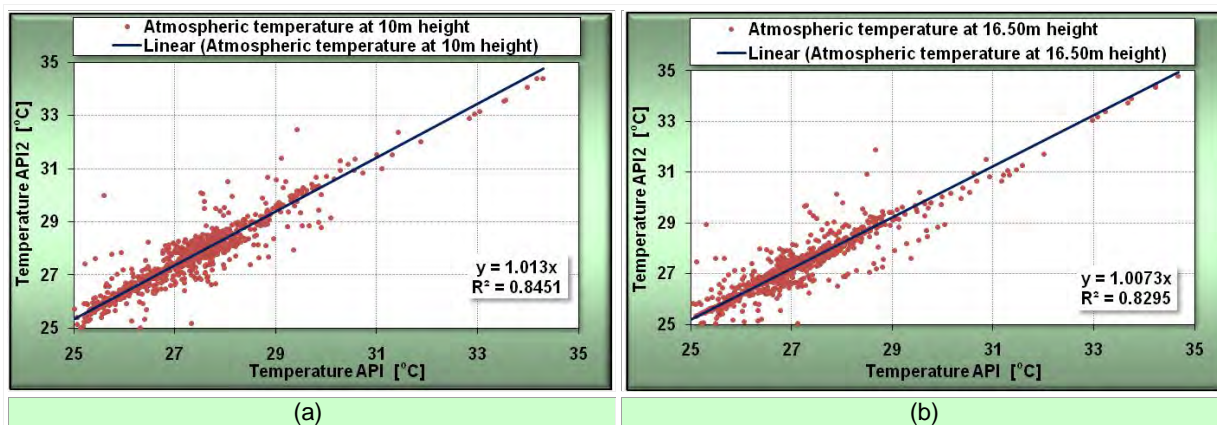


Figure V.3. Correlation between the ten minute averages of air temperature at API and API2 for both measurement heights: (a) 10m and (b) 16.5m.

V.5 Wind speed patterns

In this section, the results of the statistical analysis applied to the ten-minute averages for the wind speed will be presented. Firstly, the distribution of the data measured in directional sectors is studied on three different time scales: over the entire study period, by season and by time of day. Then, in the following two subsections, the averages of the wind speed data and the frequency distribution of the measured wind speeds are presented by direction sector, season and time of day.

Directional distribution of the measurements

The distribution of the direction data using 22.5 degree bins to cover 16 directional sectors is shown in Figure V.4. The symbol “lo” will represent the 10m height and “hi” will represent 25m height in the next figures of this chapter unless any other meaning is specified.

Figure V.4(a) shows that the winds at both measurement heights are mainly distributed in a region from the N to the SSE sectors, in a clockwise direction. The sectors outside of this region receive just less than 1% of the winds available. The majority of the wind direction distribution is clustered around a principal maximum in the NE-ENE sectors and around a secondary maximum in the ESE-SE sectors.

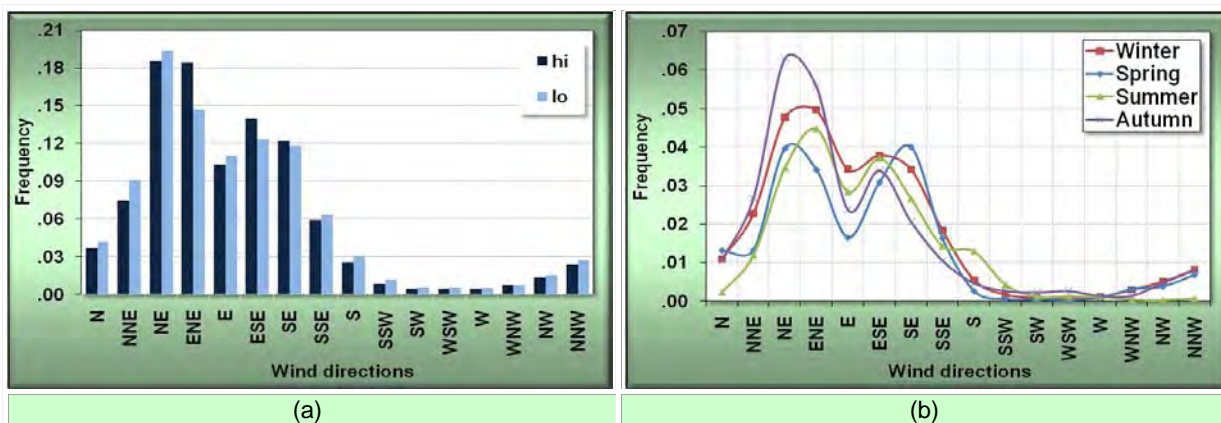


Figure V.4. Frequency distribution by direction of the measurements over the whole study period: (a) at both measurement heights and (b) during every season for the “hi” height measurements.

In Figure V.4(b), the months were grouped by season: Winter (December, January and February), Spring (March, April and May), Summer (June, July and August) and Autumn (September, October and November). Then, frequency distributions were grouped on a single chart of plots in order to simplify the comparison among the four seasons. The distribution of wind direction for each season at the “hi” height shows that all seasons displayed broadly the same distribution shown in Figure V.4(a) but there is some variation in the fraction of measurements in the NE-ENE sectors, with the greatest number seen during the Autumn season.

Figure V.5 shows, every three hours during the day, the frequency distributions of the data measured for each directional sector over the whole study period. The time period when the atmosphere goes from cooling to heating is shown in Figure V.5(a) from midnight up to 9:00 in the middle of the morning. The transition between heating and cooling, from midday to 21:00 hours, can be seen in Figure V.5(b).

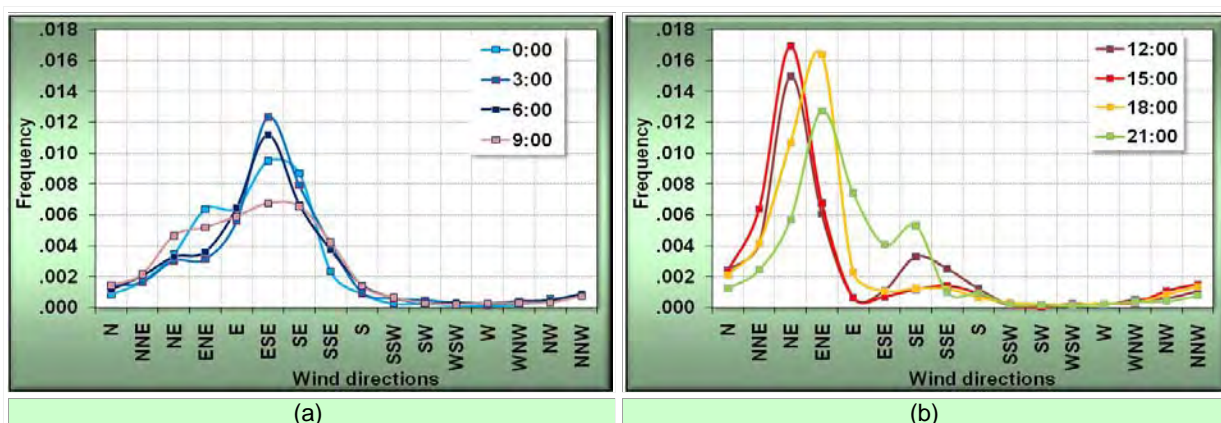


Figure V.5 Directional frequency distributions for the data measured at 8 different hours over the whole study period: (a) from midnight up to before midday, (b) from midday up to before midnight.

Figure V.6 shows the frequency distributions of the main 8 directional sectors, from N to SSE during the diurnal cycle, using the measurements recorded over the whole study period. The distributions for directional sectors between E and SSE shown in Figure V.6(a) represent the

contribution of the winds coming from the land located at the North East of the Yucatán Peninsula, see **Error! Reference source not found.**(a) and Table V.7 (a). The winds coming from the sea located around the North East of the Gulf of México are represented by the directional sectors from N to ENE, see Figure V.6(b).

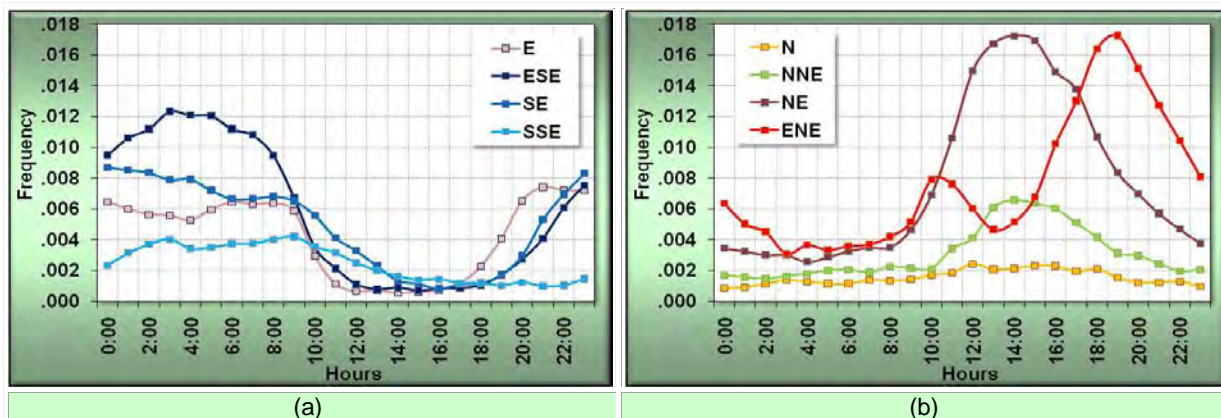


Figure V.6 Diurnal frequency distributions for the main directional sectors over the whole study period: (a) for winds coming from the land, (b) for winds coming from the sea.

Figure V.5(a) and Figure V.6(a) indicate that in the morning the wind is coming predominantly off the land, but this starts to back towards the NE between sunrise and noon. Figure V.5(b) and Figure V.6(b) show that between 12:00 and 15:00 the wind is coming predominantly from the sea. Later in the afternoon and evening the wind veers somewhat so that it is more parallel to the coast. This would seem indicative of a thermally driven sea breeze developing off the North coast of the Yucatán Peninsula which changes direction during the late afternoon as the Coriolis force takes effect.

Figure V.7 below shows a diagram summarizing the hourly periods for the dominant wind in each of the main directional sectors. It can be observed that at 09:00 in the morning, there is a transition period with no particular dominant direction when the land breeze is diminishing and the sea breeze begins to build up.

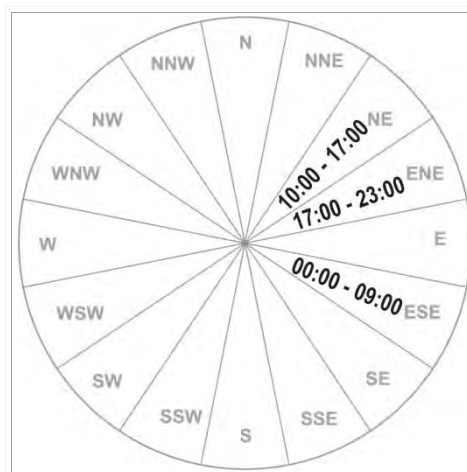


Figure V.7 Diagram for the directions of the dominant wind during the diurnal cycle.

Wind speed averages

The aggregated 10 minute wind speed averages are shown in Figure V.8 (a), (b) and (c) as a function of direction, time of day and month of the year, respectively. The highest wind speeds are seen to come from the ENE direction which also shows the greatest difference between the “hi” and “lo” wind speed averages with approximately 2m/s faster average wind speed at “hi” height. This wind coming off the sea tends to be greater in magnitude than those off the land which probably reflects the lower surface roughness.

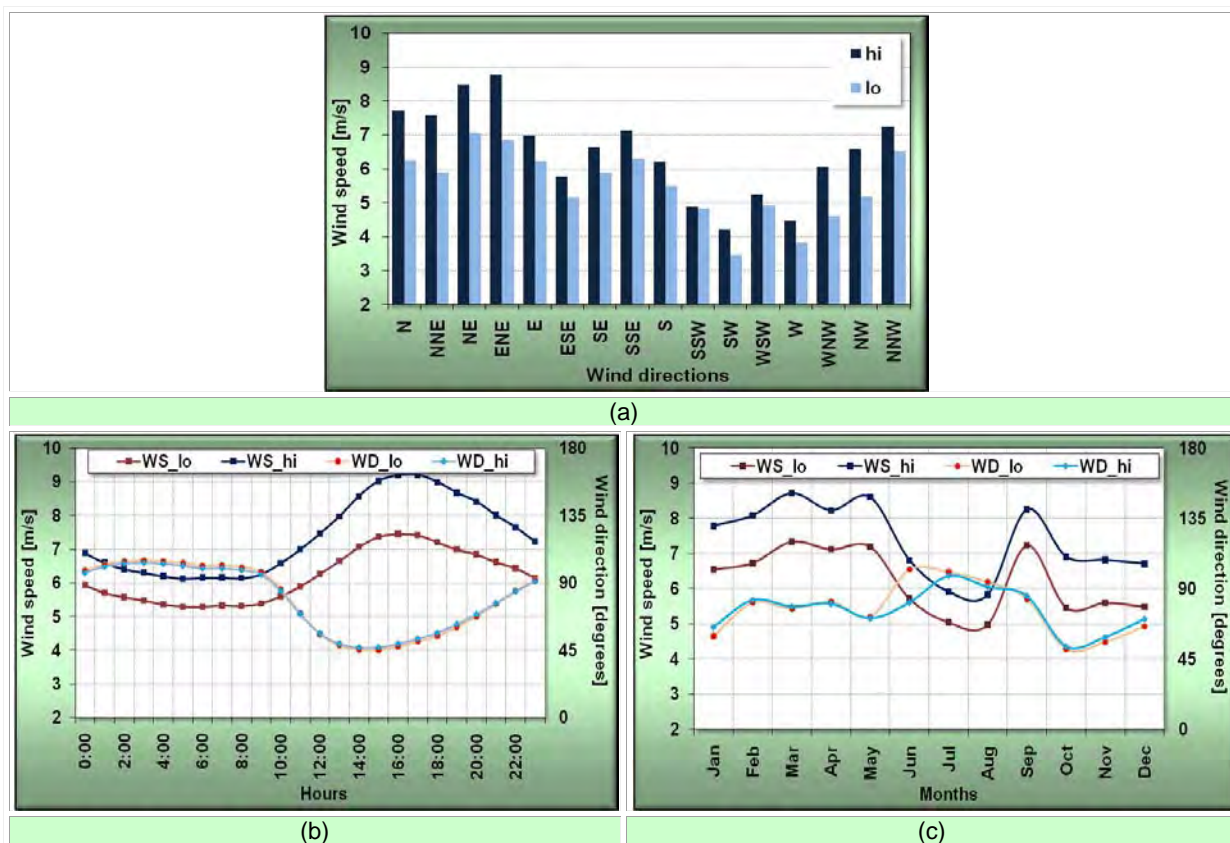


Figure V.8. Wind speed averages over the whole study period for each direction (a), diurnal cycle (b) and seasonal pattern (c).

Figure V.8(b) shows that there is a relatively constant wind speed (WS) and wind direction (WD) from midnight to early morning when the winds are mainly coming from the land around the 90 degree direction, see **Error! Reference source not found.** (a) and (b). From early morning to 14:00 in the afternoon, the winds gradually increase their intensity changing their direction to North East. At 16:00, the maximum speed is reached and the difference between the “hi” and “lo” wind also reaches its maximum. The wind direction then returns to 90 degrees from 16:00 to midnight while the wind speed decreases gradually over this period. This is much like the behaviour at RIO described in Chapter III section III.5.2 reflecting their similar coastal locations. The behaviour seen at these sites represents the combination of thermally driven winds, the effect of the sea-breeze and the effect of surface roughness, where the winds coming over the smoother sea fetch tend to be higher.

Figure V.8(c), shows a decrease in the wind speed in June, July and August; followed by a peak during September and a relatively constant wind speed during the rest of the year. The mean wind direction shows that the highest wind speeds are observed when the wind is coming from the ENE-E and reduce when the winds come from the ESE. This behaviour is again consistent with conditions described in the previous paragraph when analysing the diurnal behaviour.

Frequency distribution of the recorded wind speeds

Figure V.9 shows the wind speed frequency distribution at both measurement heights for the whole study period. It can be seen that almost 60% of the “hi” wind speeds are between 5.5m/s and 9.5m/s.

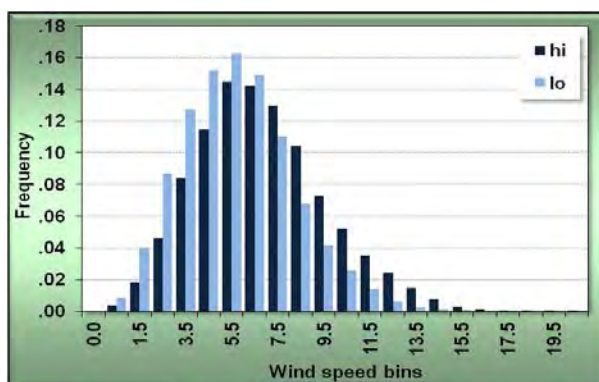


Figure V.9. Frequency distribution of the wind speeds over the whole study period at both measurement heights.

Figure V.10 shows the frequency distribution of the wind speed grouped by direction, time of day and season. In the case of the wind direction, four groups were selected considering the results of the previous chapters and the results shown in Figure V.4(a). Winds coming from the directional group NE-SSE represent more than 73% of the total available winds while less than 2% of the wind comes from the SSW-WSW group, see Figure V.10(a).

The diurnal period was divided into three groups, see Figure V.10(b), based on the behaviour shown by the wind speeds in Figure V.8(b). The period between 15:00 and 20:00 contains the strongest winds distributed around 7.5 - 8.5m/s as can be appreciated from the position of the distribution peak and from the greater proportion of wind located between 9.5m/s and 15.5m/s.

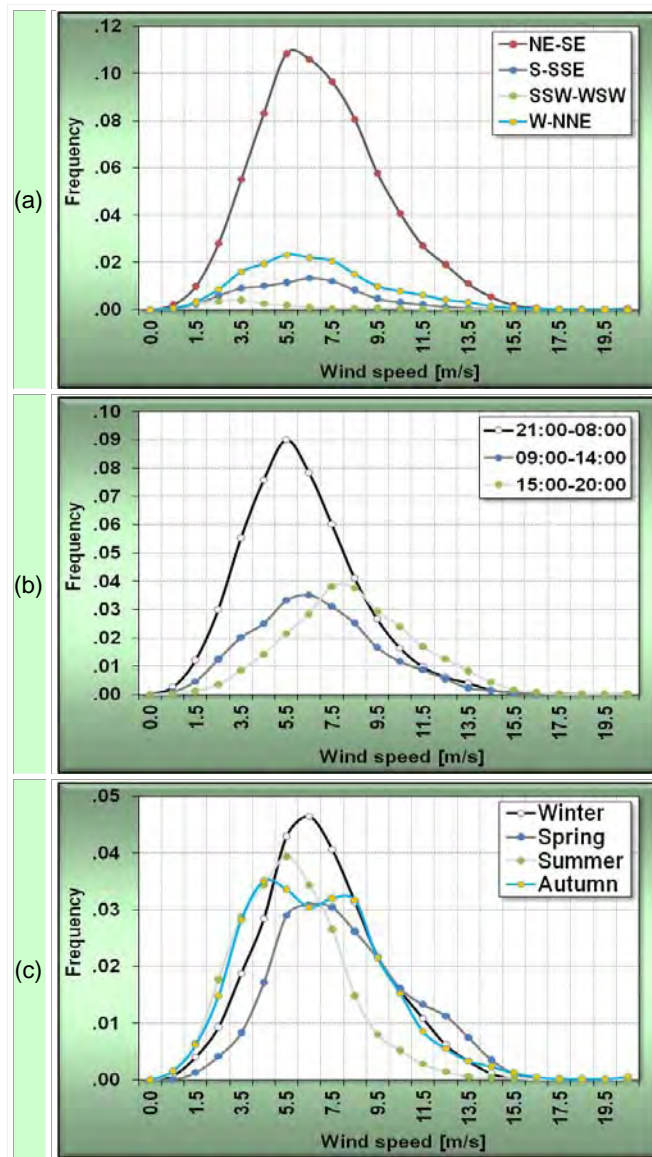


Figure V.10. Frequency distribution of wind speed over the whole study period at the “hi” height: (a) for four directional groups, (b) for three periods within the day and (c) during each season.

The strongest correlation between the wind direction and the diurnal pattern, previously presented, is consistently confirmed by the Figure V.10 (a) and (b). The distributions of wind for each season are shown in Figure V.10(c). The summer shows the weakest winds, whilst the spring season shows a significantly larger fraction of higher wind speeds and the autumn season displays a double-peaked pattern. This double peak generated by the increase in the wind speed in September, see Figure V.8(b), is almost certainly related to the end of the Hurricane season which usually includes a number of high wind speed events coming from the North to North-East sectors which is also confirmed in Figure V.4(b) for the Autumn season.

V.6 Temperature analysis

This section begins with the study of the air temperature originally measured at the API tower at the two measurement heights. Then, the atmospheric stability at the mast is inferred from onsite and remote sensing measurements and discussed. For this purpose, satellite sea surface temperature (SST) data were extracted and combined with onsite measurements. This section concludes by presenting the vertical temperature profile inferred from the measurements.

Onsite air temperature

Figure V.11 shows the average air temperature as a function of time of day and season at both measurement heights over the whole study period. The diurnal pattern in Figure V.11(a) shows a maximum around 12:00 which decreases steadily reaching a minimum at 06:00. A difference of approximately 2°C between the temperature at “lo” and “hi” height is present during the day which on this initial evidence would suggest a very unstable convective boundary layer.

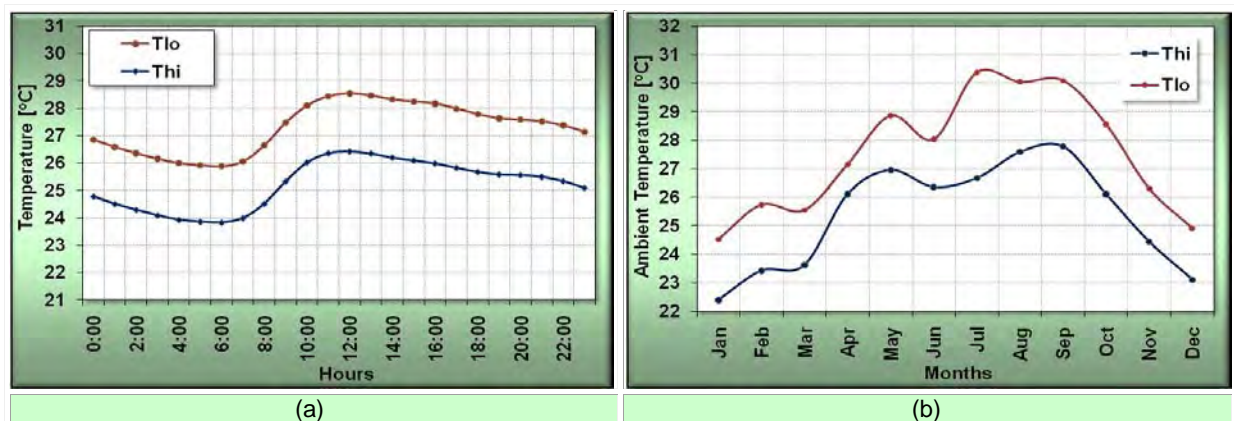


Figure V.11. Average of ambient temperature at both measurement heights: (a) Diurnal pattern and (b) Seasonal pattern

The seasonal pattern in Figure V.11(b) displays the double peak already described in previous chapters, sections II.3 and III.5 which is related to the rainy season in June-July.

V.6.1 Satellite thermal images

The GOES SST data was obtained from the JPL Physical Oceanography DAAC (Distributed Active Archive Centre) [63]. Using a decoding algorithm from NOAA, an application was developed to extract SST data expressed in degree Celsius from binary data format satellite maps. The following steps were implemented:

- Identify the SST map of the Gulf of México region between the Longitudes 80°W and 98°W; and the Latitudes 18°N and 32°N.

- Extract the region immediately around the study area (“Progreso” Pier) between the Longitudes 89.30°W, 90°W; and the Latitudes 21.25°N, 21.70°N containing an array of 18x18 SST data points.
- Extract the closest data point to the API measurement tower: Latitude 21.345836°N, Longitude 89.671496°W.

Table V.8 (a) and (b) show the geographical areas of the Gulf of México and the selected region around the “Progreso” Pier respectively. Their extracted SST images are shown in Table V.8 (c) and (d).

Table V.8 (a) Gulf of México and (b) “Progreso” pier areas with an example of an SST temperature map for each region (c) and (d).

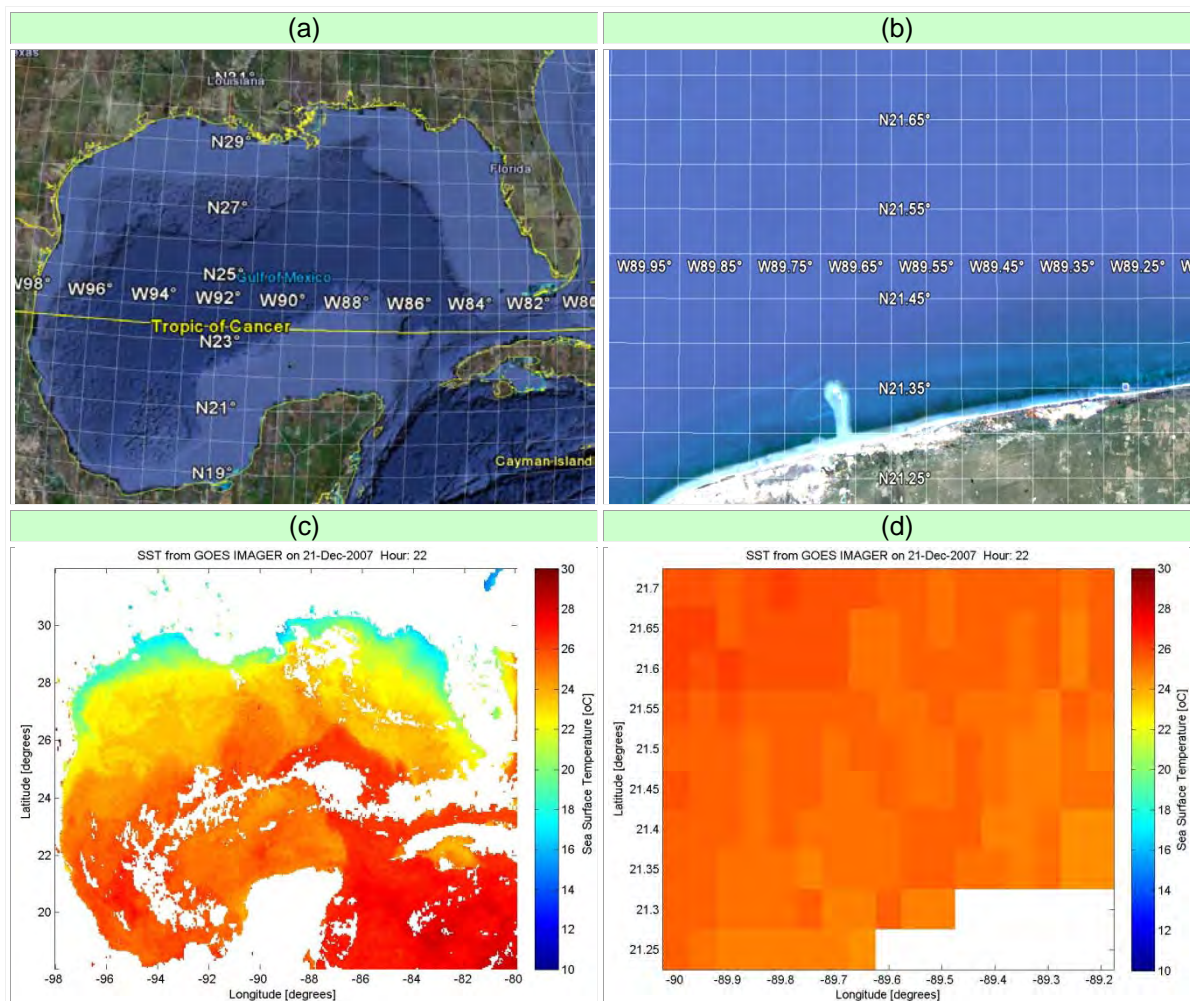


Table VIII.4., Table VIII.5. and Table VIII.6. in Appendix VIII.3 show 24 hour SST thermal maps for four example days for the Gulf of México area.

V.6.2 Correlation between Satellite SST and underwater temperature measurements

There were 105 days available of underwater temperature recorded at the API site between 2003 and 2006. These data was measured by a local coastal meteorological station using an instrument located at a water depth of approximately 3m with measurements averaged over each hour. During the period of measurement, 2046 temperature values were available corresponding to 81% availability for the recording period. The SST data for the same 105 days were extracted from the GEOS database yielding 1090 hourly values, representing 43% availability. A total of 890 hourly values (35%) were available simultaneously.

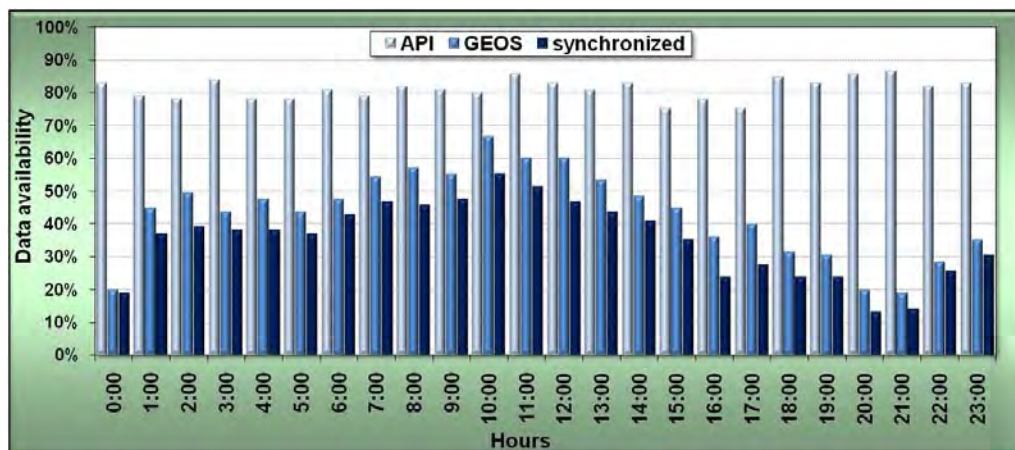


Figure V.12. Available SST measurements during the correlation period for onsite (API), satellite (GEOS) and the synchronized data where values from both sources were available simultaneously

Figure V.13 shows examples for six different days of hourly SST measured underwater at the API site and available from the GEOS Satellite.

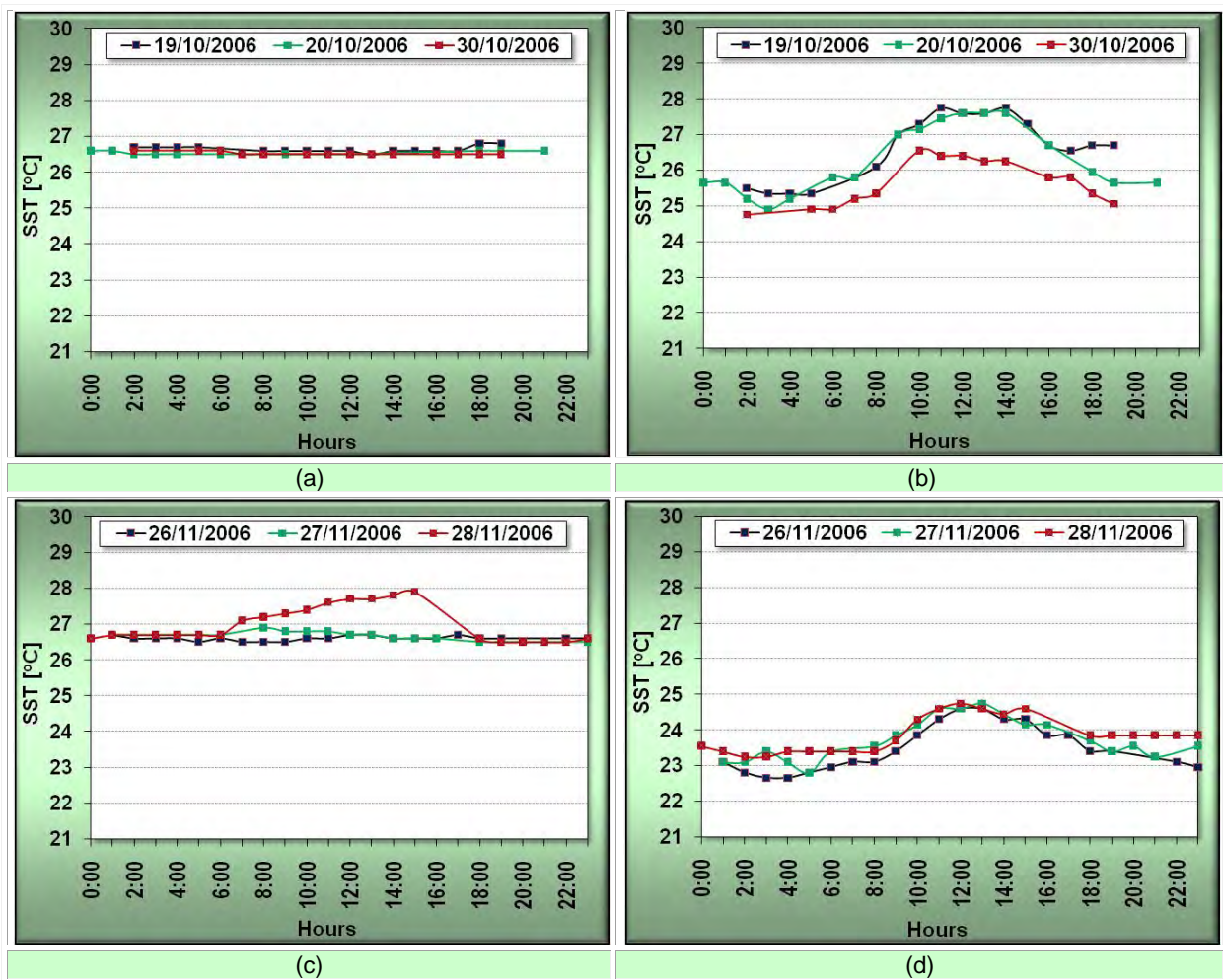


Figure V.13. Examples of hourly behaviour for: (a) and (c) underwater measurements of SST at API site; and (b) and (d) GEOS Satellite SST

The correlation for the same six day period between the measurements from the underwater sensor at the API site and from GEOS is shown in Figure V.14. The same figure shows also the daily average values during the correlation period.

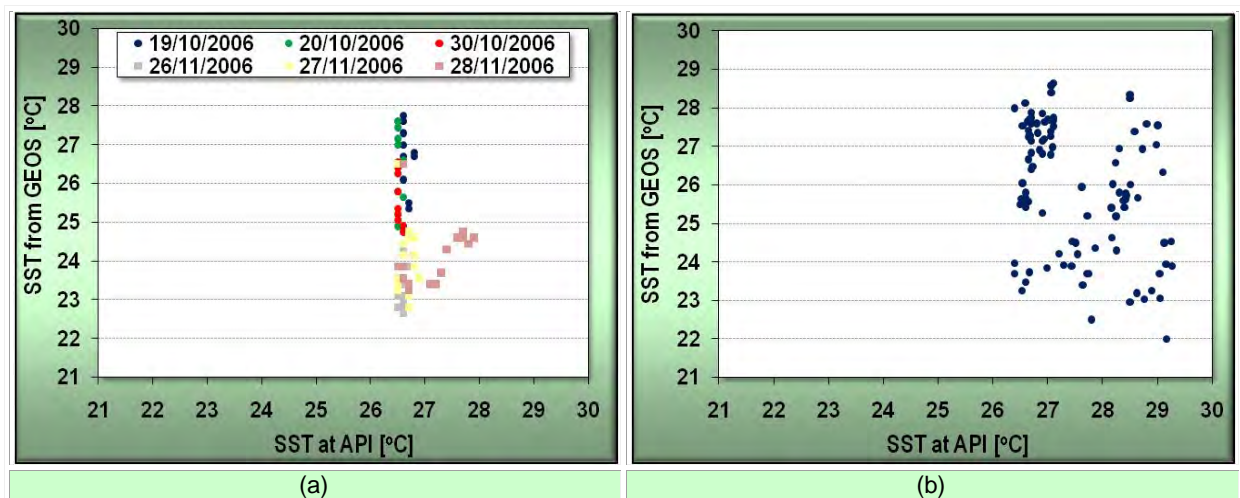


Figure V.14. Correlation between the SST measured from GEOS Satellite and the underwater measurements at API site: Examples of hourly data for six days in the correlation period (a) and daily average for the whole correlation period (b).

It can be seen that there is no significant correlation between the two datasets. The data measured from the GEOS satellite show a stronger diurnal thermal cycle than the underwater data which generally shows little diurnal variation. For the sample days, just November 28th 2006 has a slight correlation with the satellite SST. This could be caused by the fact that the underwater temperature was measured at 3m depth whilst the satellite SST data reflect the conditions of the environment immediately above the sea surface which is more significantly influenced by the atmospheric Surface Boundary Layer (SBL) conditions. For the purpose of the research presented in this thesis, the satellite SST represents a more useful parameter than the underwater temperature to study the structure of the SBL at the API site.

V.6.3 Satellite SST data for the study period

A time period between 25/07/2007 and 26/06/2009 was selected covering the period of measurements recorded on the API mast (703 days). A total of 38.5% SST values concurrent with the mast measurements was successfully extracted from the GEOS satellite thermal images corresponding to 6500 hourly values. Figure V.15 below shows the distribution of SST data available binned by hour of the day and averaged over the entire study period.

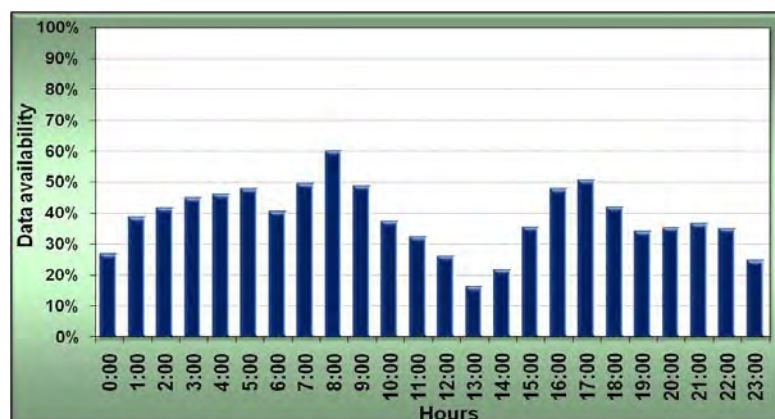


Figure V.15. SST data available from GEOS Satellite during the day averaged over the entire study period between 25/07/2007 and 26/06/2009.

Figure V.16 below shows hourly SST patterns for four example days selected from those days that had the highest availability of daily data. It can be seen that on some days, e.g. 2nd December 2007, there is little diurnal variation, but on others, e.g. the 8th May 2009, a definite diurnal cycle is observed.

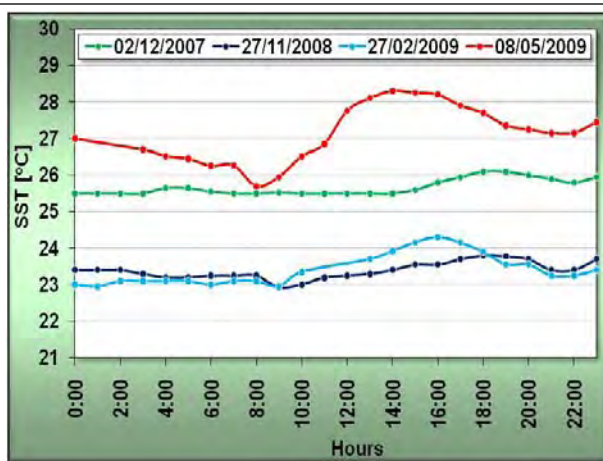


Figure V.16. Four examples of diurnal SST pattern from the GEOS Satellite.

The set of 24 hour satellite thermal images for the Gulf of México region for these four days can be seen in Table VIII.4, Table VIII.5 and Table VIII.6 of Appendix VIII.3 .

Figure V.17(a) below show the daily averages of the satellite SST data over the whole study period. The peaks in the seasonal temperature pattern discussed in previous chapters, sections II.3 and III.5 , are identifiable in September 2008 and May 2009 as well as the minimum between December and January of each year.

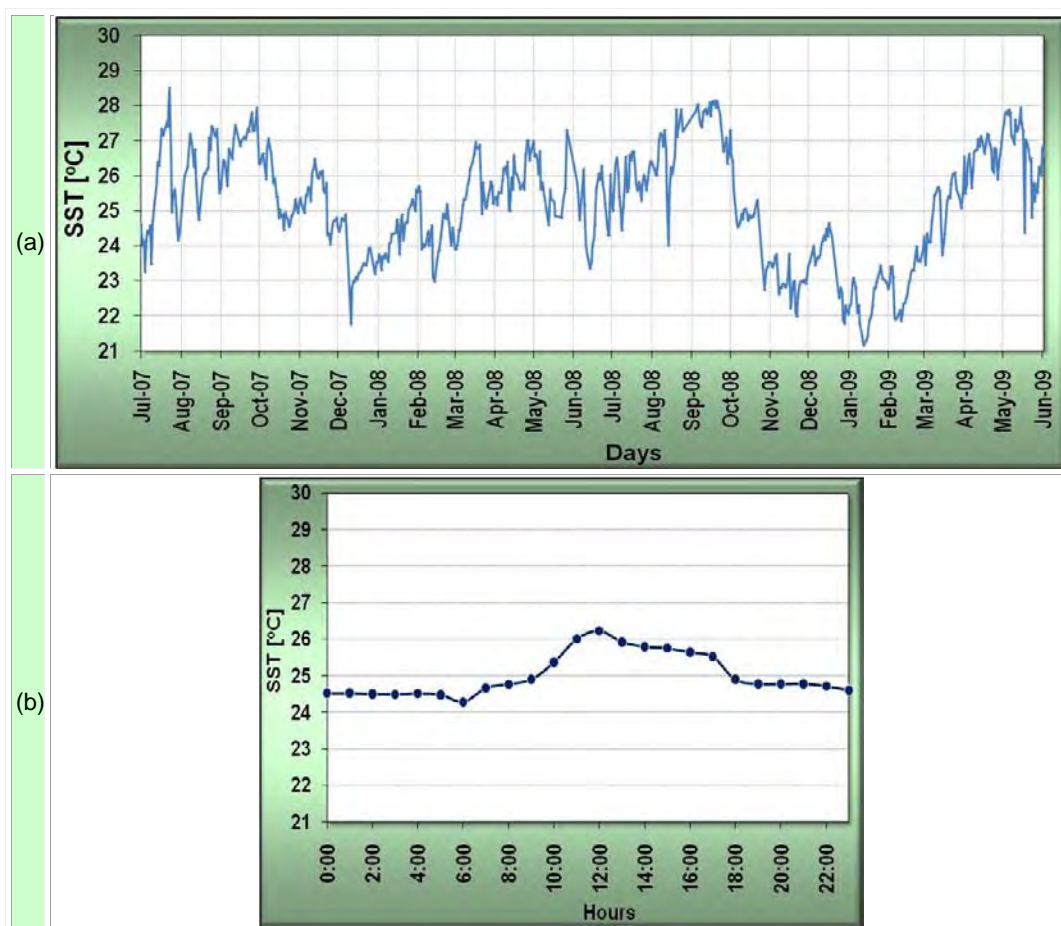


Figure V.17. Averages of SST from the GEOS Satellite over the whole study period: (a) daily and (b) hourly.

Hourly averages of the Satellite SST over the whole study period were computed and are shown in Figure V.17(b). Though the SST varies little during the day, on average there is evidence of a diurnal cycle.

V.6.4 Vertical temperature profile

Averages of the measured temperature as a function of height have been plotted in Figure V.18, for the whole study period, for every three hours during the day. The temperature trends over the day at all heights display a diurnal cycle with the highest temperature at noon and the lowest just around sunrise, e.g. 06:00. However, the ranges of temperatures differ: there is range of around 6 degrees Celsius at 10m and 25m height, but the range at the sea surface is less than 2 degrees Celsius. This is as one would expect due to the high thermal mass of the water. What is interesting to note is the lapse rate between 0m and 10m and that between 10m and 25m height. The temperatures at 10m and 25m would suggest very unstable conditions throughout the day, whereas those between 0m and 10m would suggest stable or close to neutral conditions with the most stable conditions at midday and the least stable (closer to neutral) at sunrise (06:00).

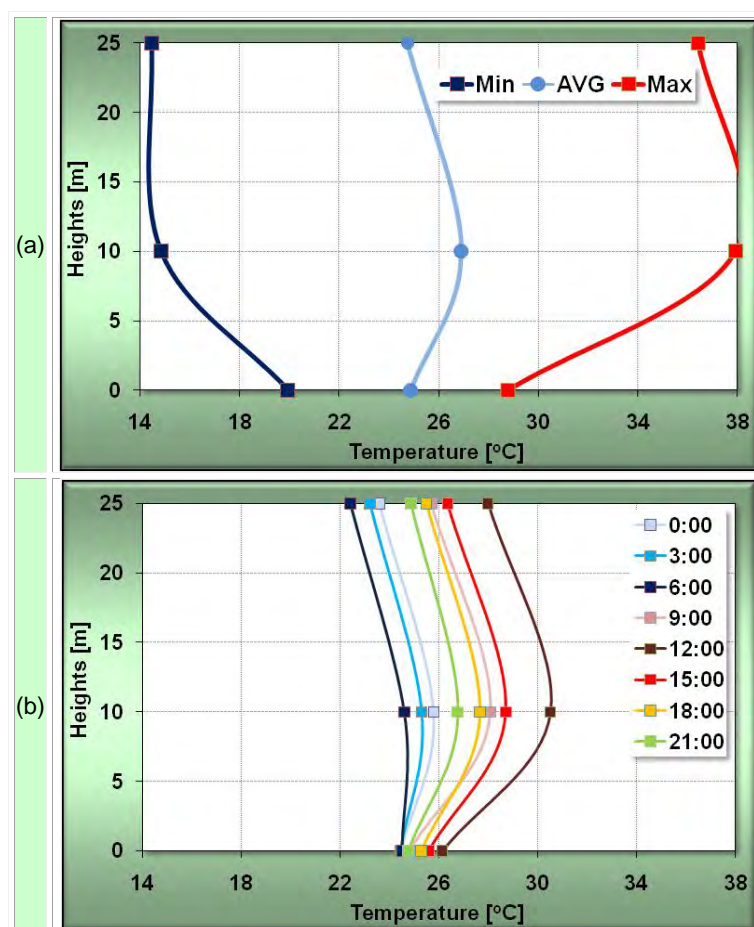


Figure V.18. Vertical temperature profile using the measurements from the GEOS Satellite for SST and from the API mast at “hi” and “lo” heights: (a) average and extreme values over the whole study period (b) hourly averages for selected times of the day.

V.7 Offshore wind speed ratio as function of stability

In this section, the ratio of the wind speeds measured at “hi” and “lo” heights have been analyzed as function of the stability through four stability measures obtained from the Gradient and Bulk Richardson numbers. The expressions to compute both Richardson numbers, equation (I.4) and equation (I.5), were presented in the general introduction. The relation presented in equation (I.3) was used to compute the stability parameter “ z/L ”. Strictly speaking this relationship is only valid for the Gradient Richardson number, though in this case it is assumed to be a reasonable approximation for the Bulk Richardson number. The wind speed ratio was then calculated using Monin-Obukhov similarity theory using equation (I.6).

Monin-Obukhov similarity theory was developed for stationary steady-state flow conditions. Thus, two filtering strategies were considered in order to exclude events which were unlikely to be representative of a steady state:

- To filter large variations in consecutive mean wind speed values (WS Filter). Each ten minute average of wind speed was compared to its two previous and to its following neighbours. Then, records with variations above a predefined Level of Filter (LoF) were discarded [30].
- To filter large variations of the standard deviation of the wind speed values (SD Filter). Samples for which the variation in standard deviation measured was above a predefined LoF were discarded.

Several LoFs were analyzed and a 20% LoF was finally selected for both filtering strategies, as this was the lowest LoF value for which no more than the 30% of the original measured data were discarded. Table V.9 below show the percentage of data filtered out for all the stability measures calculated. In the case of the Bulk Richardson number calculated from the SST, no standard deviation was available to apply the corresponding filter.

Table V.9. Percentages of remaining data after the filters were applied for each stability measure.

Filters	WS Filter	SD Filter
Ri Tho-Tlo	78.25%	70.03%
Rb Thi-Tlo	78.25%	69.38%
Rb Tlo-SST	69.59%	
Rb Thi-SST	69.57%	

The percentage of data available after the filtering to exclude conditions outside of the steady states is significant higher than the one reported by other authors. In particular, Lange [30] studying the effects of the temperature profiles in offshore conditions reported around 50% of data available after filtering with similar parameters to the ones described above.

The ratio of wind speeds measured at “hi” and “lo” height were binned every 0.01 value of the stability measure z/L , where z was taken as the lower measurement height on the API mast.

V.7.1 Stability measures derived from onsite measurements

Figure V.19 shows the measured and calculated values of the wind shear using 0.0003 as sea surface roughness length. The Obukhov length L used to bin the ratio of wind speeds was computed using the Gradient Richardson number Ri and the Bulk Richardson number Rb . Wind speed and air temperature measured at “lo” and “hi” height on the API tower were used to derive the Gradient Richardson number. Wind speed at the higher measurement height and both air temperatures were used to derive the Bulk Richardson number represented by the symbol “ $Rb_{Thi-Tlo}$ ” in Figure V.19.

No filter was applied to the wind speed data used in Figure V.19(a). The mean wind speed filter described above was applied in Figure V.19(b). The standard deviation filter described above was applied in Figure V.19(c). In general, the ratio of the wind speeds is not represented well by applying the Monin-Obukhov similarity theory. It can be seen that the filter for the mean wind speed variation does not significantly change the binned values of Ri while the binned values of “ $Rb_{Thi-Tlo}$ ” are closer to the theoretical ratio. In contrast, applying the standard deviation filter makes a significant difference particularly to “ $Rb_{Thi-Tlo}$ ” although the number of values is now significantly reduced, Figure V.19(c).

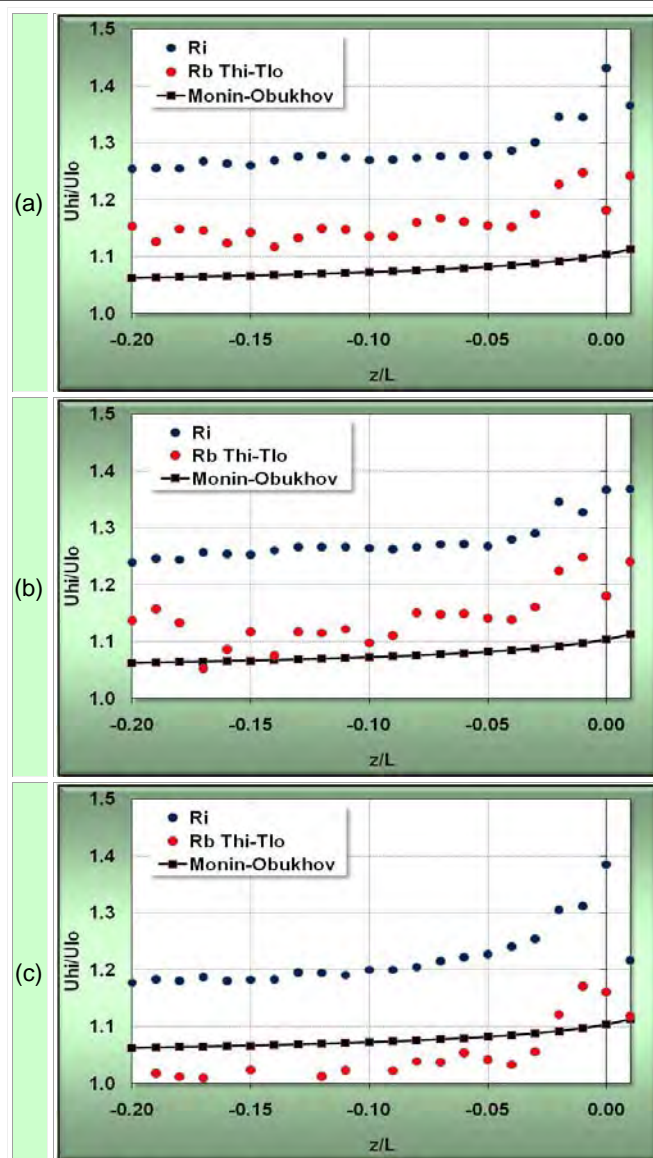


Figure V.19. Ratio of wind speed at “lo” and “hi” heights versus the stability measure z/L calculated using the Gradient Richardson number (Ri) and Bulk Richardson number (Rb Thi-Tlo). (a) No filter applied, (b) Filter applied to the wind speed variations and (c) Filter applied to the wind speed standard deviation.

Figure V.20 shows the frequency distribution of the stability measure z/L based on Ri and “Rb Thi-Tlo”. The values at the far left of the graph represent the frequency for $z/L \leq -0.21$. Similarly, the value on the far right represents the frequency for $z/L \geq 0.01$.

It can be seen that the use of either Ri or “Rb Thi-Tlo” to calculate the stability measure z/L makes a significant difference. It is well known that the use of Ri for calculating the stability can be problematic when there are small differences in the wind speed between the two heights. This problem is likely to be more acute when the situation is predominantly unstable as opposed to stable as the wind shear will be expected to be less. On the other hand, “Rb Thi-Tlo” is only an approximation to Ri and using the relationships in the General Introduction to relate Rb to z/L may not necessary be so accurate.



Figure V.20. Frequency distributions of the stability measure z/L calculated using Ri and “Rb Thi-Tlo”.

V.7.2 Stability measures derived from Satellite SST measurements

Figure V.21 shows the ratio of wind speed at both measurement heights as a function of the stability measure z/L using data filtered with the wind speed variation filter described at the beginning of this section and 0.0003 as sea surface roughness length. The stability measure was calculated using the Bulk Richardson number with SST and air temperature at “lo” height (a) and “hi” height (b). A greater scatter in the values is observed in this case compared with the results presented above in Figure V.19. It should be noted that these results were based on considerably fewer data as they were produced with hourly data synchronized with available SST data from the GEOS satellite. It can be seen that neither case is particularly consistent with the theoretical wind shear, though the higher measurements give a slightly better fit.

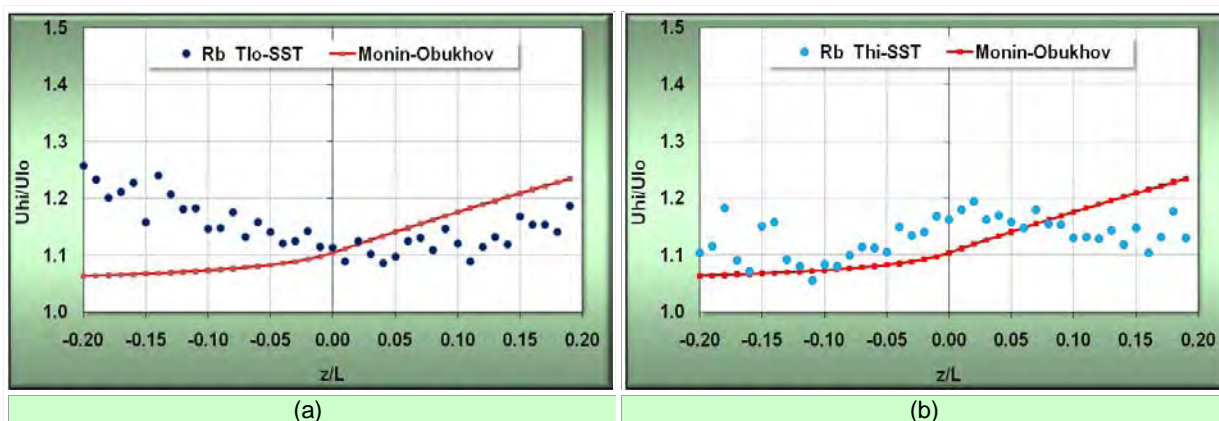


Figure V.21. Ratio of wind speeds at “lo” and “hi” height as function of the stability measure “ z/L ” using SST and air temperature at “lo” height (a) and “hi” height (b) to compute the Bulk Richardson number. The filter for mean wind speed variations was applied in both cases.

Figure V.22 shows the frequency distributions of the stability measure z/L calculated using the SST and air temperature at “lo” and “hi” height. The bin at the far left of the graph represents the frequency for $z/L \leq -0.21$. Similarly, the bin at the far right of the graph represents the frequency for $z/L \geq 0.20$. In this case, the stability computed from Tlo-SST shows a higher proportion of data in the highly stable region, as was observed from the lapse

rate patterns in Figure V.18. The value calculated using Thi-SST shows a distribution shifted to more neutral conditions.

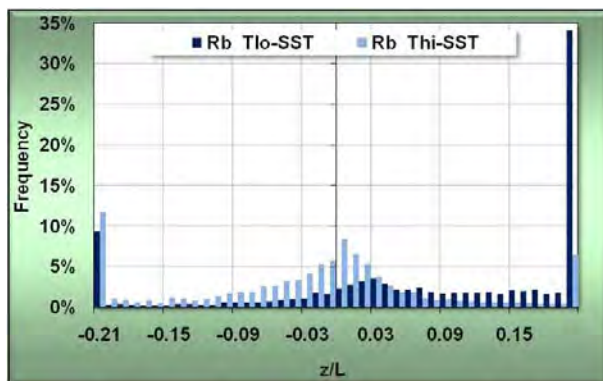


Figure V.22. Frequency distributions of the stability measure z/L computed from the SST and air temperature at “lo” and “hi” heights.

V.8 Distribution of the atmospheric stability classes

In this section, the stability classes inferred using four methods will be analyzed in more detail looking at diurnal, seasonal and directional dependence in order to cast further light on the variation in wind speed and direction at the API site off the Yucatán Peninsula. Figure V.23 below shows the distribution of the stability classes over the whole study period for the stability measure calculated from the Gradient Richardson number (Ri) and for the three stability measures calculated from the Bulk Richardson number (i.e. “Rb Tlo-SST”, “Rb Thi-SST” and “Rb Thi-Tlo”). It can be seen that there is a change from a predominance of very stable states to very unstable states when the parameters used to calculate the stability measures are measured at greater height.

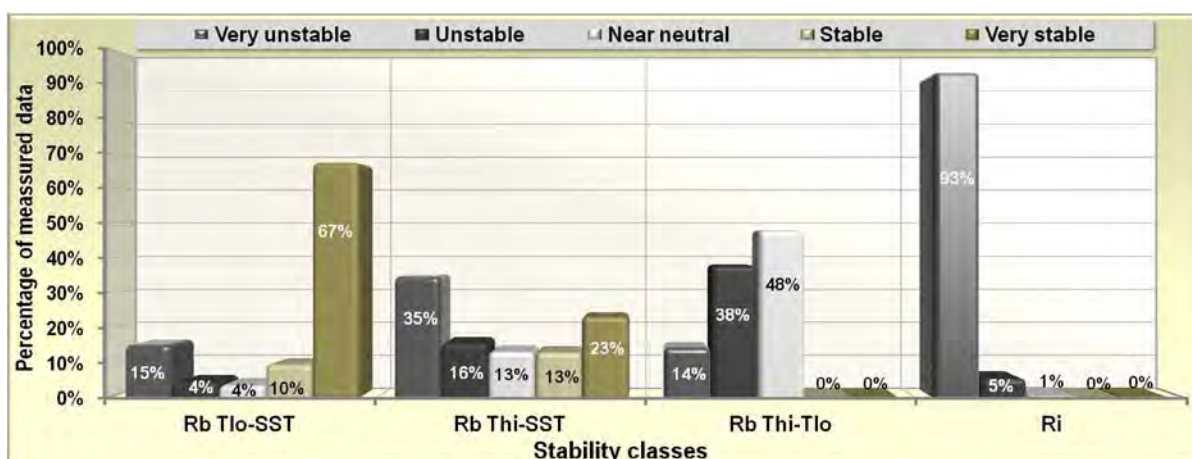


Figure V.23. Distribution of stability classes during the whole measurement period using as stability measure: (a) “Rb Tlo-SST”, (b) “Rb Thi-SST”, (c) “Rb Thi-Tlo” and (d) “Ri”.

The distribution of stability classes calculated using “Rb Tlo-SST” suggest a very stable layer close to the sea surface whereas the layer above, inferred using “Rb Thi-Tlo” suggest a

much more unstable or near neutral layer. This qualitative description will be estimated quantitatively in the next section.

Figure V.24 show the directional distribution of stability states, excluding the sectors between SSW and WNW, which receive less than 1% of the wind available (see Figure V.4). It can be seen that there is a decrease in stable states and an increase in unstable states when the winds approach the ESE direction which represent the higher contribution of the winds coming from the land, see Figure V.4. Looking back at Figure V.5(a), the wind will tend to come from the ESE direction sector during the night which would be when cooler winds would be more frequently blowing over warmer water. The greatest number of stables states are observed when the winds are coming from the sea in the NE direction which occurs most frequently (see Figure V.5(b)) during the late afternoon and early evening when the land surface (and thus the wind which originate from off the land) is more frequently warmer than the sea.

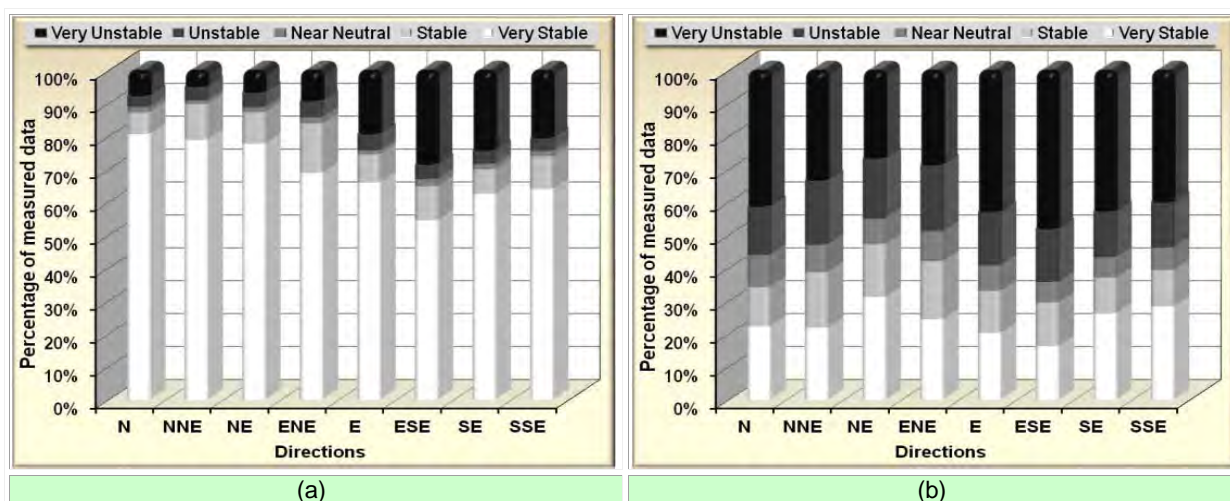


Figure V.24. Stability classes for each directional sector using as stability measure: (a) "Rb Tlo-SST" and (b) "Rb Thi-SST".

The diurnal behaviour of the stability classes is shown in Figure V.25. In this case clear diurnal patterns are seen for the fraction of stable and unstable states, consistence with the preliminary analysis of temperatures shown in Figure V.18(b). It can be seen that the fraction of stable states decreases to a minimum at sunrise (close to 06:00) when the air temperature is least, increasing to a maximum at midday (around 12:00) when the air temperature is highest. This is consistence with the results presented in the previous figure.

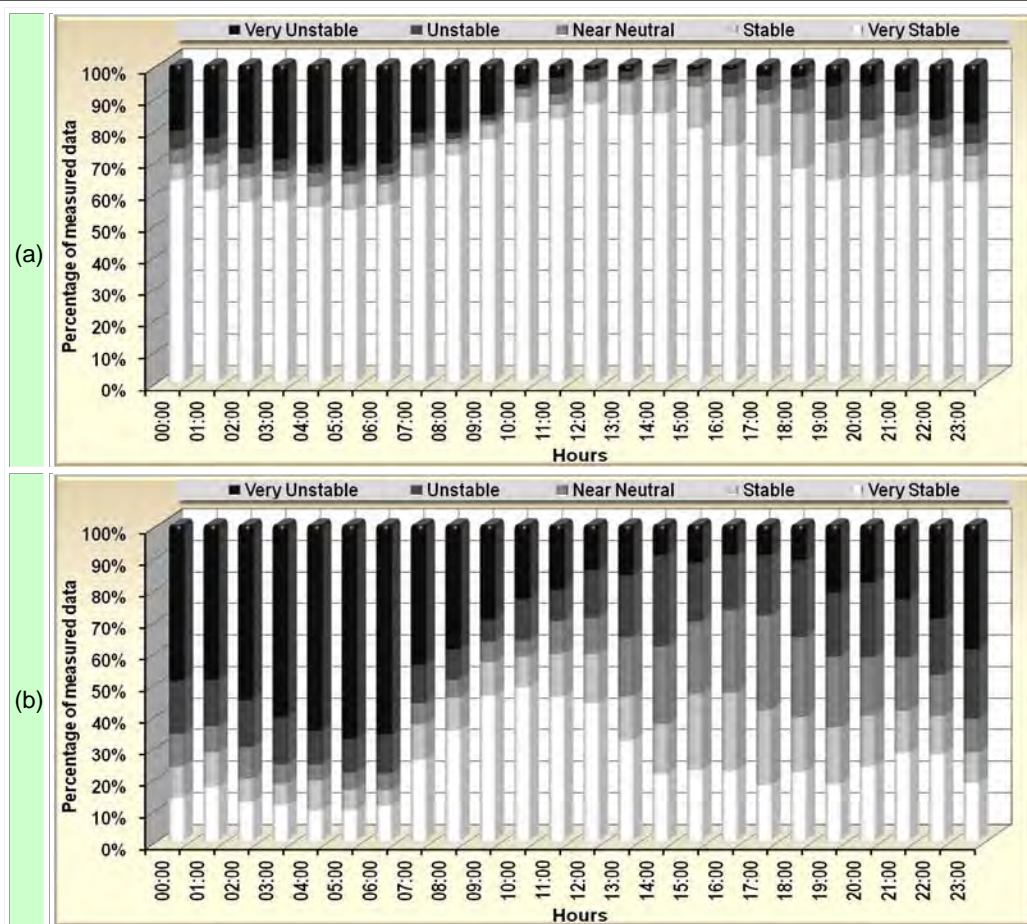


Figure V.25. Distribution of stability classes over the day using as stability measure: (a) “Rb Tlo-SST” and (b) “Rb Thi-SST”.

Figure V.26 below, shows the seasonal distribution of stability classes confirming the previous results observed for the diurnal patterns. The fraction of stable states increases in the months with higher ambient temperatures.

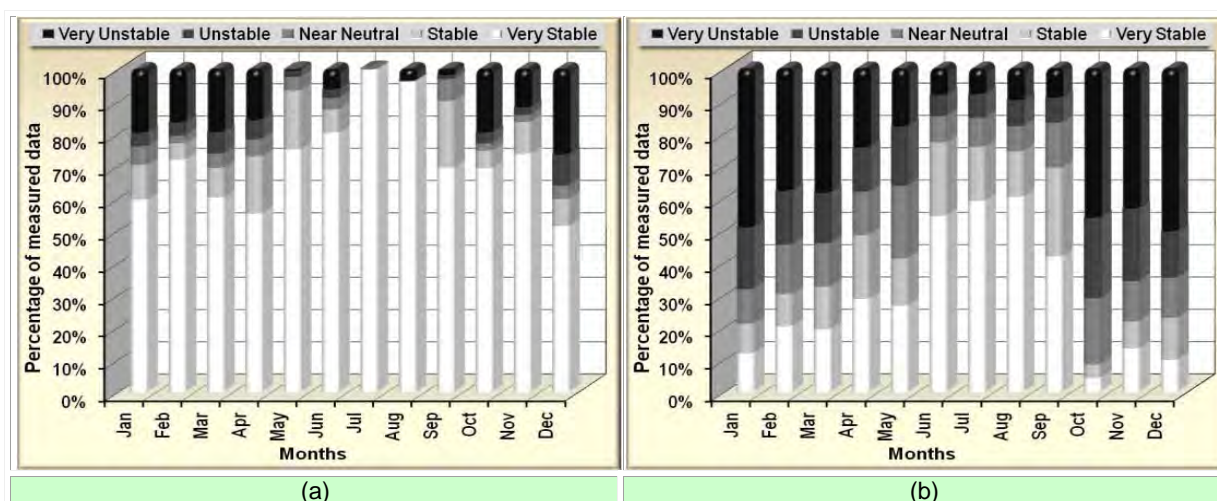


Figure V.26. Seasonal distribution of stability classes using as stability measure: (a) “Rb Tlo-SST” and (b) “Rb Thi-SST”.

The results presented above, would suggest that initially, after sunrise, the wind blows off the land over the sea. This results in a layer of warm air advecting over the sea and the

development of a thin Stable Internal Boundary Layer (SIBL). As the day develops, a more onshore sea breeze results which eventually veers to be parallel to the coast and after sunset reverts to a more offshore breeze with cooler air advecting over the sea and a diminishing of the SIBL with the development of a more Convective Boundary Layer (CBL) at night until the cycle is repeated the following day. This is an example of an inverted diurnal cycle (compared to the land).

V.9 The Stable Internal Boundary Layer.

For conditions where the wind blows off warmer land onto colder sea, a stable thermal internal boundary layer SIBL grows offshore as a result of the advection, driven by the geostrophic wind. This is due to the wind flow offshore of well mixed air from the land resulting from convective turbulence created by the heating of the land from sunrise until the early afternoon, Stull [85], see Figure V.27. If the height of the SIBL is denoted ($\delta_\theta(x)$) as a function of the distance X to the coast, then the growth rate $\partial \delta_\theta(x)/\partial x$, is less than 10^{-3} [86], thus this SIBL grows very slowly downwind as can be seen from the values shown in Figure V.27 for $\delta_\theta(100\text{km})$.

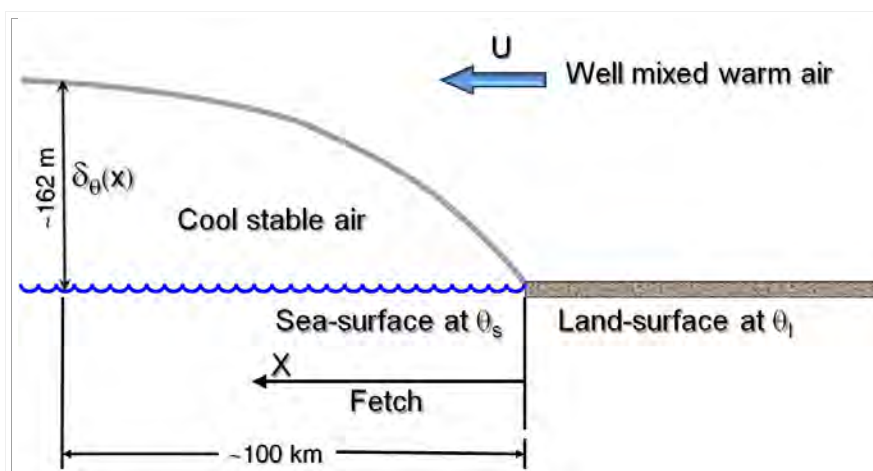


Figure V.27. Schematic of the SIBL profile ($\delta_\theta(x)$) created when warm air is advected over colder sea ($\theta_s < \theta_l$).

Through aircraft observations [87], a two dimensional numerical mesoscale model and a physical model [86]; Garratt reported an expression, see equation (V.1), to describe the SIBL height ($\delta_\theta(x)$) as a function of the fetch (X), the component of the geostrophic wind normal to the coast (U) and the potential temperature difference between the land mixed-layer air and the sea-surface ($\Delta\theta$):

$$\delta_\theta(x) = C X^{1/2} U \left(\frac{g \Delta\theta}{\bar{\theta}} \right)^{-1/2} \quad \text{with "C" independent of X and equals to 0.014} \quad \text{V.1}$$

This result was analyzed for steady state and diurnally varying flow and was found to be consistent with Mulhearn [88], Hsu [89], and Sutton [90]. Clear diurnal variations in the SIBL up to 150km from the coast and significant turbulence levels at the height of and above the SIBL up to a distance of 50km from the coast were also reported. Similar behaviour is observed in the API site at 6.65km from the shore, where the diurnal pattern can be seen and the number of unstable states increases with height revealing a higher level of turbulence for “Rb Thi-SST”, see Figure V.25.

A simpler approximation of equation (V.1) to determine the height of the SIBL in kilometres as function of the fetch downwind in metres was also reported by Hsu [91]:

$$\delta_{\theta}(x) = 12.28 X^{0.59} \quad \text{V.2}$$

This equation is very useful to estimate the approximate average height of the SIBL for the following conditions:

- For fetches (X) between 3.2km and 107.8km.
- For a component of the geostrophic wind normal to the coast (U) of between 6.7m/s and 17.9m/s.
- For a potential temperature difference between the land mixed-layer air and the sea-surface ($\Delta\theta$) of between 3.1°K and 10°K.

The average height of the predicted SIBL at the API site calculated using equation (V.2) with a fetch of approximately 6.65km is 35.4m. The height of the SIBL at a specific hour can be estimated from equation (V.1) using the results presented in chapter IV section IV.4 (which corresponds with the evaluated site closer to the API site), where at midday: $\Delta\theta=6.4^{\circ}\text{K}$, $\bar{\theta}=305.3^{\circ}\text{K}$ and $U=8.1\text{m/s}$, after extrapolation to 300m height as suggested by Kaimal and Finnigan [92]. In this case, the height of the predicted SIBL at midday is approximately 20.5m. These results confirm what was qualitatively stated in the previous sections: the sensor installed at 25m height is significantly influence by the turbulent conditions usually found at and above the SIBL height as reported by Garratt [86] which is consistent with the fraction of highly unstable states represented by “Ri Thi-Tlo” and “Rb Thi-Tlo”.

V.10 Remarks

The diurnal and seasonal behaviours identified in the previous chapters for the wind and air temperature have been consistent with the patterns resulted from the offshore analysis in offshore conditions at the North coast of the Yucatán Peninsula.

The wind speed and direction measured in the offshore conditions of the API site follow the expected pattern of a diurnal cycle produced by the difference in the heating rates between the land and the sea which drive alternating pressure gradients. There is also a significant influence of the Coriolis force which causes the sea breeze to blow in a direction more parallel to the shoreline of the North of the Yucatán Peninsula later in the afternoon.

The wind shear at the API site is not well represented by Monin-Obukhov theory, partly because of the persistent thin SIBL observed at the site, whose height is frequently between 10m and 25m with a larger level of turbulence intensity at the higher height which is close to the predicted height of the SIBL.

VI Main results, general conclusions and recommendations

Four main research subjects concerning the wind energy characteristics of the Yucatán Peninsula region have been comprehensively addressed for the first time in this thesis:

- Trends in the temporal long-term behaviour of pressure, temperature, wind speed and wind direction have been identified using daily averages recorded by meteorological observatories of periods between 10 and 20 years.
- The spatial distribution of hourly and monthly patterns of these meteorological parameters across the Yucatán Peninsula have been examined using ten minute averaged data recorded over an average period of four and a half years.
- A comprehensive analysis of the vertical wind profile has been made in terms of the directional, diurnal and seasonal patterns on an inland site using measurements at two different heights over a year and a half.
- A study of the offshore wind properties was made on a tower at 6.65km from the North coast of the Yucatán Peninsula for around two years using onsite and satellite measurements.

The results derived from the research undertaken in each chapter have been proved to be consistent among them. The main results obtained during the PhD research have been published in the scientific literature, see appendices VIII.4.1 , VIII.4.2 and VIII.4.3 , and presented in International Wind congress, see appendices VIII.4.4 and VIII.4.5 . The following integrated conclusions can be drawn from the research undertaken:

- The long-term temporal patterns showed highly directional behaviour with the majority of winds coming from the East and East-South-East sectors. Therefore, those sites located further from the East coast of the Yucatán peninsula will be dominated by land-based wind which exhibits a larger degree of temporal variations on intra-annual and inter-annual timescales.
- Weibull Probability Distributions give relatively good representations of the wind speed frequency distributions over the temporal long term period. Therefore, the use of such distributions would be reasonable in order to predict wind potential at sites around the Yucatán Peninsula.

- From the offshore buoy measurements, the atmosphere over the Western Caribbean appeared to be predominantly near neutral, whilst the atmosphere over the Eastern Gulf was predominantly unstable. These conditions produce particular spatial distributions of the wind with higher speeds on the North and North East coasts of the Yucatán Peninsula.
- The wind climatology of the Yucatán Peninsula for the inland sites reflects their geographical position in relation to the East coast. Those sites located on the North coast exhibited mixed behaviour with characteristics of both inland and coastal sites.
- The wind shear exponent of the empirical power law was inadequately represented by averaged values for inland conditions, as generally used by other authors. Instead of averages, directional and frequency distributions proved to be more effective in describing the vertical wind profile from the power law.
- Near coast inland sites exhibited expected characteristics during the night time with lower wind speeds blowing from land to sea. In contrast, non-standard wind variations and shear profiles occur during the daytime when the higher wind speeds coming from over the sea exhibit particular characteristics that reflect the two rather distinct sea thermal conditions displayed by the Gulf of México and the Caribbean Sea.
- The seasonal behaviour of the inland wind shear appears to be mainly driven by the temperature changes with the exception of the rainy season when the decrease in the air temperature reduces the effects of the convection processes.
- A preliminary correlation was identified between inland wind speed and rate of change of temperature reflecting stable conditions during periods of cooling and unstable conditions during periods of heating.
- The rate of change of inland air temperature may be used as a proxy for vertical temperature gradient to infer atmospheric stability when temperature measurements are only available at one height, particularly where winds are dominated by thermal conditions. However, more data and a thorough analysis would be required to develop this further.
- The offshore wind speed and direction at the North coast follow the expected pattern of a diurnal cycle produced by the difference in the heating rates between the land and the sea which drive alternating pressure gradients. There is also a significant influence of the Coriolis force which causes the sea breeze to blow in a direction more parallel to the shoreline of the North of the Yucatán Peninsula during the late afternoon.
- The offshore wind shear at the API site is not well represented by Monin-Obukhov theory, partly because of the persistent thin SIBL observed at the site, whose height is frequently between 10m and 25m and partly because of the number of non steady-state events.

The results presented in this thesis have established for first time the basis for the development of a Yucatán Wind Atlas. Historical (long-term) and geographically distributed analysis have been established from the most reliable meteorological measurements which can be used to extrapolate the wind characteristics through Measure-Correlate-Predict algorithm to other regions in the Yucatán Peninsula. Nevertheless, future work needs to consider data collected at more than one height at several sites in order to analyse the wind shear profile and allow an accurate extrapolation to potential wind turbine hub height.

The analysis of the offshore data revealed a non-uniform surface boundary layer and it is clear that more detailed profile measurements are required offshore to gain greater insight into the atmospheric boundary layer offshore. The application of numerical models, e.g. mesoscale models, would help to give more detail on the horizontal and vertical fluxes in this region. If offshore wind power is to be developed then this further work is necessary to provide confidence in the predicted wind speed at potential wind turbine hub height.

It is also recommended that the data recorded at the offshore site be used to identify the behaviour of the rate of change of temperature as function of the other atmosphere stability parameter evaluated in the last chapter. It is also highly recommended to undertake, at the end of the research project, a carefully comparison of the temperature measure by the sensors used placing them at the same height and without any change in the connections conditions, in order to identify any calibration issue.

VII References

1. Global Wind Energy Council (GWEC). Global Wind Report 2006. WEB site: http://www.gwec.net/uploads/media/gwec-2006_final.pdf; 2007 [retrieved 21.11.07].
2. Global Wind Energy Council (GWEC). Global Wind Report 2008. WEB site: <http://www.gwec.net/fileadmin/documents/Global%20Wind%202008%20Report.pdf>; 2010 [retrieved 19.02.10].
3. Herbert GMJ, Iniyamb S, Sreevalsanc E and Rajapandiand S. A review of wind energy technologies. *Renewable and Sustainable Energy Reviews* 2007;11(6): 1117-1145.
4. Essa KSM and Embaby M. Statistical Evaluation of Wind Energy at Inshas, Egypt. *Wind Engineering* 2005;29(1): 83-88.
5. Li M, Li X. Investigation of wind characteristics and assessment of wind energy potential for Waterloo region, Canada. *Energy Conversion and Management* 2005;46(18-19): 3014-3033.
6. Farrugia R and Scerri E. Analysis of wind characteristics in the Maltese Archipelago. *Renewable Energy* 1997;12(4): 339-350.
7. Shata ASA and Hanitsch R. Evaluation of wind energy potential and electricity generation on the coast of Mediterranean Sea in Egypt. *Renewable Energy* 2006;31(8): 1183-1202.
8. Shata ASA and Hanitsch R. The potential of electricity generation on the east coast of Red Sea in Egypt. *Renewable Energy* 2006;31(10): 1597-1615.
9. Sahin B, Bilgili H and Akilli H. The wind power potential of the eastern Mediterranean region of Turkey. *Journal of Wind Engineering and Industrial Aerodynamics* 2005;93(2): 171-183.
10. Rehman S. Wind energy resources assessment for Yanbo, Saudi Arabia. *Energy Conversion and Management* 2004;45(13-14): 2019-2032.
11. Rehman S and Ahmad A. Assessment of wind energy potential for coastal locations of the Kingdom of Saudi Arabia. *Energy* 2004;29(8): 1105-1115.
12. Tchinda R, Kaptoum E. Wind energy in Adamaoua and North Cameroon provinces. *Energy Conversion and Management* 2003;44(6): 845-857.
13. Akpinar EK, Akpinar S. Determination of the wind energy potential for Maden-Elazig, Turkey. *Energy Conversion and Management* 2004;45(18-19): 2901-2914.
14. Akpinar S, Kavak Akpinar E. Wind energy analysis based on maximum entropy principle (MEP)-type distribution function. *Energy Conversion and Management* 2007;48(4): 1140-1149.
15. Vicente RT. Influence of the fitted probability distribution type on the annual mean power generated by wind turbines: A case study at the Canary Islands. *Energy Conversion and Management* 2008;49(8): 2047-2054.
16. Rehman S, Ahmad A. Assessment of wind energy potential for coastal locations of the Kingdom of Saudi Arabia. *Energy* 2004;29(8): 1105-1115.

17. Rehman S, Wind energy resources assessment for Yanbo, Saudi Arabia. *Energy Conversion and Management* 2004;45(13-14): 2019-2032.
18. Al-Nassar W, Alhajraf S, Al-Enizi A, Al-Awadhi L. Potential wind power generation in the State of Kuwait. *Renewable Energy* 2005;30(14): 2149-2161.
19. Essa KSM, Mubarak F. Survey and Assessment of Wind-speed and Wind power in Egypt including Air Density Variation. *Wind Engineering* 2006;30(2): 95-106.
20. Sahin B, Bilgili M, Akilli H. The wind power potential of the eastern Mediterranean region of Turkey. *Journal of Wind Engineering and Industrial Aerodynamics* 2005;93(2):171-183.
21. Troen I, Mortensen NG, Petersen EL. WASP Wind Atlas Analysis and Application Programme. User's Guide. Risoe National Lab, Roskilde, Denmark, 1988.
22. Akpinar EK and Akpinar S. An assessment on seasonal analysis of wind energy characteristics and wind turbine characteristics. *Energy Conversion and Management* 2005;46(11-12): 1848-1867.
23. Akpinar S and Akpinar EK. Estimation of wind energy potential using finite mixture distribution models. *Energy Conversion and Management* 2009;50(4): 877-884.
24. Ramachandra TV and Shruthi BV. Wind energy potential mapping in Karnataka, India, using GIS. *Energy Conversion and Management* 2005;46(9-10): 1561-1578.
25. Jaramillo OA, Saldaña R and Miranda U. Wind power potential of Baja California Sur, México. *Renewable Energy* 2004;29(13): 2087-2100.
26. Cancino-Solórzano Y and Xiberta-Bernat J. *Statistical analysis of wind power in the region of Veracruz (México)*. *Renewable Energy* 2009;34(6): 1628-1634.
27. Van Wijk AJM, ACM Beljaars, AAM Holtslag and WC Turkenburg. Evaluation of stability corrections in wind speed profiles over the North Sea, *Journal of Wind Engineering and Industrial Aerodynamics* 1990;33: 551–566.
28. Coelingh JP, AJM van Wijk and AAM Holtslag. Analysis of wind speed observations over the North Sea, *Journal of Wind Engineering and Industrial Aerodynamics* 1996;61(1): 51-69.
29. Coelingh JP, AJM van Wijk and AAM Holtslag. Analysis of wind speed observations on the North Sea coast, *Journal of Wind Engineering and Industrial Aerodynamics* 1998;73(2): 125-144.
30. Lange B, Larsen S, Højstrup J and Barthelmie RJ. The influence of thermal effects on the wind speed profile of the coastal marine boundary layer, *Boundary Layer Meteorology* 2004;112: 587–617.
31. Pryor SC and Barthelmie RJ. Analysis of the effect of the coastal discontinuity on near-surface flow, *Annals of Geophysics* 1998;16: 882–888.
32. Pryor SC and Barthelmie RJ. Statistical analysis of flow characteristics in the coastal zone, *Journal of Wind Engineering and Industrial Aerodynamics* 2002;90(3): 201-22.
33. Lapworth A. The diurnal variation of the marine surface wind in an offshore flow, *Quarterly Journal of the Royal Meteorological Society* 2005;131(610), Part B: 2367-2387.

34. Barthelmie RJ, Courtney MS, Højstrup J and Larsen SE. Meteorological aspects of offshore wind energy: observations from the Vindeby wind farm, *Journal of Wind Engineering and Industrial Aerodynamics* 1996;62: 191-221.
35. Barthelmie RJ, Grisogono B and Pryor SC. Observations and simulations of diurnal cycles of near-surface wind speeds over land and sea, *Journal of Geophysical Research*, 1996;101(D16): 21327–21337.
36. Farrugia RN. The wind shear exponent in a Mediterranean island climate, *Renewable Energy* 2003;28(4): 647-653.
37. Rehman S and Al-Abbadib NM. Wind shear coefficients and their effect on energy production, *Energy Conversion and Management* 2005;46(15-16): 2578-2591.
38. Rehman S and Al-Abbadib NM. Wind shear coefficients and energy yield for Dhahran, Saudi Arabia, *Renewable Energy* 2007;32: 738-749.
39. Kirchhoff RH and Kaminsky FC. Wind shear measurements and synoptic weather categories for siting large wind turbines, *Journal of Wind Engineering and Industrial Aerodynamics* 1983;15(1-3): 287-297.
40. Ramazan K. An evaluation of wind energy potential as a power generation source in Kütahya, Turkey, *Energy Conversion and Management* 2004;45(11-12): 1631-1641.
41. Jiang Y, Yuan X, Feng J and Cheng X. Wind Power Density Statistics Using the Weibull Model for Inner Mongolia, China, *Wind Engineering* 2006; 30(2): 161–168.
42. Bailey BH and McDonald SL. *Wind resource assessment handbook*. Albany-New York: AWS Scientific Inc; 1997.
43. Amador JA, Alfaro EJ, Lizano OG and Magaña VO. Atmospheric forcing of the east tropical Pacific: A review. *Progress in Oceanography* 2006; 69: 101-142.
44. Arya SP. *Introduction to Micrometeorology*. SanDiego/California: Academy; 2001.
45. Lalas DP and Ratto CF. *Modeling of atmospheric flow fields*. Singapore: World Scientific Publishing, 1996.
46. Rehman S, Halawani TO and Husain T. Weibull parameters for wind speed distribution in Saudi Arabia. *Solar Energy* 1994;53(6): 473-479.
47. Lun IYF and Lam JC. A study of Weibull parameters using long-term wind observations. *Renewable Energy* 2000;20(2):145-153.
48. Persaud S, Flynn D and Fox B. Potential for wind generation on the Guyana coastlands. *Renewable Energy* 1999;18:175-189.
49. Shamilov A, Kantar YM and Usta I. Use of MinMaxEnt distributions defined on basis of MaxEnt method in wind power study. *Energy Conversion and Management* 2008;49: 660-677.
50. Ramirez P and Carter JA. The use of wind probability distributions derived from the maximum entropy principle in the analysis of wind energy. A case study. *Energy Conversion and Management* 2006;47: 2564-2577.
51. Ulgen K and Hepbasli A. Determination of Weibull parameters for wind energy analysis of Izmir, Turkey. *International Journal of Energy Research* 2002;26: 495-506.

52. Seguro JV and Lambert TW. Modern estimation of the parameters of the Weibull probability density distribution for wind energy analysis. *Journal of Wind Engineering and Industrial Aerodynamics* 2000;85: 75-84.
53. Celik AN. A statistical analysis of wind power density based on the Weibull and Rayleigh models at the southern region of Turkey. *Renewable Energy* 2003;29: 593-604.
54. Ahmad MR, Ali AS and Asaad AM. Estimation Accuracy of Weibull Distribution Parameters, *Journal of Applied Sciences Research* 2009;5(7): 790-795.
55. Celik AN. Energy output estimation for small scale wind power generators using Weibull-representative wind data. *Journal of Wind Engineering and Aerodynamics* 2003;91: 693-707.
56. Genc A at al. Estimation of Wind Power Potential Using Weibull Distribution, *Energy Sources, Part A: Recovery, Utilization, and Environmental Effects* 2005;27(9): 809-822.
57. Gore, R.H. *The Gulf of Mexico*. Pineapple Press Inc. Sarasota, Florida, 1992.
58. National Renewable Energy Laboratory. Renewable Resource Data Center: Wind Energy Resource Information-Wind Energy Resource Atlas of the United States, Web site: (<http://rredc.nrel.gov/wind/pubs/atlas/tables/1-1T.html>) 2010 [retrieved 22.02.10] .
59. Breaker LC, Krasnopolsky VM and Maturi EM. GOES-8 imagery as a new source of data to conduct ocean feature tracking. *Remote Sensing of Environment* 2000;73(2):.198-206.
60. Legeckis R and Zhu T. Sea surface temperatures from the GOES-8 geostationary satellite. *Bulletin of the American Meteorological Society* 1997;78(9): 1971-1983.
61. May DA and Osterman WO. Satellite-derived sea surface temperatures: Evaluation of GOES-8 and GOES-9 multispectral imager retrieval accuracy. *Journal of Atmospheric and Oceanic Technology* 1998;15(3): 788-797.
62. Wu X, Menzel WP and Wade GS. Estimation of sea surface temperatures using GOES-8/9 radiance measurements. *Bulletin of the American Meteorological Society* 1999;80(6): 1127-1138.
63. JPL Physical Oceanography DAAC (Distributed Active Archive Center). GOES SST data. Web site (ftp://podaac.jpl.nasa.gov/pub/sea_surface_temperature/goes/goes11-12/data/), 2009, [retrieved [01.07.09].
64. Bryant WR, Antoine JW, Ewing M and Jones B. Structure of Mexican continental shelf and slope, Gulf of Mexico. *American Association of Petroleum Geologists Bulletin*. 1968;52: 1204-1228.
65. Murray, G.E. *Geology of the Atlantic and Gulf coastal province of North America*. New York: Harper and Bros, 1961.
66. Salvador A. *The Gulf of Mexico Basin, the Geology of North America*. Geological Society of America, Boulder, Colorado, 1991.
67. Nowlin WD. Water masses and general circulation of the Gulf of Mexico. *Oceanology* 1971;5(2): 28-33.
68. Businger JA, Wyngaard JC, Izumi Y, Bradley EF. Flux Profile Relationships in the Atmospheric Surface Layer. *Journal of Atmospheric Sciences*. 1971;28: 181–189.

69. Högström U. Nondimensional Wind and Temperature Profiles. *Boundary Layer Meteorology* 1988;42: 55–78.
70. Troen IB and Petersen EL. *European Wind Atlas*, Risoe National Laboratory, Risoe, Denmark, 1991.
71. Arya SP. *Introduction to Micrometeorology*. San Diego/California: Academy, 2001.
72. Dai A. and Wang J. Diurnal and semidiurnal tides in global surface pressure fields. *Journal of Atmospheric Sciences* 1999;56: 3874-3891.
73. National Oceanic and Atmospheric Administration (NOAA), 2008. "NOAA's National Data Buoy Center (NDBC) website", <http://www.ndbc.noaa.gov>, [retrieved [10.01.08].
74. Van-Wijk AJM, Beljaars ACM, Holtslag AAM and Turkenburg WC. Evaluation of stability corrections in wind speed profiles over the North Sea. *Journal of Wind Engineering and Industrial Aerodynamics* 1990;33: 551-566.
75. Grachev AA and Fairall CW. Dependence of the Monin–Obukhov Stability Parameter on the Bulk Richardson Number over the Ocean. *Journal of Applied Meteorology* 1997;36: 406-414.
76. Monin AS and Obukhov AM. Basic laws of turbulent mixing in the surface layer of the atmosphere. *Tr. Geofiz. Inst. Akad. Nauk SSSR*, 1954;151: 163-187.
77. Larsen SE. Observing and Modelling the Planetary Boundary Layer', in E. Raschke and D. Jacob (eds.), *Energy and Water Cycles in the Climate System*, ASI series I, Vol. 5, Springer, Berlin, 1993: 365-418.
78. Foken T. 50 Years of the Monin–Obukhov similarity theory, *Boundary Layer Meteorology*, 2006;119: 431-447.
79. Holtslag AAM. Estimation of diabatic wind speed profile from near-surface weather observations, *Boundary Layer Meteorology*, 1984;29: 225-250.
80. Van Delden A. Observational evidence of the wake-like character of the sea breeze effect, *Beilr. Phys, Atmosph*, 1993;66(1 2): 63-72.
81. Businger JA. A note of the Businger-Dyer profiles, *Boundary Layer Meteorology*, 1988;42: 145-151.
82. Panofsky HA and Dutton JA. *Atmospheric Turbulence*, Wiley Interscience, New York, 1984, 397.
83. Ozerdem B and Turkeli M. An investigation of wind characteristics on the campus of Izmir Institute of Technology, Turkey, *Renewable Energy* 2003;28(7): 1013-1027.
84. Locke LF, Silverman SJ and Spirduso WW, 2nd edition, *Reading and Understanding Research*, SAGE Publications, Inc, 2004.
85. Stull RB, *An Introduction to Boundary Layer Meteorology*, Kluwer Academic Publishers, Dordrecht, The Netherlands, 1988.
86. Garratt JR. The Stably Stratified Internal Boundary Layer for Steady and Diurnally Varying Offshore Flow, *Boundary Layer Meteorology*, 1987;38: 369-394.
87. Garratt, J.R. and Ryan B.F. *The structure of the stably stratified internal boundary layer in offshore flow over the sea*. *Boundary Layer Meteorology* 1989;47(1): 17-40

88. Mulhearn PJ. On the Formation of a Stably Stratified Internal Boundary Layer by Advection of Warm Air over a Cooler Sea, *Boundary Layer Meteorology* 1981;21: 247-254.
89. Hsu SA. On the Growth of a Thermally Modified Boundary Layer by Advection of Warm Air Over a Cooler Sea, *Journal of Geophysics Research* 1983;88: 771-774.
90. Sutton OG, *Micrometeorology*, McGraw-Hill, New York, 1953.
91. Hsu SA, *A verification of an analytical formula for estimating the height of the stable internal boundary layer*. *Boundary Layer Meteorology* 1989;48(1): 197-201.
92. Kaimal JC and Finnigan JJ. *Atmospheric Boundary Layer Flows: Their Structure and Measurement*. Oxford University Press, New York, 1994.

VIII Appendices

VIII.1 Classified critical literature review

Reflecting the wind data available for the Yucatán Peninsula, an initial detailed literature review was organized into three main groups, which later derived the three research dimensions defined in the introduction section:

- **Temporal assessments:** related to research using at meteorological observations over at least a 10 year period, a limited number of sites compared with the whole study zone, and with typically daily average values.
- **Spatial assessments:** related to research undertaken mainly using data from meteorological stations during time periods of less than 10 years at a large number of sites that cover the whole study zone and with data averaging periods no greater than an hour.
- **Inland vertical wind profile:** Research from sites instrumented to study the wind resource at two different heights, generally at one site, specially installed for wind resource evaluation instead of meteorological purposes. These measured data should be recorded at least every two seconds and average values stored every 10 minutes.

The most up to date papers have been included in the critical review, chosen covering the three categories, and mainly dealing with close to coastal or island zones. A summary table of the publications included in each group followed by their chronological critical review is presented for each research paper. Each critical review included the following elements [84]:

- **Research:** Title of the published paper.
- **Summary:** Outline of the research undertaken considering five analysis areas:

Analysis areas	Main question to answer in each stage
Purposes	Aim of the research
Context	Where is the proposed study situated within the wider research field?
Methods	How the research was conducted?
Results	What was found?
Conclusions	Which are the meaning and implications of the obtained results?

- **Evaluation:** A judgement of the research on the basis of the five analysis areas.

VIII.1.1 Temporal assessment

The papers selected were published between 2004 and 2006. One of the papers deals with basic daily data while the others use hourly data. The sites cover two coastal zones and one inland site with study periods between 10 and 14 years. The Table VIII.1 below summarises the basic information for each paper.

Table VIII.1. Temporal data researches.

Year	Reference	Study Period [years]	Average period	Met Stations	Site's location
2004	[11]	14	Hourly	5	Coastal locations of the Kingdom of Saudi Arabia
2005	[9]	12	Hourly	7	Eastern Mediterranean region of Turkey
2006	[41]	10	Daily	1	Zhurihe, Inner Mongolia region in China

Critical reviews:

Research:

Assessment of wind energy potential for coastal locations of the Kingdom of Saudi Arabia [11].

Purposes: The authors propose to undertake a wind data analysis including seasonal and diurnal behaviour, energy generation and capacity factor for onshore sites of Saudi Arabia.

Context: The authors draw attention to the environmental effects and energy potential of the wind energy in a global context. Some examples of the fundamental role played by the wind data analysis to properly evaluate the wind energy potential were also mentioned. After a brief exploration of previous works done in the Kingdom of Saudi Arabia, related with studying and using the wind energy potential, the authors summarise their motivations and establish that using relatively windy sites in the Kingdom of Saudi Arabia, analysis of seasonal and daily wind behaviour and calculation of the parameters related with wind energy generation will be the main content of the proposed research.

Methods: Considering the availability of meteorological data, locations in coastal sites were chosen as data source. The following table summarizes the main described parameter of such sites:

Main measurement characteristics	
Measurement sites	5 Meteorological stations in the coastal locations of the Kingdom of Saudi Arabia (Dhahran, Yanbo, Al-Wajh, Jeddah, and Gizan).

Measurement height	10m
Average frequency	Hourly
Study period	14 years (1970-1983)
Data Source	Not directly specified

Some general procedures to discard erroneous data values from the data bank were also presented. The authors did not introduce any formal research plan.

Results: The long-term hourly mean wind speed data were used to estimate the mean values at 3 different heights (40, 50 and 60m above ground level a.g.l.) by means of the 1/7th wind power law. Then, the authors present the hourly mean wind speeds during the day (Diurnal behaviour) and the monthly mean wind speeds during the year (seasonal behaviour) at four different heights for each site as well as a comparison among all the sites at 10m height. Then, the percent frequency distribution at 10m was presented for all sites.

The power curve of nine wind generators with power from 150kW to 2.5MW were considered to compute the energy output in MWh and the capacity factor at 10m and 50m height for all study sites.

Conclusions: The authors concluded that the seasonal variations were significant just in three (Dhahran, Yanbo and Gizan) of the five studied sites. It was also mentioned that the seasonal and diurnal behaviour match respectively the summer and daily electrical load requirements. The authors range Yanbo and Dhahran as the best sites in reference to their energy production and capacity factor.

Evaluation: The topic of the study was introduced in general terms citing some previous investigations but despite of the purpose being clearly stated, the authors did not establish a clear relation between the proposed study and previous studies. The introduction section supports the proposed research using general arguments about the importance of the wind energy to Middle Eastern countries

No specific explanations were provided to justify the selection of the five study sites and the chosen study period. The authors did not establish a research methodology and it was not explicitly expressed why the computations made were specially selected for the proposed study. A general procedure was described to validate the source data but there was not any mention of the relevant technical details of the sensors used. No arguments were presented to support the power selection of the wind generators included in the research and the brief description about how compute the energy output in "MWh" was not enough clear or it should have included the corresponding mathematical equation.

The conclusions make a review of the obtained results in relation with the daily and yearly electric load but the author did not present any additional information to support this fact. In general, just qualitative conclusions were presented and finally the authors

match the conclusions with the results and the research purpose stating that “Yanboo” was the best site to install wind power generators.

Research:

The wind power potential of the eastern Mediterranean region of Turkey [9].

Purposes: The authors declared as research purpose: “to quantify the wind energy potential of the east Mediterranean region of Turkey and identify locations with the best wind source”.

Context: The authors described some general arguments about the fast development of the Turkey, its energetic requirements and the potential of the wind energy in the region. Some results of previous papers issued about the wind power potential in Turkey and in other parts of the world were also presented. The authors indicated that the proposed research was dealing with sites not covered in previous studies about wind energy availability.

Methods: The data were selected from seven sites located mainly in coastal regions. The following table summarizes the main described parameters of the sites:

Main measurement characteristics	
Measurement sites	7 Met stations, Eastern Mediterranean region of Turkey
Measurement height	Between 8 and 17m (in sites from 4 to 100m above sea level).
Average frequency	Hourly
Study period	10 years (1992–2001)
Data Source	Turkish Meteorological Service

A map with the study sites was presented as well as a table with the average directions of the wind speed for the seven study sites.

Results: The Weibull parameters were computed for all sites using the last 5 years of the study period. The wind speed frequency distribution was plotted for each site and the daily behaviour of the hourly wind speed for all the sites were graphically presented, showing that all sites had the lowest wind speeds around the seven o'clock in the morning and the highest during the afternoon. Yearly mean wind speeds for all stations were also plotted in the same graph making evident which was the site with better wind resource. The monthly mean wind speed was separately plotted for each site during the last 5 years of the study period. These graphs showed a seasonal pattern where the highest wind speeds were during July and August and the lowest during November and December, in almost all the studied stations.

Using the WASP model, a table was presented to show the percentage of decrease in wind speed as a consequence of surrounding obstacles for all the sites, in each

direction and for 10, 25, 50 and 100m height. Finally, the authors presented two maps of the study region showing the mean energy potential at 10 and 25m heights.

Conclusions: The authors concluded that there were many areas with potential for wind power generation within the study region.

Evaluation: The authors stated that not all the regions of Turkey had been properly studied. No clear arguments were presented to explain the site selection. There was no explanation as to how the Weibull parameters were computed and why just 5 years were selected to calculate them. The table of Weibull parameters listed the mean wind speed and energy density but it was not clearly stated if these values were calculated from the measured data or derived from the Weibull parameters. The authors did not explain properly the procedure followed to compute the wind speed in each direction for 10, 25, 50 and 100m height. The first part of the conclusions included statements that cannot be directly derived from results obtained in the presented research.

Research:

Wind Power Density Statistics Using the Weibull Model for Inner Mongolia, China [41],

Purposes: Calculate the probability distribution function and the wind power density for the region of Inner Mongolia in China.

Context: The authors reviewed the availability of wind energy reported by previous studies. The region of study is described as a zone without electrical grid supplies and with important wind energy potential. Thereafter, the authors mention that few studies have been made in the study zone and consequently the proposed that research could contribute to an improved knowledge of the wind energy distribution in this part of China.

Methods: A meteorological station located at Zhurihe at an elevation of 1151m above sea level has been chosen as the source of data:

Main measurement characteristics	
Measurement sites	1 Met station in Zhurihe, Northeast of Inner Mongolia, China
Measurement height	10m above ground level, at an altitude of 1151 m.
Average frequency	Daily
Study period	10 years (1991–2000)
Data Source	China Meteorological Administration

The Zhurihe station was selected for analysis because it has the largest long term (10 years) record of wind speed measurements in Inner Mongolia. The average wind speed is 5.5m/s at 10m height.

Results: A method to calculate and validate the Weibull distribution and the mean power density for Weibull distribution was presented. The authors have calculated the monthly mean wind speed and the corresponding Weibull parameters. Then the “goodness of fit” was studied finding good correlation values.

The frequency distribution for the measured wind speed was plotted for each month of the 10 years of data. Then, the probability density and cumulative distribution were plotted for the whole study period. In a comparison bar graph, the wind power density for the measured data and the wind power density calculated from the Weibull function were presented to finally show the monthly error derived from the wind power density calculated with the Weibull function.

Conclusions: The conclusions summarised the main calculations undertaken in the research: Weibull distribution model, wind speed probability density and wind power density to finally outline that the Weibull function represented the measured data and allowed to estimate the power density.

Evaluation: The authors presented a general introduction that identified the research proposed in the context of the wind energy assessment in China but some concrete examples about previous research in China and in the study region could have helped to fit better the proposed research in what is already known for this country. More details about how was computed the “goodness of fit” were required to support the values presented and the graph that represented the monthly probability derived from the measured data should have included the corresponding monthly probability computed with the Weibull model.. A seasonal graph on a yearly basis and an hourly analysis on a daily basis could have being helpful

VIII.1.2 Spatial assessment

Published papers were selected from the last three years and cover regions with costal zones. The density of measurement sites per study area allows a reasonable characterization of the geographical zone under investigation. Table VIII.2, summarizes the sites selected:

Table VIII.2. Spatial data researches.

Year	Reference	Study Period [years]	Average period	Met Stations	Site's location
2004	[25]	1	10 minutes	15	State of “Baja California Sur”, México
2005	[18]	9	Hourly	6	State of Kuwait
2006	[19]	5	15 minutes	18	Egypt

Critical reviews:**Research:**

Wind power potential of Baja California Sur, México, Renewable Energy [25]

Purposes: To study of the wind potential of “Baja California Sur” in the North-West of México and to estimate the wind energy output, the capacity factor and the production costs by means of the Weibull probability distribution function.

Context: A general introduction about the state of the wind energy evaluation in México was presented by the authors in order to mention the support given by the Government of the State of “Baja California Sur” to undertake the assessment of wind energy on its geographical region. Thus, the authors established that the proposed research will be focused in studying the wind power density along the shore line of the study region and through the Weibull function to evaluate in one site the energy output and the capacity factor for two generators.

Methods: A set of measurement sites were installed along the coastline of “Baja California Sur” and a year of data was collected. Some characteristics of the sensors used and the measurement procedure were also described. The general parameters are summarized in the following table:

Main measurement characteristics	
Measurement sites	15 wind stations located along the western coastline of “Baja California Sur”, México.
Measurement height	10 m
Average frequency	10 minutes
Study period	13 months (February 1997 to February 1998)
Data Source	The Electrical Research Institute

The models used to compute the Weibull function, the wind power, the energy density, the vertical wind profile (power law) were also presented.

Results: A table with the yearly mean wind speed, the standard deviation, the Weibull parameters, the power and energy were presented as results of the whole study period for each of the 15 sites. After this, the authors selected “El Cardón” to study its wind speed monthly behaviour, its wind rose and its calculated (Weibull) and measured frequency distribution. Using the power law, the authors extrapolated the wind speed up to 55m height and using two different generators of 750 W a calculation was made to the annual energy production, the capacity factor and the production cost.

Conclusions: The authors concluded that there were good conditions to develop a wind farm at the site called “El Cardon” with capacity factor close to 25% and production costs between 4.5 and 6.2 US¢/kW h (considering investment of 1000-1100 US\$/kW).

Evaluation: The content of the study was introduced in logical and general terms considering the lack of research in México about the wind energy resource.

The measurement sites were directly presented without any description to support their selection in terms of the amount of sites and their geographical locations, mainly considering that these sites were installed specially for the proposed study.

The quality and reliability of the data was not assessed. There was no mention of the method used to compute the Weibull parameters. The selection of the “El Cardon” as the site that better describes the complete region was not fully supported. The authors had also over-simplified the presented criterion to choose a coefficient of 1/7 in the estimation of the vertical wind profile by means of the power law.

Finally, the conclusions were just presented in terms of the evaluation made at just one site and there was no discussion related with the results obtained by others.

Research:

Potential wind power generation in the State of Kuwait [18].

Purposes: Evaluate the wind energy potential in Kuwait.

Context: The research purpose was to as “assess the wind energy potential in Kuwait” and a brief description about the measurement stations, study period and main calculations that will be obtained during the proposed research.

Methods: A historical data set covering 46 years of monthly averages, extreme winds and wind directions from the Kuwait International Airport at 10m height were presented. The measurement conditions were defined as follows:

Main measurement characteristics	
Measurement sites	6 meteorological stations in the State of Kuwait
Measurement height	10m above ground level
Average frequency	Hourly
Study period	4 years (January 1998 - December 2002)
Data Source	Meteorological stations in the State of Kuwait

Mathematical formulations to compute the vertical wind profile by means of the power law, the Weibull parameters and wind power density were presented. A computer program was designed to execute some basic validation tasks.

Results: Monthly averages for the wind power density at 10m height and their extrapolation to 30m height were tabulated for each study site highlighting the summer season with the highest power available. Weibull parameters were also computed and tabulated for each site to compare the mean wind power density predicted by Weibull with the one computed from the measured values of wind speed. Also wind speed frequency distribution and the corresponding Weibull function were plotted in the same graph for

each site at 10m height. Finally, the authors presented a map with the distribution of the wind power density over Kuwait.

Conclusions: The authors summarised the main results for the annual average of wind speed and wind power density underlying that the summer season was identified with higher wind power, coinciding with the high electricity demand season during the year in Kuwait. Finally, the authors conclude that the higher wind power was found at open flat desert areas in the northern, north-western and southern parts of Kuwait and proposed studies to implement wind farm on those areas.

Evaluation: The site selection and measurement conditions were accurately described, the authors introduced a set of results of 46 years wind data corresponding, but from a site not included in the proposed study. This information creates some confusion. The authors generated the Kuwait wind power density map at 30m height but without presenting how it was derived and which roughness values, digital elevation and obstacles information were used.

Research:

Survey and Assessment of Wind-speed and Wind power in Egypt including Air Density Variation [19]

Purposes: The authors did not explicitly establish the study purpose and the better way of summarize a purpose is by means of the research title: "Survey and Assessment of Wind-speed and Wind power in Egypt including Air Density Variation"

Context: The introduction briefly described that meteorological data will be analyzed from several stations around Egypt.

Methods: Meteorological data from stations around Egypt were used to process the wind speed, temperature and atmospheric pressure. The next table gives information about these stations:

Main measurement characteristics	
Measurement sites	18 Met stations, throughout Egypt.
Measurement height	10m
Average frequency	15 minutes
Study period	5 years (since 9/3/2000 to 31/12/2004)
Data Source	It is not explicitly specified

The equation to calculate the power density was shown and an analysis of an air density correction factor to sites not at sea level was developed. Here, the authors define the cross correlation coefficient between the wind speed cube and the air density, the correction factor and finally the coefficient of variation of air density and of

the wind speed cube. The authors established that the random variability in daily temperature, pressure, air density and wind speed will be presented for 18 Egyptian stations during 5 years.

Results: A table was presented with averages of wind speed, maximum, minimum and frequency distribution during 5 years for all study sites. A clear oscillating pattern in daily behaviour of the air density was showed for two sites and a table was included with the calculations for all study sites about the statistical properties of air density and wind speed cube. Tabulated values were presented for the sites showing the defined cross-correlation, coefficient of variation, correction factor and power density.

The formulation to compute Weibull function and several derived parameters was described by the authors and years 2003 and 2004 were selected to compute the hourly, daily, monthly and yearly of the wind speed, frequency distribution and wind power. Then for 2004 the stations with lowest and highest wind speed averages were selected to represent the yearly frequency distribution and the monthly averages of the energy potential with values measured and with values computed by Weibull and Rayleigh functions. The best fitting were obtained in all cases for Weibull function. Finally, tables with monthly and yearly averages for wind speed were presented for all stations and for 2003 and 2004.

Conclusions: The authors concluded the following:

- In the Red Sea the wind was strongest in the summer while at the Mediterranean coast zones wind was strongest in winter and spring seasons.
- The random wind energy potential formulation showed that the average wind energy production was not only a function of the coefficient of variation of the air density and wind speed cubed, but also of the cross-correlation coefficient.
- The Red Sea, Mediterranean (except El-Arish) and some Inland zones (Aswan and Ismailia) can be chosen as favorable locations for wind energy.

Evaluation: The caption of the table that shows the statistical data for all the study station during 5 years was incomplete and produces several doubts that must be solved reading the text. The authors selected years 2003 and 2004 to derive the Weibull and Rayleigh parameters but did not explain why only two of the five years of data were used. The authors come to acceptable conclusions classifying their comments by geographical areas and presenting facts related with the obtained results to underlying the better regions and seasons.

VIII.1.3 Inland vertical wind profile

In this case, papers were selected considering those sites specially installed to measure the wind characteristics at two different heights. The papers were published between 2003 and 2004 and include one coastal site and two others inland sites close to shore zones. The Table VIII.3 shows general information about the mentioned researches.

Table VIII.3. Vertical wind profile researches.

Year	Reference	Study Period [Months]	Average period	Meass. Heights	Site's location
2003	[36]	72	10 minutes	10 and 25m	Swatar, on Malta's South West coast
2003	[83]	16	10 minutes	10 and 30m	Campus of Izmir Institute of Technology, Turkey
2004	[40]	20	10 minutes	10 and 30m	Dumlupinar University, Kütahya, Turkey

Critical reviews:

Research:

The wind shear exponent in a Mediterranean island climate [36].

Purposes: Study the wind shear exponent of the power law using measurements at two different heights on the central Mediterranean island of Malta.

Context: The role of the wind shear by means of the power law to estimate wind speed was expressed by the authors, mainly considering that usually wind data records come from meteorological stations installed on average at 10m height. The use of the 1/7 value for the wind shear exponent has proved to be useful, said the authors, to describes atmospheric wind profiles in the lower boundary layer when neutral stability conditions apply. However, wind shear also depends on others parameters related with wind speed, roughness length, and the height interval. Thus, the authors draw attention to significant errors that could be made by using a single exponent wind shear. Finally, the authors proposed a research to find more descriptive values for the wind shear by means of measurements of the wind speed made at different heights in the case of a Mediterranean island

Methods: A special tower was installed in a typical Maltese farmland with low height trees on a site at 216m above mean sea level. The following table shows the main details:

Main measurement characteristics	
Measurement sites	Swatar, on Malta's South West coast
Measurement height	10m and 25 m.
Average frequency	10 minutes

Study period	72-month period (August 1995–July 2001)
--------------	---

None validation procedure was used with the measured data and just the power law expression was presented without any particular research plan.

Results: The wind shear exponent for the whole study period was estimated using the mean wind speeds at 10 and 25 m. The obtained value was 0.36 which means that an error of 17% could be introduced if the wind speed had been estimated from 10 to 25m by means of the 1/7th exponent. A table and a graph were presented to show the monthly wind shear during the whole period and a clear decrease in wind shear is observed in the summer season. Finally, a daily behaviour of the wind share was plotted to illustrate its decrease in the middle of the day.

Conclusions: The authors state that the computed value for the wind shear could be useful in other Mediterranean sites and a mention was made about the increase in the precision of the expected energy generated by the wind turbine.

Evaluation: The authors did not present enough quantitative material to establish the boundaries of the 1/7 exponential approximation for the wind shear. Consequently, it was not clearly established the role of the proposed research in the study field. The measurement conditions were described but considering the study length, some validation procedure should have been applied to increase the reliability of the results. The monthly average values of the wind share should not be tabulated because they were better represented by the graph that clearly shows the seasonal wind share behaviour. It could be useful that the authors had included the yearly behaviour of the wind share to complete the presented research..

Research:

An investigation of wind characteristics on the campus of Izmir Institute of Technology, Turkey [83].

Purposes: Contribute to increase the reliability of the wind data for Turkey by means of studying the wind characteristics on one site close to coastline of the Aegean Sea.

Context: The authors made a general and qualitative introduction about the cost effective of the electricity produced by wind generators compared with others renewable technologies. Some mention was also made relative to the importance of developing wind data measurement to design reliable wind conversion systems. Some authors were also named because of their work related with the study of wind energy in Turkey

and finally the authors of the current paper declared that their study was an “attempt to bridge the gap” of the “absence of a reliable and accurate Wind Atlas of Turkey”.

Methods: A 30m height measurement tower was installed at 460m height over the sea level in the Izmir Institute of Technology campus. A set of sensors were installed to measure wind speed and wind direction, atmospheric pressure, temperature and relative humidity. The wind speed was measured at two heights such as is summarized in the following table:

Main measurement characteristics	
Measurement site	Izmir Institute of Technology campus, Turkey
Measurement height	10m and 30m
Average frequency	1 hour before 2001 and 10 minutes after 2001
Study period	16 months (July 2000 and November 2001)

The authors provided a table with the main properties of the used sensors and mentioned that just the 3.7% of the data was missing. “Encarta Digital Atlas” was used as a source for digital height counter map and surface roughness map. All data was processed using the “WinPro” software.

Results: A table was presented with the monthly averages values of the atmospheric pressure, relative humidity and temperature. Thereafter, the authors will always present the results for both 10 and 30m heights. The monthly behaviour of the wind speed were computed and plotted. The wind speed, wind direction and turbulence intensity for the whole study period were also showed. A table with the Weibull parameters, the calculated mean wind speed, the frequency and the wind shear were shown. The wind speed frequency distribution for the measured data and using the Weibull function were plotted in the same graph for each direction (using 12 sectors). Finally, the authors presented a map of the study area and plots with the turbulence intensity computed by frequency and by direction.

Conclusions: The authors conclude that the studied site presented “high wind potential” and claimed that “an attempt to promote wind energy in Turkey and to bridge the gap in order to create prospective Turkish Wind Atlas”. Weibull model was expressed as better than Rayleigh one. A mention also was made to express that the importance to the study of the computed turbulence intensity.

Evaluation: More quantitative information should have been included to describe the previous work made in Turkey and to show the lack of reliability of the previously used wind data. The authors described the site selection and the sensors but there was no explanation about how the measured data with hourly averages was used in conjunction with the 10 minutes averages to evaluate the site. Also, the resolution of the digital heights and roughness data used was not specified and the areas selected in both cases were introduced without any supporting argument. The monthly wind speed at 10 and 30m should have been presented in the same plot to simplify the comparison between the two heights and the wind shear was mentioned and showed

in a table but the authors do not analysis this result in any way. The plots that represent the behaviour of the wind speed, wind direction and turbulence intensity did not contribute to the discussion presented.

There was no mention as to how the Weibull parameters were calculated. In this sense, another questionable aspect was the conclusion that the Weibull distribution was better than Rayleigh one. This conclusion were not supported by the results presented because the authors did not compare Weibull and Rayleigh distributions against the measured data, they just said "Shape factor (k) for 30m height is 2.473 which means that measured data differ from the Rayleigh distribution" and this is not enough to say that the Weibull distribution was the best one to the study site. Another shortcoming was the turbulence intensity results, in this case the authors did not clearly define the concept and the representation presented was not the one found in the usual Wind Energy literature.

Research:

An evaluation of wind energy potential as a power generation source in Kütahya, Turkey [40].

Purposes: Study the potential of wind energy to be used as electricity supply in the region of Kütahya (Turkey) by means of a measurement site at the Dumlupınar University Main Campus.

Context: The necessity of sites specially designed to evaluate the wind energy potential was established by the authors. The author indicated that a site had been installed at University campus to develop a reliable characterization of the wind energy potential at the central western part of Turkey.

Methods: A mast of 30m height was installed at 1100m above sea level with no surrounding obstacles. The technical information about the sensors: two cup anemometers, one wind vane, ambient Temperature, relative humidity and atmospheric pressure data was provided by the authors. The following table shows the relevant parameters of the site:

Main measurement characteristics	
Measurement sites	Kütahya, at the central western part of Turkey
Measurement height	10m and 30 m
Average frequency	10 minutes
Study period	20 months, (July 1, 2001 and February 28, 2003)

Some comments were made by the author about the calibration of the sensors and the missing data, which was less than 2%. None formal research plan was established.

Results: A table was presented with the monthly averages of the wind speed at 10 and 30m, wind direction, direction of the strongest winds, temperature, relative humidity and

atmospheric pressure during the 20 study months using the 10 minutes average data. The author also graphs the monthly average of wind speed at 10 and 30m height. The frequency distribution of the measured data at 30m and the Weibull and Rayleigh probability distribution function were shown graphically when the Weibull parameter were computed applying the variable least square method. Finally, the author had chosen a wind generator of 600 kW at 65m height and presented graphically the power duration curve of the wind turbine for the measured data, Weibull and Rayleigh functions. The capacity factor was 15.6% to produce 1372.2MWh during the 20 study months.

Conclusions: General statements were made by the author about the use of wind energy potential in Turkey, prior to conclude that the available technology was not enough to use efficiently the measured wind energy in the study site. The measurements should be evaluated in the long term, said the author, in accordance with technological developments and reduction in the cost of turbines.

Evaluation: The author presented fairly qualitative information, and the research could not be considered an evaluation exercise.

The strongest argument that supported the study “The wind data from meteorological sites are not fully reliable for wind power prediction in Turkey” was not clearly established until the section number 3 “Material and Methods”. The measurement system used in the research and their configuration procedure were well presented by the author but the results and analysis done were insufficient, considering the available data and the research purpose.

The detailed evaluation showed that despite some weaknesses in analysis, the selected research papers have made important contributions to the study of the wind characteristics. This initial review of the scientific literature, about research undertaken in regions with similar characteristics to the Yucatán Peninsula, was the support to define the base structure and a relevant research direction for this PhD. Consequently, three initial research subjects were initially selected to be developed in the following conditions:

Temporal wind characteristics.	
Data measurement conditions:	
Wind data used	From three meteorological observatories in the Yucatán Peninsula
Measurement height	10m a.g.l.
Average frequency	Daily
Study period	10 - 20 years (1986-2005).
Data Source	Department within the Mexican national meteorological service (CNA).

Spatial evaluation of wind energy distribution.	
Data measurement conditions:	
Wind data used	From nine weather stations around the Yucatán Peninsula.
Measurement height	10m a.g.l.
Average frequency	10 minutes
Study period	3 - 7 years (2000-2007)
Data Source	Department within the Mexican national meteorological service (CNA).


Online wind vertical profile	
Data measurement conditions:	
Wind data used	From a 33 m tower installed in Mérida, Yucatán, México.
Measurement height	10m and 30m a.g.l.
Average frequency	10 minutes
Study period	1.5 years (2003-2005)
Data Source	Faculty of Engineering of the Autonomous University of Yucatan

A wider selection of scientific papers was included in the next stages of the research, see general introduction section I.2 , as well as the vertical wind profile in offshore conditions. The research subjects identified in the tables showed above were developed during the course of this PhD research and the results were presented in Chapters II , III and IV . Finally, a set of three research papers were published covering these subjects, which are attached in Appendices VIII.4.1 , VIII.4.2 and VIII.4.3 .


VIII.2 Devices and sensors

This appendix presents tables that summarizes the main characteristics of the sensors and devices used to configure the measurement stations installed during the PhD project to obtain the results presented in chapters IV and V .


Polar Mechanical Anemometer Sensor: RM Young 03001-5

	Specifications	Sensor	
		Wind Speed	Wind Direction
	Measurement Range	0 - 50 m/s	0 – 360° (mechanical) 0 – 355° (electrical)
	Starting Threshold	0.5 m/s	0.8 m/s (10°) 1.8 m/s (5°)
	Distance Constant	2.3 m	N/A
	Operating Temperature Range	-50 to 50 °C	-50 to 50 °C
	System Error	± 0.1 m/s	±5°

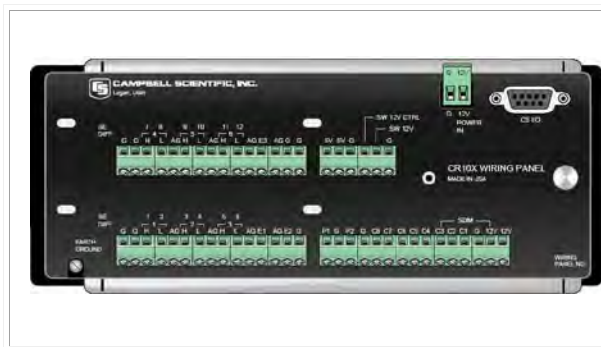
Orthogonal Ultrasonic Anemometer: Gill WindSonic 2D

	Specifications	Sensor	
		Wind Speed	Wind Direction
	Measurement Range	0 – 60 m/s	0 - 360°
	Starting Threshold	0.01 m/s	0.01 m/s
	Operating Temperature Range	-35 to 70 °C	-35 to 70 °C
	System Error	±2 %	±3 %
	Recording Resolution	0.01 m/s	1°

Temperature and Relative Humidity Sensor: Vaisala CS500

	Specifications	Sensor	
		Temperature	Relative Humidity
	Measurement Range	-40 to 60 °C	0 to 100 %
	Operating Temperature Range	-40 to 60 °C	-40 to 60 °C
	Operating Humidity Range	0 to 100 %	0 to 100 %
	System Error		0 – 10% RH: N/D 10 – 90% RH: ± 3 % 90 – 100% RH: ± 6 %

Datalogger: Campbell CR10X.



Specifications	Values
Differential analogue Channels	6
Digital Ports	8 I/O
Maximum Input Voltage	± 2500 mV
Resolution	0.33 µV
A/D Bits	16
Execution Rate	64 Hz
Data Storage (Data points)	62,280
Operation Temperature Range	-25 to 50 °C

Ethernet communication module: Campbell Network Link interface NL100.



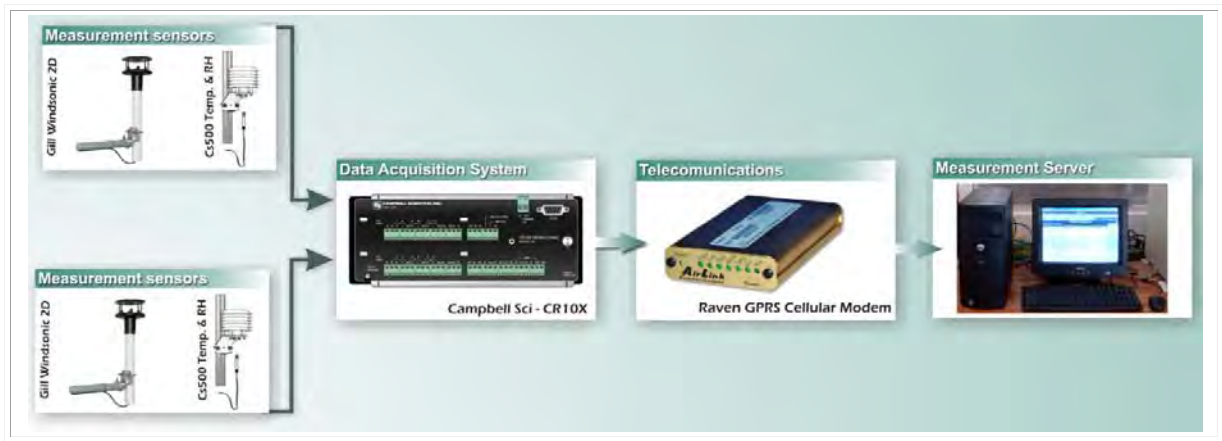
Specifications	Values
Communication Protocol	TCP/IP
Power supply	12 VDC
Current	130 mA
Temperature range	-25° to +50°C

Mobile communication module: GPS Digital Mobile Modem – AirLink/Raven 110



Specifications	Values
Communication Protocol	Cingular digital cellular networks.
Communication speed	Up to 384 Kbps
Transmit power	1.0 W for 1900 MHz
Power supply	12 VDC
Current	20 – 250 mA
Temperature range	-30° to +70°C

Configuration of the measurement system installed at the API site:



Using the raw data measured from the digital ultrasonic sensors, the scalar parameters of wind speed and wind direction were calculated through the definitions show in the following table:

Parameter	Definition	Where:
Scalar mean wind speed (S)	$S = \frac{\sum_i^N s_i}{N}$	$s_i = \sqrt{U_{ei}^2 + U_{ni}^2}$
Resultant mean wind speed (\bar{U})	$\bar{U} = \sqrt{U_e^2 + U_n^2}$	$U_e = \frac{\sum_i^N U_{ei}}{N} \quad U_n = \frac{\sum_i^N U_{ni}}{N}$
Resultant mean wind direction (Θ_U)	$\Theta_U = \text{ArcTan}\left(\frac{U_e}{U_n}\right)$	

On this table, **N** represents the number of measured samples within the corresponding ten minutes averaging period. It should be 300 samples when there were not data lost.

VIII.3 Sea surface temperature maps from GEOS Satellite

Table VIII.4. Example of hourly Satellite SST images of the Gulf of México region selected from four days with the higher amount of images available. The temperature-colour scale is the same introduced in Table V.8 (c) and (d). N/A stands for “Not Available” in the following tables.


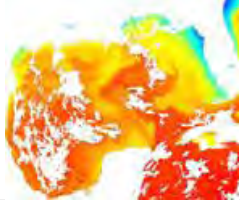
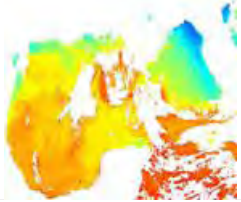

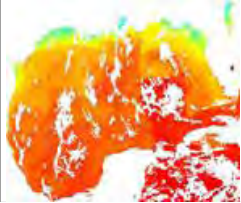
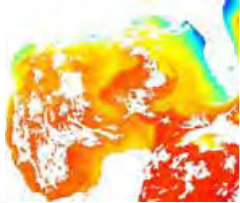
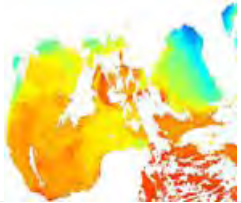
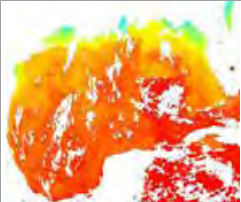
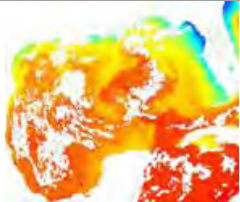
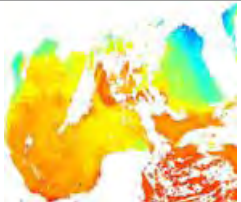
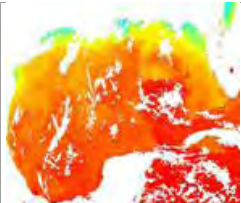
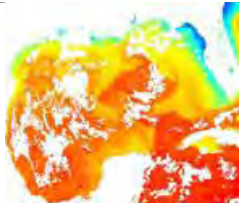
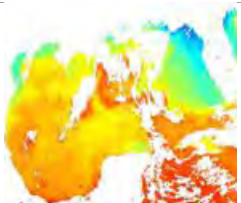

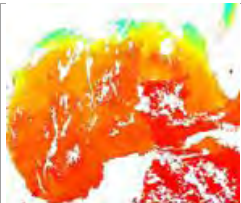
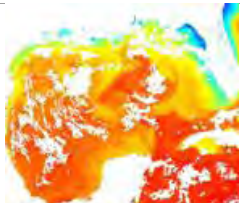
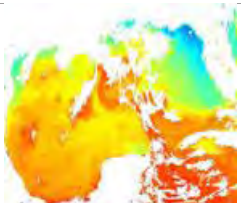



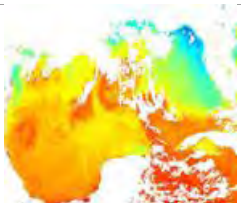



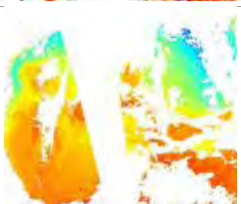
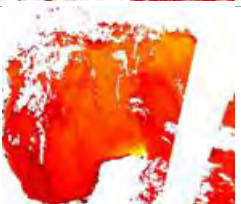
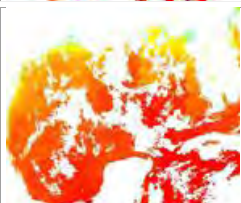
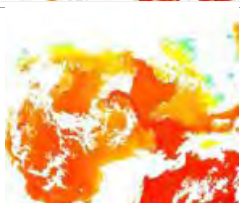


Hours	02/12/2007	27/11/2008	27/02/2009	08/05/2009
0				
1				N/A
2				N/A
3				
4				
5				
6				
7				

Table VIII.5. Continuation of Table VIII.4

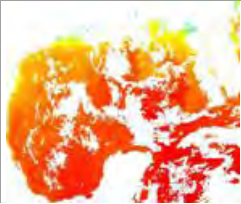
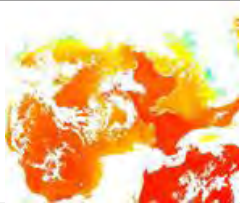
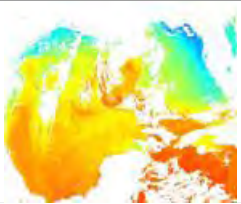
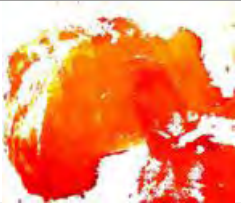
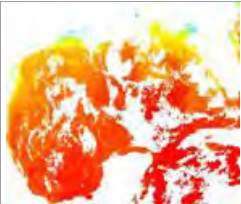
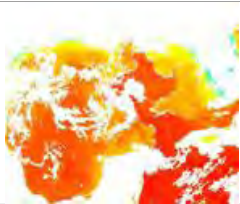
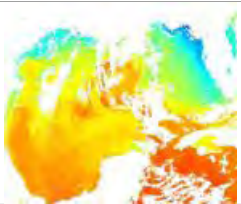
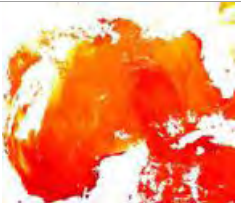
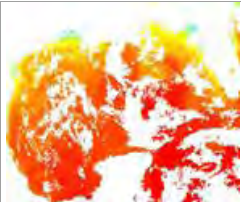
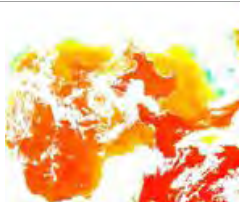
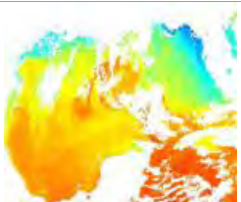
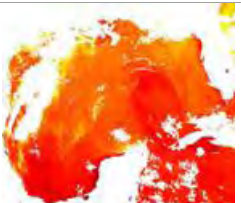



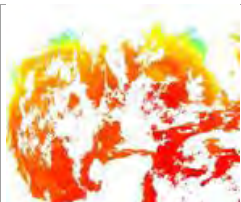

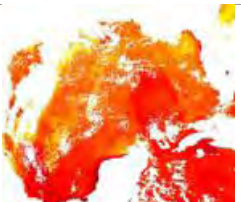
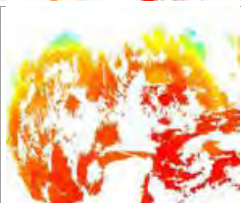
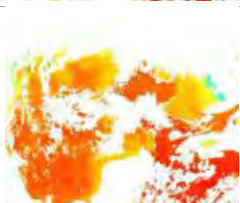
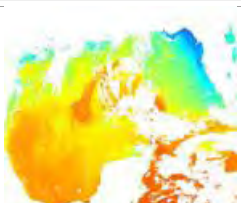
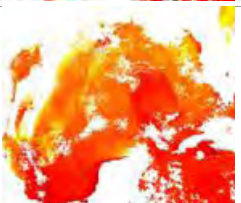


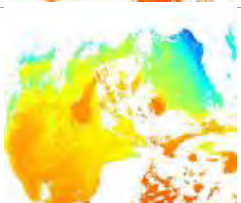



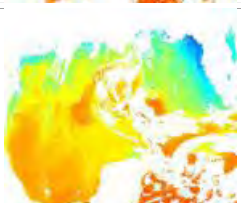
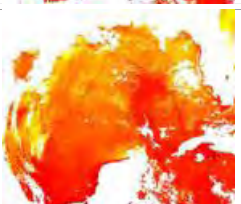
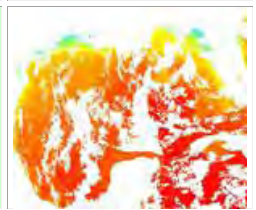
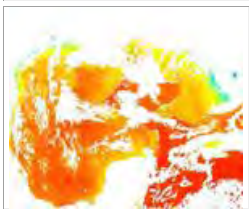
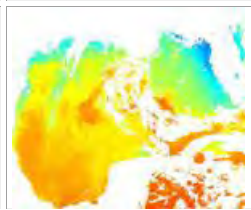
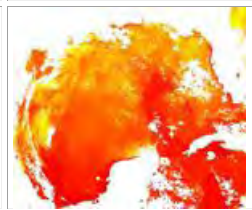
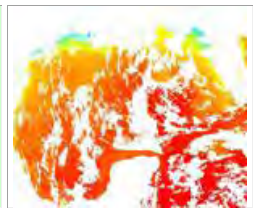
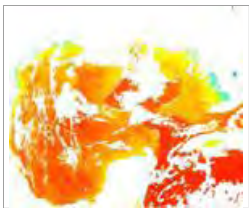
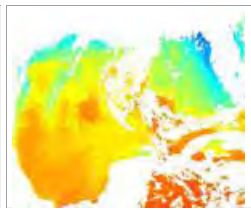
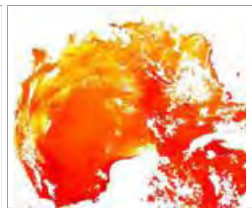

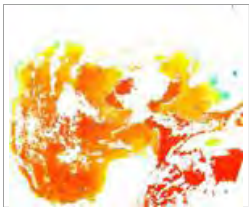
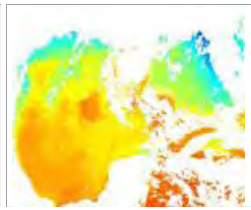

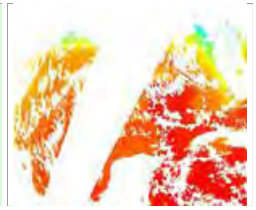
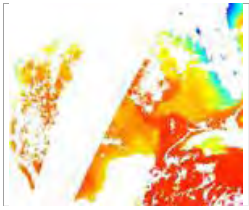
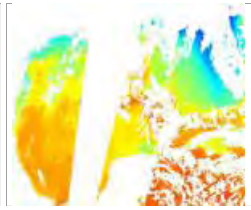

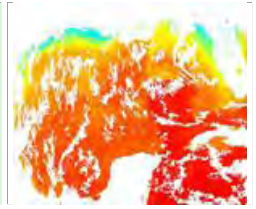
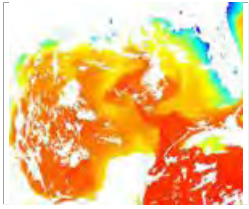
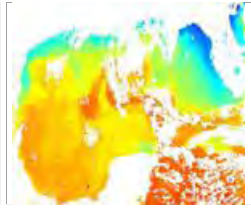

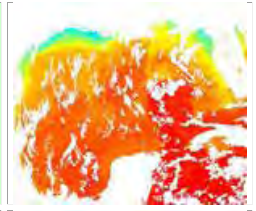
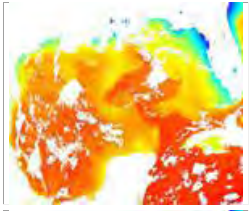
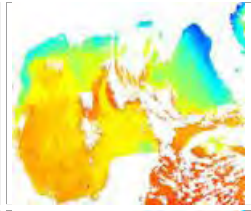

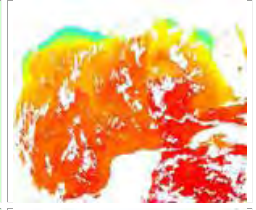
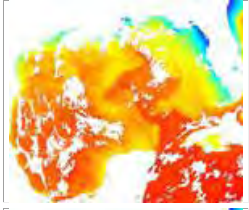
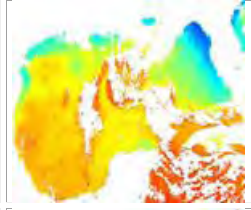

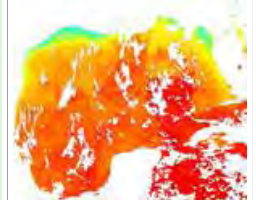
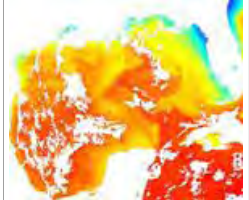
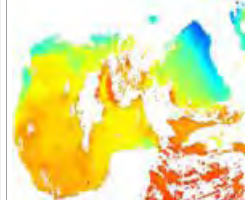

Hours	02/12/2007	27/11/2008	27/02/2009	08/05/2009
8				
9				
10				
11			N/A	
12			N/A	
13				
14				
15				

Table VIII.6. Continuation of Table VIII.5

Hours	02/12/2007	27/11/2008	27/02/2009	08/05/2009
16				
17				
18				
19				
20				
21				
22				
23				

VIII.4 Published results

The research subjects initially identified with the detailed reference review of the scientific literature and presented in Chapters II , III , IV were published in three scientific journal as follow:

- R. Soler-Bientz, S. Watson, and D. Infield, Preliminary study of long-term wind characteristics of the Mexican Yucatán Peninsula. *Energy Conversion and Management*, 2009. **50**(7): p. 1773-1780.
- R. Soler-Bientz, S. Watson, and D. Infield, Wind characteristics on the Yucatán Peninsula based on short term data from meteorological stations. *Energy Conversion and Management*, 2010. **51**(4): p. 754–764.
- R. Soler-Bientz, S. Watson, and D. Infield, Evaluation of the Wind Shear at a Site in the Northwest of the Yucatán Peninsula, México. *Wind Engineering*, 2009. **33**(1): p. 93-107.

Also, selections of the results described in the chapter V were also presented in the **European Wind Energy Conference:**


- R. Soler-Bientz, S. Watson and D. Infield. Study of the offshore winds and its propagation inland of the northern zone of the Yucatan Peninsula, Eastern Mexico. in *European Wind Energy Conference and Exhibition (EWEC2009)*. 2009. Marseille, France.
- R. Soler-Bientz, S. Watson, and D. Infield. Preliminary results of a statistical wind resources analysis in offshore conditions in the Eastern Gulf of Mexico. in *European Wind Energy Conference and Exhibition (EWEC2010)*. 2010. Warsaw, Poland.

The next subsections display the first page of the published papers.

VIII.4.1 Energy Conversion and Management Journal, 2009


Energy Conversion and Management 50 (2009) 1773–1780

Contents lists available at ScienceDirect



Energy Conversion and Management

journal homepage: www.elsevier.com/locate/enconman



Preliminary study of long-term wind characteristics of the Mexican Yucatán Peninsula

Rolando Soler-Bientz^{a,b,*}, Simon Watson^a, David Infield^{c,1}

^aCentre for Renewable Energy Systems Technology, Department of Electronic and Electrical Engineering, Holywell Park, Loughborough University, Loughborough, Leicestershire LE11 3TU, United Kingdom
^bEnergy Laboratory, Faculty of Engineering, Autonomous University of Yucatán Facultad de Ingeniería, Av. Industrias no contaminantes s/Aullo periférico norte s/n, Mérida, Yucatán, Mexico
^cInstitute of Energy and Environment, University of Strathclyde, Glasgow, United Kingdom

ARTICLE INFO

Article history:
Received 9 October 2007
Received in revised form 5 August 2008
Accepted 14 March 2009
Available online 11 April 2009

Keywords:
Monthly wind pattern
Wind rose
Wind resource assessment
Weibull distribution
Wind power density

ABSTRACT

Mexico's Yucatán Peninsula is one of the most promising areas for wind energy development within the Latin American region but no comprehensive assessment of wind resource has been previously published. This research presents a preliminary analysis of the meteorological parameters relevant to the wind resource in order to find patterns in their long-term behaviour and to establish a foundation for subsequent research into the wind power potential of the Yucatán Peninsula. Three meteorological stations with data measured for a period between 10 and 20 years were used in this study. The monthly trends of ambient temperature, atmospheric pressure and wind speed data were identified and are discussed. The directional behaviour of the winds, their frequency distributions and the related Weibull parameters are presented. Wind power densities for the study sites have been estimated and have been shown to be relatively low (wind power class 1), though a larger number of suitable sites needs to be studied before a definitive resource evaluation can be reported.

© 2009 Elsevier Ltd. All rights reserved.

1. Introduction

Wind power is seen as one of the most effective means available to combat the twin crises of global climate change and energy security, providing a possible solution to the problems associated with volatility in the fossil fuel markets for coal, gas and oil. The "Global Wind Energy Council" (GWEC) in their report "Global Wind Report 2006" [1] presented the state of development of wind energy for leading countries in each geographical region for the period 2000–2006 and a global forecast for 2007–2010 of the cumulative capacity of wind energy installations, which is expected to reach 149.5 GW by 2010. According to this report, the annual market for wind energy grew at a rate of 32% in 2006, with over 15,000 MW of new capacity installed worldwide. The market continued to broaden with installations in over 70 countries, establishing wind power as the leading renewable energy technology. Globally, the value of new generating plant installed in 2006 reached US\$24 billion. While Europe continues as the world leader, with 65% of the global market, the United States was the leader in terms of new installed capacity in 2006 with 2500 MW of new installed plant. On the other hand, new capacity installed in Latin America and the Caribbean during 2006 was 296 MW, increasing the total installed capacity to 508 MW. Mexico is one of the most promising areas for wind energy development being in the list of countries that more than doubled its installed capacity with 87 MW mainly located in the Isthmus of Tehuantepec in the State of Oaxaca.

A basic requirement when developing wind power projects is to study the geographical distribution of wind and its main characteristic parameters. Herberta et al. [2] presented in 2007 a general review of wind energy technologies briefly describing the main results published in the scientific literature, covering more than 20 research projects undertaken around the world. This review was particularly concerned with wind resource assessment. Average wind speed and temporal wind patterns have been identified using short-term measurements, such as in the study by Essa and Embaby [3] to describe the winds of a site close to the Egyptian Mediterranean coast over one year. Similarly, Li and Li [4] analyzed data over 5 years to determine the annual, seasonal and diurnal wind characteristics for the Waterloo region in Canada.

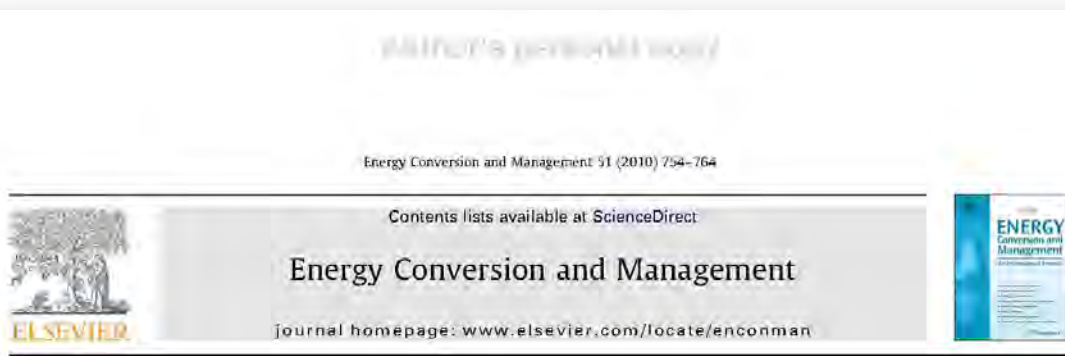
Long-term studies for periods of at least 10 years have been reported using wind data measured at meteorological stations on

^{*} Corresponding author. Address: Centre for Renewable Energy Systems Technology, Department of Electronic and Electrical Engineering, Holywell Park, Loughborough University, Loughborough, Leicestershire LE11 3TU, United Kingdom. Tel.: +44 1509 635338; fax: +44 1509 635341.
E-mail addresses: sbientz@msn.com, sbientz@uady.mx (R. Soler-Bientz).

¹ David Infield was involved with this research when based at Loughborough University.

0196-8904/\$ - see front matter © 2009 Elsevier Ltd. All rights reserved.
doi:10.1016/j.enconman.2009.03.018

VIII.4.2 Energy Conversion and Management Journal, 2010



Wind characteristics on the Yucatán Peninsula based on short term data from meteorological stations

Rolando Soler-Bientz^{a,b,*}, Simon Watson^a, David Infield^c

^a CREST, Department of Electronic and Electrical Engineering, Loughborough University, LE11 3TU, UK
^b Energy Laboratory, Faculty of Engineering, Autonomous University of Yucatán, Mérida, Yucatán, Mexico
^c Institute of Energy and Environment, University of Strathclyde, Glasgow, UK

ARTICLE INFO

Article history:
 Received 25 March 2009
 Accepted 30 October 2009
 Available online 16 December 2009

Keywords:
 Diurnal wind variation
 Monthly wind variation
 Wind resource assessment
 Atmospheric stability

ABSTRACT

Due to the availability of sparsely populated and flat open terrain, the Yucatán Peninsula located in eastern México is a promising region from the perspective of wind energy development. Study of the diurnal and seasonal wind resource is an important stage in the move towards commercial exploitation of wind power in this Latin American region. An analysis of the characteristics of the wind resource of the Yucatán Peninsula is presented in this paper, based on 10 min averaged wind speed data from nine meteorological stations, between 2000 and 2007. Hourly and monthly patterns of the main environmental parameters have been examined. Highly directional behaviour was identified that reflects the influence of winds coming from the Caribbean Sea and the Gulf of México. The characteristics of the wind speed variation observed at the studied sites reflected their proximity to the coast and whether they were influenced by wind coming predominantly from over the land or predominantly from over the sea. The atmospheric stability over the eastern seas of the Yucatán Peninsula was also analysed to assess thermal effects for different wind directions. The findings were consistent with the variation in average wind speeds observed at the coastal sites where winds came predominantly from over the sea. The research presented here is to be used as a basis for a wind atlas for the Yucatán Peninsula.

© 2009 Elsevier Ltd. All rights reserved.

1. Introduction

Wind energy has seen average annual growth of 30% globally over the last 10 years [1]. This explains why it is now the leading renewable energy source and is positioned to help in the mitigation of the polluting effects of fossil fuel combustion for the production of electricity. In order to assess the increasing contribution that wind energy could make worldwide, studies of the wind characteristics in potential regions need to be undertaken. A brief overview of regionally based resource assessment is presented below.

Wind energy potential for five coastal regions of the Kingdom of Saudi Arabia was evaluated by Rehman and Ahmad [2] using hourly mean values of wind speed and wind direction and covering a period of almost 14 years between 1970 and 1983. The authors analysed seasonal and diurnal changes in wind speed values and identified Yanbo site as the best location for use the power of wind. This site was later studied in detail by Rehman [3]. On the North-West of the Saudi Arabia, in the State of Kuwait, Al-Nassar et al. [4]

presented a study with hourly averaged wind speeds from six meteorological stations made at 10 m above ground level (a.g.l.) over a four year period (January 1998–December 2002). Monthly averages for the wind power density at 10 m a.g.l. and their extrapolation to 30 m a.g.l. were tabulated for each study station by means of the power law. The authors highlighted that the summer season showed higher potential wind power coinciding with the period of highest electricity demand during the year.

An assessment of wind energy in Egypt was carried out by Essa and Mubarak [5]. Data were collected from 18 meteorological stations around Egypt measuring at 10 m a.g.l. and recording averages every 15 min over a five year period (April 2000–December 2004). The hourly, daily, monthly and yearly behaviour of the wind speeds were computed. The authors concluded that the Red Sea, Mediterranean (El-Arish) and some Inland zones (Aswan and Ismailia) would be favourable locations for wind energy applications and that the Red Sea winds were strongest in the summer while in the Mediterranean coastal zones, winds were strongest in winter and spring seasons.

The eastern Mediterranean region of Turkey was studied by Sahin et al. [6] using hourly data from seven meteorological stations which were measured between 1992 and 2001. The authors computed the wind energy at 10 m and 25 m a.g.l. using a linear wind flow model (WASP) developed by Troen et al. [7]. Three areas with

* Corresponding author. Address: CREST, Department of Electronic and Electrical Engineering, Loughborough University, LE11 3TU, UK. Tel.: +44 1509 635338; fax: +44 1509 635341.
 E-mail address: sbientz@msn.com (R. Soler-Bientz).

VIII.4.3 Wind Engineering Journal, 2009

WIND ENGINEERING VOLUME 33, No. 1, 2009 PP 93-107

93

Evaluation of the Wind Shear at a Site in the North-West of the Yucatan Peninsula, Mexico

Rolando Soler-Bientz,^{1,2,*} Simon Watson¹ and David Infield³

¹Centre for Renewable Energy Systems Technology (CREST), Department of Electronic and Electrical Engineering, Loughborough University, United Kingdom
Tel: +44 1509 635338, Fax: +44 1509 635341, E-mail: sbientz@msn.com

²Energy Laboratory, Faculty of Engineering, Autonomous University of Yucatan, Mexico

³Institute of Energy and Environment, University of Strathclyde, Glasgow, United Kingdom

ABSTRACT

Extrapolations from 10m above the ground up to the wind turbine hub height are frequently made to the data available for wind power assessments. Because of its simplicity, the power law profile has been one of the most popular mathematical formulations to predict the vertical wind shear. This paper presents an analysis of wind speed and wind shear in terms of the directional, diurnal and seasonal patterns for a site at the Autonomous University of Yucatan which experiences the tropical conditions of the Yucatan Peninsula in Mexico. This analysis takes a detailed look at frequency distributions to facilitate a comprehensive understanding of the local climatic conditions. Diurnal wind speed variations are shown to be affected in particular by the differing wind conditions associated with fetches over two distinct offshore regions. Seasonal behaviour suggests some departure from the oscillations expected from temperature variation. In addition, the use of rate of change of temperature at one height is proposed as an alternative to vertical temperature gradient inferred from two heights as an indicator of atmospheric stability which will affect the wind shear. The work presented is part of a regionally funded research program to evaluate the onshore and offshore wind potential in the north of the Yucatan Peninsula.

Keywords: Wind shear, Wind direction, Frequency distribution, Diurnal variation, Atmospheric stability, Seasonal variation.

1. INTRODUCTION

The yield of a Wind Energy Conversion System (WECS) is highly dependent on the precision of the wind speeds used to compute the wind energy potential. In order to assess the wind potential for a wide area, it may not be feasible to install a large number of masts with measurements made at typical wind turbine hub heights (presently 60 m-80 m). Wind speed data from existing meteorological stations are often used initially for this purpose. Usually wind speed data from meteorological stations are measured at 10 m above ground level (a.g.l.). The wind speed at the turbine hub height must then be determined from estimates of the site wind shear based upon locally available data. A number of papers have been published to address this subject depending, among other factors, on the amount and kind of meteorological data available, the geographical location (inland, onshore or offshore), the

VIII.4.4 European Wind Energy Conference 2009

European Wind Energy Conference and Exhibition 2009, Marseille, France



Study of the offshore wind and its propagation inland of the northern zone of the Yucatan Peninsula, Eastern Mexico

PO.60

Rolando Soler-Bientz^{1,2*}, Simon Watson¹, David Infield³

¹ CREST, Electronic and Electrical Engineering, Loughborough University, UK

² Energy Laboratory, Faculty of Engineering, Autonomous University of Yucatan, México. *email: sbientz@msn.com

³ Institute of Energy and Environment, University of Strathclyde, UK

ABSTRACT

A preliminary study of the wind characteristics of the northern zone of the Yucatan Peninsula, Eastern Mexico was undertaken for offshore and coastal sites using data measured from three measurement sites. Ten minutes averages of wind speeds, wind directions and ambient temperatures at two different heights were recorded from data measured over a year. The usual wind statistics analysis was undertaken to evaluate the atmospheric stability and the relation between the offshore and onshore winds. The results were compared with the models previously proposed by Monin-Obukhov and by Hsu.

1. INTRODUCTION

The winds in the offshore environment have better characteristics for wind energy applications than winds in inland flat regions because offshore winds tend to show less variability, there is reduced turbulence intensity that can fatigue turbine components and offshore wind speeds are normally higher due to a lower surface roughness. However, these potentially better wind conditions need to be evaluated as the benefits are to some extent offset by higher installation, operation and maintenance costs for wind farms in offshore environments. One alternative option is consider the wind conditions at a coastal site which may benefit from some of the features of an offshore site but is far more accessible in terms of installation, operation and maintenance.

Among the factors affecting wind speeds in mainly flat coastal regions are the latitude of the site, differences between the air and sea temperatures, water depth and distance from the coastline. The flow of winds over a coastal discontinuity face changes in roughness, availability of heat and moisture which alter the turbulent mixing and momentum transfer creating different stability conditions offshore and onshore sites and influencing the wind profile behaviour [1]. By means of data measured from an offshore wind farm in Denmark, Barthelmie studied the changes in the onshore and offshore stability and their impact in the wind profile [2].

Barthelmie and Palutikof [3], introduced a couple of methods to predict wind speeds at offshore coastal regions using an empirical approach and a solution with the internal boundary layer theory. On the other hand, McQueen and Watson [4], studied different methodologies to predict the offshore wind speeds concluding that more research should be undertake to evaluate the impact of the atmosphere stability on the sea-land discontinuity conditions.

The research presented in this paper is focused in to identify the directional and diurnal patterns of the winds over the north-West of the Yucatan Peninsula, to classify the stability stages of the atmosphere over the measurement period and to evaluate the correlation between the offshore and onshore winds. Three strategic locations have been chosen around the North-West coast of the Yucatan peninsula. Two stations are located at coastal sites and one station is located 6.4km offshore. Ten minutes averages of ambient temperature and wind speed and direction at two different heights were recorded during a full measurement year in each study site.

2. STUDY REGION

Three measurement stations were installed on communication towers at the North-West of the Yucatan Peninsula: one offshore (API) and two onshore (CHM and TCP) as can be seen below in the map and the tower images of the Figure 1. A couple of ambient temperature and wind speed and direction sensors were

VIII.4.5 European Wind Energy Conference 2010

European Wind Energy Conference and Exhibition 2010, Warsaw, Poland



Preliminary results of a statistical wind resources analysis in offshore conditions in the Eastern Gulf of Mexico

PO.89

Rolando Soler-Bientz^{1,2*}, Simon Watson¹, David Infield³

¹ CREST, Electronic and Electrical Engineering, Loughborough University, UK

² Energy Laboratory, Faculty of Engineering, Autonomous University of Yucatan, México *email: sbientz@msn.com

³ Institute of Energy and Environment, University of Strathclyde, UK

ABSTRACT

A statistical analysis of the wind resources has been undertaken by mean of data measured on a communication tower installed on a pier which extends 6.65km from the coastline. A set of wind and temperature sensors were installed to record the ten minute averages over approximately two years. As a complement, hourly values of Sea Surface Temperature, extracted from GEOS satellite measurements over the study region, were also included in the research presented. The results have confirmed that the offshore wind is thermally driven by differential heating of land and sea producing sea breezes which veer to blow parallel to the coast in the late afternoon under the action of the Coriolis force. Air temperature and sea surface temperature profiles suggested largely unstable conditions and the potentially development of a shallow Stable Internal Boundary Layer.

INTRODUCTION

In offshore conditions, the differences between the air and sea temperatures, water depth and distance from the coastline are among the principal factors influencing the wind speeds and the stability conditions in the atmospheric boundary layer. The flow of winds over a coastal discontinuity face changes in roughness, availability of heat and moisture which alter the turbulent mixing and momentum transfer creating different stability conditions in offshore sites and influencing the wind profile behaviour [1]. By means of data measured from an offshore wind farm in Denmark, Barthelmie studied the changes in the onshore and offshore stability and their impact in the wind profile [2].

In the case of offshore conditions, Van Wijk et al. [3] obtained good estimates for the seasonal mean wind speed in the North Sea after applying their "diabatic" method to calculate the wind speed profile as a function of height, when wind speed, sea water temperature and air temperature are known. This diabatic method was also used by Coelingh et al. to study offshore [4] and onshore sites [5]. These two studies of the North Sea and its coastal areas concluded that diurnal variations are very similar in autumn and winter and that the thermal circulation leads to sea breezes with important effects up to 30km offshore for wind speeds lower than 7m/s.

For the marine environment of the Danish Baltic Sea, Lange et al. [6] studied the influence of thermal effects on wind speed profiles reporting that the standard Monin-Obukhov theory predicted lower wind speed values than measured for stable and near-neutral conditions, especially at large distances from the shore. Using wind speed and air temperature data measured from one onshore site and two offshore towers, Pryor and Barthelmie [7] studied the wind speed, stability and surface roughness. They reported that wind speed distributions onshore and offshore were statistically different for heights less than 20m regardless of the atmosphere stability conditions, at distances less than 2km from the shore. In an extended study using data from the Danish monitoring network [8], the same authors concluded that sites located within 2km from the coastline could experience significant vertical shear and differing turbulence because the wind speeds close to the sea surface were frequently decoupled from the wind characteristics above 30m in height.

Lapworth [9] reported diurnal patterns with maximum winds overnight and minimum values occurring during the afternoon for the offshore surface winds around the English coast after applying numerical models for stable boundary layers to offshore measurements made in static vessels. On the other hand, Barthelmie et al. [10] studying the coastal meteorology of Denmark found that the offshore sites which receive winds from over the land showed a typical onshore pattern with lowest wind speeds overnight and highest wind speeds during the afternoon. Generally, the increase in offshore wind speeds overnight is produced by the lower roughness of the sea surface and the transition from stable conditions over land to less stable conditions over sea. During the day, the transition from unstable conditions over land to stable conditions offshore means that the surface layer becomes decoupled from higher wind speeds aloft and the wind speed close to the surface layer is lower, as was reported by Barthelmie et al. [11].